MURDOCH
UNIVERSITY
PERTH, WESTERN AUSTRALIA

Honours Engineering Thesis
Design, Planning and Implementation of the Dilution and Recycle Section of the Engineering Pilot Plant

---

Author

Radomir Sebesta

Academic Supervisor

Associate Professor Graeme Cole

A thesis submitted to the Murdoch University School of Engineering and Information Technology
to fulfil the requirements for the Bachelor of Engineering Honours Degree
in the discipline of
Industrial Computer Systems Engineering and Instrumentation and Control Engineering

School of Engineering and Energy, Murdoch University, Western Australia

29 November 2018

© Radomir Sebesta 2018

This page is intentionally left blank

AUTHOR'S DECLARATION

I declare that this thesis is my own account of my research and contains as its main content work which has not previously been submitted for a degree at any tertiary education institution.

X

Radomir Sebesta

The main body of this document has a word count of approximately 17000 words.

ABSTRACT

The Murdoch University Engineering Pilot Plant simulates a Bayer process in which alumina is extracted from bauxite. Water is utilised as the process medium for teaching purposes. Recently, table salt has been introduced into the process for conductivity testing purposes. As the plant comprises of 316 grade stainless steel construction, the presence of salt within the plant presents corrosion concerns. Additionally, the Water Corporation advises that a maximum of 20,000 g/L of total dissolved solids inclusive of salts, can be sent to drain as a result of plant activities.

The design and planning of the dilution and recycle section of the Engineering Pilot Plant was successfully completed. This allows the salt concentration to be diluted within a holding tank arrangement attached to the current output of the pilot plant, before being pumped to drain. This is only possibly when below permissible limits. If further dilution is required, the recycle stream is employed to recycle product within this arrangement until the desired concentration is achieved. This provides a feasible solution to these problems. Additionally, an operational Foundation Fieldbus communications network was established within the plant to provide future students with alternate means of plant communications.

In the absence of an implemented dilution and recycle section addition to the plant, a process model was derived from fundamental principles instead. An overall mass balance and salt component balance were utilised for this purpose. Differential equations were then derived. A simulation based on these equations was then implemented via Mathwork's simulation program, Simulink.

The method of direct synthesis was then used to derive both Proportional and Proportional and Integral controllers. Both types of controllers were then applied to both of the desired process variables: holding tank level and conductivity. The performance of each controller was assessed for set point tracking and

disturbance rejection capabilities using both statistical process control and integral error criteria. The PI controller was found to have the most desired system response for both level and conductivity.

A fully operational Foundation Fieldbus network was also successfully established within the pilot plant. This entailed the use of a Fieldbus interface module, power conditioner, segment coupler and a Foundation Fieldbus instrument in the plant. This network will provide future students with the option of utilising a new communications network with diagnostic capabilities for future plant and instrument implementation.

ACKNOWLEDGEMENTS

Associate Professor Graeme Cole

Project Supervisor, Murdoch University

Professor Parisa Bahri

Professor of Engineering, Murdoch University

Mr Will Stirling

Technical Officer, Murdoch University

Mr Mark Burt

Technical Officer, Murdoch University

Mr Graham Malzer

Technical Officer, Murdoch University

This page is intentionally left blank

TABLE OF CONTENTS

LIST OF FIGURES

LIST OF TABLES

LIST OF ABBREVIATIONS

Acronym	Definition
AC	Alternating Current
A/D	Analogue/Digital
AWG	American Wire Gauge
CB	Control Builder
CEE	Control Execution Environment
CPU	Central Processing Unit
CS	Configuration Studio
CSTR	Continuously Stirred Tank Reactor
CUSUM	Cumulative Sum
DC	Direct Current
DCS	Distributed Control System
DD	Device Description
DLL	Data Link Layer
DMC	Dynamic Matrix Control
DP	Differential Pressure
EEPROM	Electronically Erasable Programmable Read Only Memory
EPP	Engineering Pilot Plant
FAS	Fieldbus Access Sublayer
FF	Foundation Fieldbus
FIM	Fieldbus Interface Module
FMS	Fieldbus Message Specification
FTE	Fault Tolerant Ethernet
GMC	Generic Model Control
GPM	Gallons Per Minute
HMI	Human Machine Interface
HSE	High Speed Ethernet
HVAC	Heating, Ventilation and Air Conditioning
ICE	Instrument and Control Engineering
I/O	Input/Ouput
IOTA	Input/Ouput Termination Assembly

ISO	International Standards Organisation
LabVIEW	Laboratory Virtual Instrument Engineering Workbench
LAN	Local Area Network
LCD	Liquid Crystal Display
LCL	Lower Control Limit
MSEDE	Microsoft Excel Data Exchange
MV	Manipulated Variable
NaCl	Sodium Chloride
OPC	Open Platform Communications
OSI	Open Systems Interconnect
P	Proportional
PDU	Protocol Data Unit
PI	Proportional and Integral
PID	Proportional, Integral and Derivate
PKS	Process Knowledge System
PLC	Programmable Logic Controller
PSI	Pounds per Square Inch
PTFE	Polytetrafluoroethylene
PV	Process Variable
RAM	Random Access Memory
RPM	Revolutions Per Minute
SCADA	Supervisory, Control And Data Acquistion
SCM	Sequential Control Module
SP	Set Point
SPC	Statistical Process Control
SS	Stainless Steel
TCP	Transmission Control Protocol
UCL	Upper Control Limit
VSD	Variable Speed Drive

1 INTRODUCTION

The purpose of this project was to provide a novel solution to several problems that have arisen due to recent plant upgrades. These include plant corrosion concerns and pumping excessive amounts of table salt to drain. Both these problems and solutions with be discussed through this report.

1.1 PROJECT BACKGROUND

The Murdoch University pilot plant, shown in Figure 1, is a representation of the Bayer process required to extract alumina from bauxite on a smaller scale than normally seen in industry [1]. It is fitted with instrumentation and other control equipment commonly encountered in industry. Automation is achieved though the Honeywell Experion C300 controller utilising its Process Knowledge System (PKS) Distributed Control System (DCS) [2] [3]. Collaboration between the Murdoch University Engineering department, Alcoa of Australia, Honeywell and Control and Thermal Engineering brought about the inception of the EPP [4].

As a requirement of a penultimate year ICE major unit, ENG322 Process Control Engineering II, students operate the EPP to gain hands-on understanding of controlling a real-world process [5]. Advanced control schemes are implemented within the plant during the fourth year ICE major unit ENG445 Instrumentation and Control Systems Design. These include interaction analysis and subsequent design and implementation of decouplers, Generic Model Control (GMC) and Dynamic Matrix Control (DMC) schemes [6].

FIGURE 1 MURDOCH UNIVERSITY ENGINEERING PILOT PLANT

This thesis is the latest addition to previous projects performed on the EPP since its installation at the South Street campus. Past contributions include general upgrades to the plant and associated instrumentation, implementation of new communication networks and upgrades to the plant control architecture [7] [8] [9] [10] [11]. Previous work has allowed students to interact with the plant in increasingly sophisticated ways. This project aims to add further complexity to the existing process whilst providing an appropriate solution to the project problem. This will give future students more opportunities than currently possible, to understand process interaction and implement complex control strategies.

1.2 PROJECT SCOPE

The project scope was to design, plan and implement a dilution and recycle subsystem of the EPP. This included the design, planning and selection of new plant and associated instrumentation for future implementation. It also included the implementation of Foundation Fieldbus communications between the plant and the Honeywell Experion PKS DCS.

Proposed new plant and equipment comprised of:

- A holding tank arrangement:
    - Eight interconnected tanks;
    - Each tank with an agitator controlled by an associated motor.
- One conductivity sensor;
- One differential pressure level transmitter;
- One plug type control valve;
- Two integral orifice flow transmitters;
- Three 24 V solenoid valves;
- One positive displacement pump;
    - One variable speed drive (VSD).
- Foundation Fieldbus communications:
    - Foundation Fieldbus Interface Module;
    - Foundation Fieldbus Single Channel Power Conditioner;
    - Foundation Fieldbus Segment Coupler;
    - Two 4-20mA to Foundation Fieldbus Converters.
- All necessary interconnecting tubing and wiring.

Figure 2 indicates the required changes in red for the successful implementation of the full scope. This would entail the installation of a holding tank arrangement on the outlet of CSTR3. If the holding tank contains only water, it can be recycled back to the supply tank to prevent water wastage. Salt can be added to the process via the dye tank during conductivity testing within the CSTR arrangement. If the salt concentration present is above permissible limits of 20000 mg/L set by the Water Corporation, it cannot be dumped to drain. This solution can then be recycled back to the CSTR arrangement for further dilution instead. Raw water can also be applied via the dilution stream to bring down the concentration of salt present in the holding tank. Should the salt content be below the permissible limits, it can then be pumped to drain.

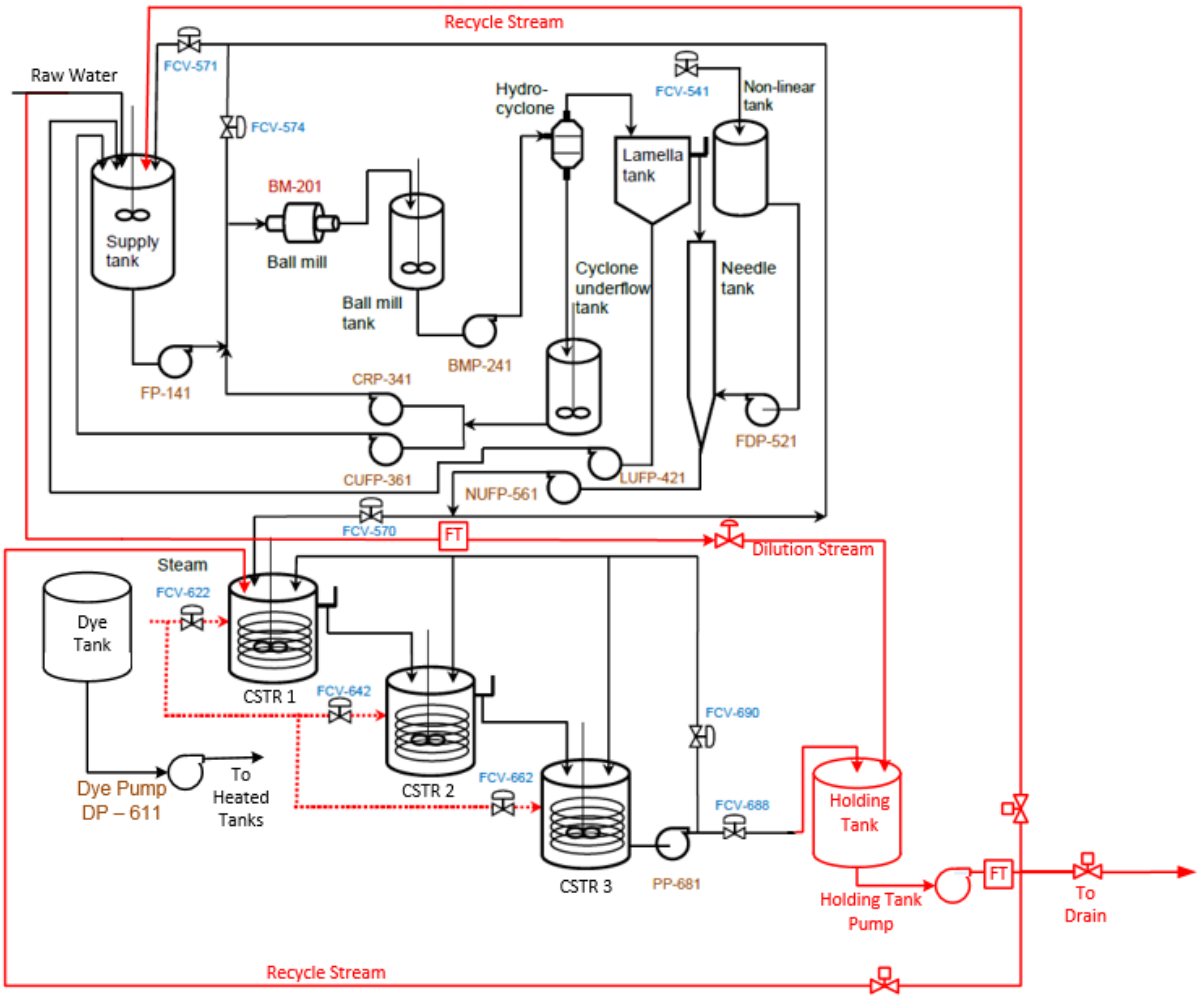

FIGURE 2 ENGINEERING PILOT PLANT PROPOSED CHANGES

The scope included the following objectives:

- Identify the amount of raw water pumped to drain daily during teaching weeks;
- Research salt water effects on plant equipment within the EPP;
- Liaise with relevant authorities to obtain permissible trade waste limits;
- Design an appropriate solution to dilute and recycle plant output stream;
- Create an accurate system model of the dilution and recycle addition to the plant from fundamental principles;
- Design and test appropriate control schemes;
- Implement a new communications network.

Successful implementation of this project will extend the lifespan of the existing plant by preventing the recycling of saline solution through the entire plant. It will also add further options for communication within the plant. Furthermore, conductivity testing within the pilot plant will become a viable option. Students will be able to learn how dilution affects salt concentrations in water. Most importantly, when concentration testing is not being undertaken, water previously being pumped to drain will be recycled throughout the plant.

1.3 ENGINEERING PILOT PLANT OVERVIEW

The history of the Murdoch University EPP can be assessed most efficiently by starting from the initial inception of the EPP at Murdoch University and then describing each major upgrade implemented by staff or students in a chronological fashion finishing at the current iteration of the EPP. This will help explain the need for the work contained within this thesis report. A detailed overview is located in Appendix A Detailed Engineering Pilot Plant Overview.

2 PROJECT REQUIREMENT

To develop an appreciation for the requirements for this project, the following areas were explored:

- Changes in Process control;
- Water wastage;
- Effects of salt on plant equipment;
- Process Recycle streams;
- Trade waste discharge regulations.

2.1 CHANGES IN PROCESS CONTROL

The origins of feedback control can be traced back to a period two thousand years ago. Ancient water clocks were operated using float regulators in Alexandria (Egypt) and Baghdad (Iraq) during this period. Before the 1940s, most processing plants were run manually by process operators. In the 1940s and 1950s, higher performance equipment and processes were developed. The 1960s saw the rise of dynamic analysis and control theory. A sudden increase in energy costs saw the rise of advanced control systems in the 1970s. By the 1980s and 1990s, control hardware went through a transitional period. Pneumatic control was upgraded to analogue/electric control that was microprocessor-based. After this, came the introduction of Distributed Control Systems (DCS) introducing various advanced control possibilities [12].

The role of process control has evolved over the years. Traditionally, in industrial applications, process variables are maintained near their desired values. This is done to increase safety, reduce environmental impact and optimise the process. There was also the need to be able to move the process from one operating point to another. With the introduction of computer control systems like DCS, this role has been expanded. It now includes functions such as information processing, process control, online optimisation and scheduling [12].

2.2 WATER WASTAGE

Consistent daily plant water usage measurement for an entire year was not a feasible approach. Instead, a logical sequence of calculations based on average plant use was utilised to calculate average yearly plant water usage. Every teaching week, two sessions have been run on weekdays for a total of eight hours a day. The output of the EPP was taken from the Continuously Stirred Tank Reactor (CSTR) 3 via the product pump. First, the average operating percentage of the product pump, PP-681 was obtained during student pilot plant sessions. Next, a calibration curve for the pump was obtained by obtaining flow measurements at set increments from 0 to 100% flow. Both of these data sets were then used to calculate that on a daily average, 2320L of water was being pumped to drain, during plant operation. This results in an estimated 324,800L of raw water being wasted each year as a direct result of pilot plant operations.

2.3 EFFECTS OF SALT ON PLANT EQUIPMENT

Table salt otherwise known as Sodium Chloride (NaCl), is a highly corrosive element when in contact with metals. 316 grade Stainless Steel (SS) is utilised in many applications due to its high corrosion resistance. When in contact with NaCl however, SS becomes subject to a form of corrosion known as pitting. The result in the formation of rust on the surface of the metal. This occurs when moisture present in the pipework condenses and forms droplets or thin electrolyte layers containing chloride ions due to a drop in temperature or a fall in relative humidity [26]. Murdoch University staff have raised their concerns about the introduction of NaCl into the EPP. The plant is predominantly stainless-steel construction.

2.4 PROCESS RECYCLE STREAMS

Recycle streams are commonly applied in both chemical and industrial process. Several reasons for implementing a recycle stream occur within process applications. These include [13]:

- Recovery and reuse of unconsumed reactants;
- Recovery of a catalyst;
- Dilution of a process stream;
- Control of a process variable;
- Circulation of a working fluid.

Currently, in the absence of a recycle stream, saline solution is being pumped directly to the drain. This occurs during conductivity testing in the CSTR arrangement of the EPP. This is in direct violation of the Water Corporation's trade waste regulations [14]. As the addition of salt during conductivity testing is a manual application, high salt concentrations entering the CSTRs are feasible. The addition of a recycle stream would allow for process medium exhibiting a salt concentration above 20,000 mg/L to be recycled back to the holding tank arrangement for further dilution before being pumped to drain.

2.5 TRADE WASTE DISCHARGE REGULATIONS

The Water Corporation defines trade waste as "any wastewater discharged from your business other than waste from office facilities or staff amenities" [14]. Any trade waste discharged by an organisation requires an appropriate trade waste permit from the Water Corporation. This is to ensure that there is appropriate mitigation against consequential harm to the environment or the wider public [14]. Currently, the Water Corporation trade waste acceptance criteria for total dissolved salts is a maximum of 20,000 mg/L [15]. A trade waste application was obtained with the help of Murdoch University Facility staff for the Murdoch University EPP. This allowed for continued operation during conductivity testing.

3 TECHNICAL REVIEW

Following is a detailed technical review of all major plant and instrumentation planned for future implementation or installation.

3.1 HOLDING TANK ARRANGEMENT

The holding tank allows outgoing process medium to reside in a location before being pumped elsewhere based on the salt concentration measured. In the absence of one large holding tank due to budget restrictions, eight smaller vessels were considered.

3.1.1 SIZE REQUIREMENT CALCULATION

From previous EPP operation, the maximum Needle Tank Pump, NUFP-561 flowrate was measured as 0.0974L/s. This sets the normal maximum flowrate from the Product Pump, PP-681. It was deemed that a residence time of thirty minutes was appropriate in this circumstance. Residence time is usually associated with continuous process flow through a vessel. It can be defined as the average time taken by a fluid particle to pass through a vessel during continuous process operation [16]. The simplest way to calculate this value is shown in (1) [17].

$$Mean\ Residence\ Time\ (s) = \frac{Volume\ of\ vessel\ (m^3)}{Flowrate\ of\ fluid\ through\ vessel\ (\frac{m^3}{s})} \quad \textbf{(1)}$$

Rearranging (1) to solve for required volume results in (2).

$$Volume\ of\ vessel\ (m^3) = Residence\ Time\ (s) \times flowrate\ of\ fluid\ through\ vessel\ (\frac{m^3}{s}) \quad \textbf{(2)}$$

By substituting known parameters, the required holding tank arrangement volume is calculated via (3):

$$V\ (m^3) = 30min \times \frac{60s}{min} \times 0.0974\ \frac{\mathrm{L}}{s} \times \frac{1m^3}{1000L} = 1800s \times 9.74 \times 10^{-5} \frac{m^3}{s} = 0.175m^3 \qquad \textbf{(3)}$$

By multiplying 0.175m^3 by 1000L/m^3, a required holding tank volume of 175L was found to be required. This was increased to 200L to allow room for any errors in calculation. As the desired steady state level would reside around 50% of tank level, the overall tank volume required will be 400L.

3.1.2 REPURPOSING EXISTING EQUIPMENT

A common theme throughout the project was the need to source and repurpose as much existing plant and instrumentation as possible before resorting to ordering new equipment. For this reason, with the help of EPP technical staff, eight small vessels were repurposed for this scope. Figure 3 shows one of these vessels.

FIGURE 3 HOLDING TANK VESSEL AND IMPELLER

Each vessel, has an internal diameter of 0.345m and height of 0.495m. The cross-sectional area of each tank, 0.0935m^2, was calculated utilising (4) [18].

$$A = \pi r^2 \quad \textbf{(4)}$$

Multiplying 0.0935m^2 by 8 resulted in a total holding tank arrangement cross-sectional area of 0.748m^2. The cross-sectional area dimensions would be required during modelling activities carried out later. A volume of 0.046m^3 per holding tank was then calculated utilising (5) [18]. This was multiplied by 8 to obtain a complete holding tank arrangement volume of 0.370m^3.

$$V = \pi r^2 h \quad \textbf{(5)}$$

This resulted in a holding tank volume of 46.27L and a holding tank arrangement volume of 370.19L. This allows operation within the vessel arrangement at just under half the total volume to provide a residence time of 30 minutes when operating near 50% level set-point. Should the vessel be operated at a higher level set point, the residence time would increase.

3.1.2.1 AGITATORS AND IMPELLERS

Associated Lightnin L5U08F mixer motors were also located in a cupboard within the EPP. These are the original motors that controlled the A310 axial flow impellers in a past application. Each single-phase motor, shown in Figure 4 outputs a maximum of 550 revolutions per minute (RPM) with a rated maximum power of 75W. These motors require 230V to operate. This type of impeller is standard issue for all Lightnin gear drive portable mixers [19] and is shown in Figure 5.

FIGURE 4 AGITATOR MOTOR

FIGURE 5 AXIAL FLOW IMPELLER

3.2 CONDUCTIVITY INSTRUMENTATION

Instrumentation has already been implemented in each of the CSTRs as part of a prior thesis project. For this reason, the same type of conductivity sensor was considered for use within the holding tank arrangement. The Endress+Hauser supplied Liquiline CM444 transmitter and three CLS50D conductivity sensors were already installed in the EPP. For this project, an extra CLS50D conductivity sensor is to be installed on the holding tank arrangement to measure the conductivity of process fluid within this vessel arrangement.

3.2.1 CONDUCTIVITY

When salts, acids or bases are dissolved in water, ions carrying opposing charges move in opposite directions through the solution. The motion of these electrically charged particles creates a current. Liquids that conduct electricity this way are termed electrolytes. Conductance, measured in Siemens (S), is a measure of the current-carrying capability of an electrolyte. Conductivity, therefore, is the conductance of an electrolyte per unit length. It has units of Siemens per metre (S/m). This is the simplest method of indicating the dissolved solids or ionic content of a solution [20].

3.2.1.1 EFFECTS OF DILUTION AND TEMPERATURE

Dilution decreases the amount of dissolved electrolyte and consequently forms ions within the solution. Conversely, it also reduces the concentration of the electrolyte. This being the number of ions per unit volume. This, in turn, reduces the conductivity of the fluid [20]. The viscosity of a fluid decreases with an increase in temperature. This, in turn, affects the mobility of ions within an electrolytic solution. As the temperature of an electrolyte solution is increased, the conductivity of that solution will also increase [21]. The effects of temperature on conductivity, however are deemed outside the scope of this thesis and not further explored.

3.2.2 LIQUILINE CM444

The Liquiline CM444 transmitter is capable of obtaining multiple parameters. These include Conductivity, Oxygen, Chlorine and Turbidity amongst others values from any Memosens type sensor available. This digital transmitter possesses four channels allowing connection of up to four Memosens sensors. It supports communication via 4-20mA, HART, Profibus DP, Modbus TCP and Ethernet amongst other protocols [22].

This transmitter was already implemented as part of a prior thesis project [11]. The configuration of this transmitter contained a base module (BASE-E). This provides two 4-20mA outputs, an alarm relay and further provision for two other sensors [23]. As three channels were already occupied by previously installed Indumax CLS50D conductivity sensors, provision for installation of the last sensor is provided via the fourth channel as shown in Figure 6.

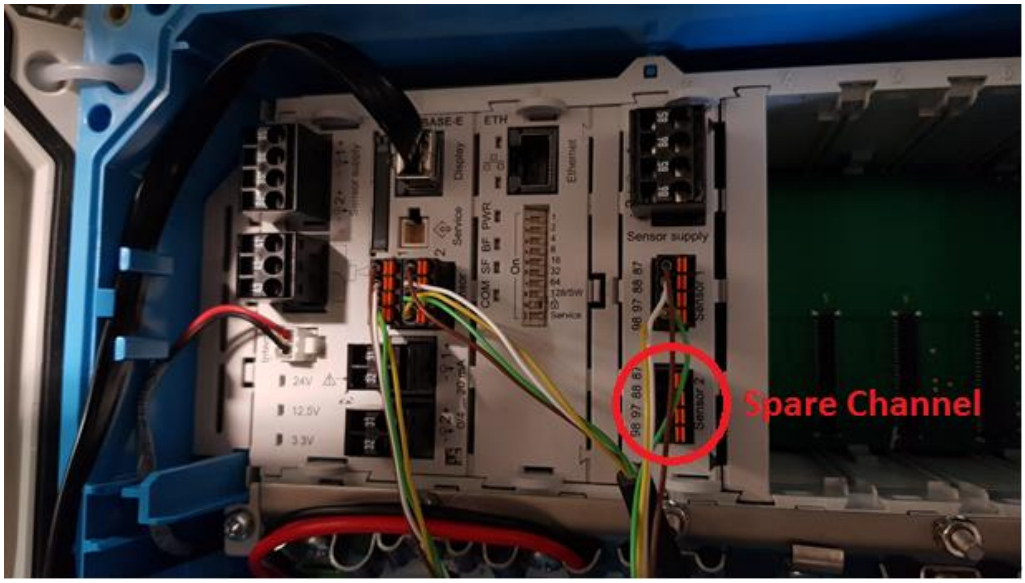

FIGURE 6 LIQUILINE CM44 TRANSMITTER SPARE CHANNEL

3.2.3 INDUMAX CLS50D

The Indumax CLS50D is a digital conductivity sensor. It possesses an inductive measurement principle. Features include high durability and resistance to chemicals. The design of the sensor ensures there is no direct contact with the process. This is due to the sensor coating comprising of highly resistant materials [24]. The Indumax CLS50D conductivity sensors are used to measure conductivity (μS/cm) and temperature (^{o}C) in each CSTR within the EPP. They can also measure concentration (% or mg/L) [25]. It is anticipated that one of these sensors will be installed in the holding tank arrangement once implemented.

3.2.3.1 MEASUREMENT PRINCIPLE

Figure 7 outlines the measurement principle for inductive conductivity. This involves an oscillator (1) generating within the primary coil (5), an alternating magnetic field that induces a current flow in the medium (4). The strength of this current is reliant on the conductivity in the process medium. The current flow generates a magnetic field in the secondary coil (3). The current induced in this coil is measured in the receiver (2) and determines the conductivity of the solution [25]. The sensor is factory calibrated.

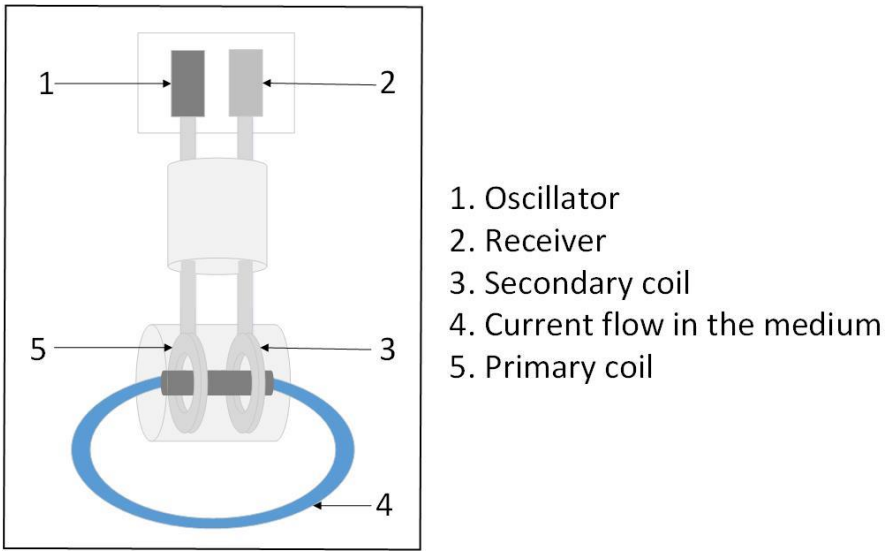

FIGURE 7 INDUCTIVE CONDUCTIVITY MEASUREMENT – ADAPTED FROM [25]

3.3 LEVEL MEASUREMENT

A Honeywell ST 3000 smart Differential Pressure (DP) type transmitter was selected for level measurement in the holding tank arrangement. It was chosen as it was already available and allows easy integration into the Honeywell Experion PKS DCS. It is accurate, reliable and stable. The ST 3000 transmitter also provides comprehensive diagnostics to assist with maintenance activities. The communication method employed by this transmitter is Foundation Fieldbus (FF) [26]. This presented a challenge as no prior Foundation Fieldbus had been implemented prior at Murdoch University.

3.3.1 MEASURING LEVEL WITH DIFFERENTIAL PRESSURE

There is a direct relationship between hydrostatic head pressure and liquid level in a vessel. As the hydrostatic pressure exerted by a column of liquid is directly related to its height and specific gravity in an open tank, this relationship can be utilised to infer a liquid height reading. As atmospheric pressure is exerted on the surface of the liquid in the vessel, the DP transmitter is referenced to the atmosphere as it measures gauge pressure. This way, any change in atmospheric conditions is accounted for by both sides of the instrument as shown in Figure 8 [27]. The same application will be used for the holding tank arrangement.

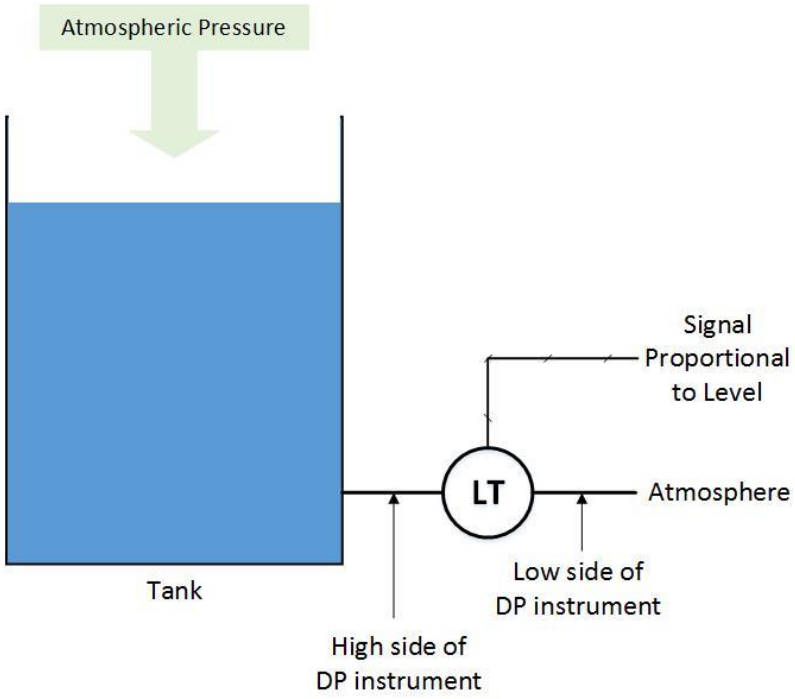

FIGURE 8 LEVEL MEASUREMENT WITH A DP TRANSMITTER – ADAPTED FROM [27]

3.4 CONTROL VALVE

A 0.5 inch Baumann 51000 series 4-20mA control valve was repurposed for this project. This valve is a V-ported plug type valve. It is optimally designed for low flow, high-pressure control applications in both laboratories and pilot plants [28]. The valve will provide control of raw water from the water supply into the holding tank arrangement. This provides control of the water stream providing dilution of the saline solution within the holding tank. The characteristics of this modified equal percent control valve were obtained via calibration curves obtained with EPP staff assistance. These can be found in Figure 11.

3.4.1 OPERATION PRINCIPLE

Plug valves provide quick closing or opening with leak-proof closures. They are ideal for high flows at low-pressure drops and low flow control applications. The valves usually cost less and are lighter in weight than comparable globe or gate valves. The V-ported plug valve, shown in Figure 9, is used for control of fluids containing fluids in suspension [17]. Flow is guided over a valve plug and directed through a single V-notch path as the plug moves above the Polytetrafluoroethylene (PTFE) ring providing precise flow control. In the instance that the V-notch is below the PTFE ring, flow is completely restricted [28] [29].

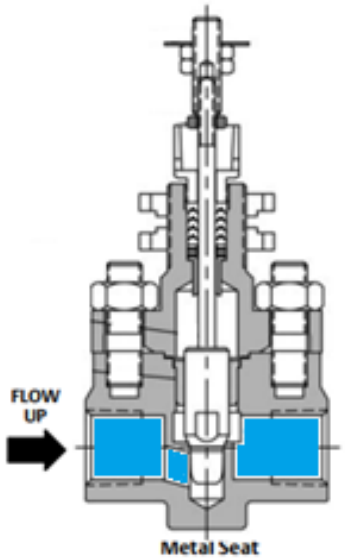

FIGURE 9 BAUMANN 51000 SERIES PLUG VALVE – ADAPTED FROM [28]

3.4.2 SELECTION OF APPROPRIATE VALVE TYPE

First, the question was asked – is a control valve even the best choice for this application? This led to consideration of two potential alternatives: regulators and variable speed pumps. Regulators were not considered further as these are designed to keep the process at a particular static state. Variable speeds pumps were also not a valid option due to associated expenses. Existing EPP stock included both a 0.25 inch and 0.5 inch Baumann 51000 series 4-20mA control valve. In order to choose the most suitable valve for this application several factors were considered [17]:

- Pressure drop across the valve;
- Control valve performance;
    - Characteristics and gain;
    - Valve rangeability.

3.4.2.1 PRESSURE DROP ACROSS THE VALVE

The pressure drop across the valve had to be considered. The higher the pressure drop across the valve, the more affect it will have on the process. It will also waste more pumping energy supplying process fluid in that line. Pressure drop across the valve is dynamic. Pressure drop available for the control valve decreases as the total flow through the system rises. This is because during high flow scenarios, the pump discharge pressure will be lower and pressure drop through the pipework will increase. Thus, control valves do not work with a fixed pressure drop or a fixed percentage of system pressure drop. Instead, the pressure drop across the control valve is the remaining pressure in the line after considering other pressure drops across the system [17].

3.4.2.2 CONTROL VALVE PERFORMANCE

Good control valve performance is determined by several factors. It must exhibit stability across the full operating range of the process. The valve must not operate near either of its fully open or closed positions to prevent unnecessary wear. Lastly, it must operate fast enough to compensate for disturbances in the process [17].

3.4.2.2.1 CHARACTERISTICS AND GAIN

By selecting the correct characteristics, the valve will exhibit stability across the full operating range of the process. This is only possible if all the process, sensor, controller and valve gains are constant. Gain is defined as the change in output divided by the change in input [30]. This will also enable the valve to operate in time when accounting for process disturbances. As the gain of the process decreases with flow through the control valve, an equal percentage valve is appropriate. This type of valve possesses a gain that increases with load. Figure 10 visually depicts this principle. As such, this combination serves to keep the loop gain relatively constant. The EPP is a predominantly friction type system. This means that an increase in flow will result in a drop in available pressure drop across the control valve. Again, an equal percentage valve is required in this scenario [17].

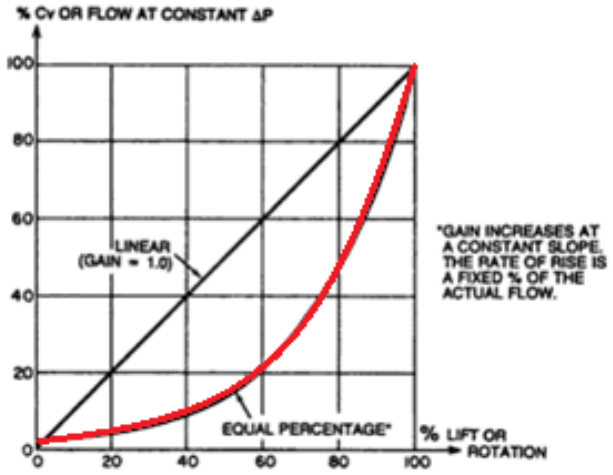

FIGURE 10 INHERENT CHARACTERISTICS OF CONTROL VALVES – ADAPTED FROM [17]

3.4.2.2.2 VALVE RANGEABILITY

The required rangeability for a control valve should be calculated as a ratio. This ratio is between the valve capacity coefficient, C_v required at maximum flow (and minimum pressure drop) and the C_v required during minimum flow (and maximum pressure drop) conditions. C_v is the flowrate in gallons per minute (GPM) of water that passes through a valve at a pressure drop of one pound per square inch (PSI). This decision on valve rangeability is usually made with the aid of a plot of valve gain versus C_v. If the valve exhibits 25% difference or less across the full C_v range between actual and theoretical valve gain, the rangeability of the valve is said to be acceptable [17].

3.4.3 FLOW REGIME CALCULATIONS

It was imperative to ascertain which type of flow regime would be present in the system the control valve was to be employed in. It was established experimentally by Osborn Reynolds in 1883, that two main flow regimes exist; laminar and turbulent [31]. During laminar flow situations present at low flow rates, the layers of fluid flow alongside each other. Fluid particles in a layer of fluid stay within the same layer. Turbulent flow, on the other hand, is present during high flow rates. This introduces eddies and vortices that mix the fluid by moving particles around the cross section of pipework they are within. Flow rates in between these two regimes are termed transitional [32].

To calculate which flow regime was present, first average velocity of the flow had to be obtained. In order to calculate average velocity, volumetric flow rate, Q (m^3/s) is divided by cross-sectional area A (m^2) as shown in (6) [32]. Area was calculated via (7) [32] Volumetric flow rates were obtained during valve calibration testing with the assistance of EPP technical staff. 0.5 inch tubing was used for the testing as this is the same size as that currently employed within the EPP.

$$V = \frac{Q}{A} \quad \text{where} \quad A = \frac{\pi D^2}{4} \qquad \textbf{(6), (7)}$$

Average velocity was calculated as being 0.921m/s based on a measured volumetric flowrate of $1.17*10^{-4}m^3/s$ within a pipe of 0.5 inch (12.7mm) diameter [33].

The method for distinguishing which flow regime is present in a pipe and when it changes is determined by the Reynolds number (dimensionless) shown in (8) [32],

$$Re = \frac{\rho VD}{\mu} = \frac{VD}{v}, \qquad \textbf{(8)}$$

where V is the average velocity of flow within the pipe (m/s), D is the inside diameter of the tube (m), ρ is the fluid density (kg/m^3), μ is the dynamic viscosity of the fluid and v is the kinematic viscosity of the fluid (m^2/s). The kinematic viscosity of water is $1.0034*10^{-6}$ m^2/s at 20°C and normal atmospheric pressure [33]. Flow with a Reynolds number equal to or less than 2100 is said to be laminar while flow with a Reynolds number equal to or above 4000 is turbulent. Reynolds numbers between these two figures are attributed to transitional flow [18]. Based on the figures above, the calculated Reynolds number was 116.3. This defines the flow regime in the fresh water input stream as laminar.

3.4.4 PRESSURE LOSS IN PIPEWORK, FITTINGS AND VALVE

It is important to account for the pressure loss attributed to the pipework, fittings and valves within the control system. First, the Fanning friction factor must be calculated via (9). This applies to laminar flow conditions only [18].

$$f = \frac{16}{N_{Re}} \tag{9}$$

Using the previously obtained Reynolds number of 116.3, the friction fanning factor (dimensionless) was calculated as $137.6*10^{-3}$.

The Darby or 3-K method is applicable across a wide range of applicable Reynolds numbers in determining the loss coefficient, K_f. This method employs the use of the three K's (K_1, K_i and K_d) along with pipe diameter, D_n (inches) and a Reynolds number to calculate the loss coefficient [31]. This was crucial in the later calculation of the pressure drop across fittings and valves when designing a system. For the fresh water feed system, a total of two threaded long radii 90^o elbows and one straight through plug valve were considered. The loss coefficient is calculated as shown via (10) [31].

$$K_f = \frac{K_1}{N_{Re}} + K_i\left(1 + \frac{K_d}{D_n^{0.3}}\right) \tag{10}$$

A total loss coefficient, Kf of 17.71Pa.m^3/kg was calculated for the two fittings and the plug valve. (11) [31], was used to calculate the energy dissipated per unit mass of fluid due to friction attributed to these elements within the fresh water feed stream.

$$e_{f,fittings} = \frac{\Delta P}{\rho} = \frac{K_f \times V^2}{2} \tag{11}$$

Multiplying through by the density of water at 20°C (998.2kg/m^3) allowed for derivation of the pressure drop across both the fittings and the plug valve. This was found to be 7.495kPa at a volumetric flowrate of 1.17*$10^{-4}$$m^3$/s. As 1PSI is equivalent to 6.895kPa, the pressure drop is equivalent to 1.087PSI [18].

Next the pressure drop attributed to friction through the piping itself required calculation. This began again with a calculation of the major energy losses. (12) [18], was used in this instance. Here the previously calculated fanning factor, f (137.6*10^{-3}) and average velocity, ū (9.21*10^{-1}m/s) along with a nominal pipework length of 3m was applied.

$$e_{f,major} = \frac{\Delta P}{\rho} = 2f\frac{\bar{u}^2 \times L}{2} \quad \textbf{(12)}$$

Major energy losses due to pipework in the fresh water stream were calculated. Again, as before, the density of water at 20°C (998.2kg/m^3) was multiplied through to obtain pressure drop across the pipework. This was found to be 55.044kPa at an average velocity of 9.21*10^{-1}m/s. Utilising the previous conversion, this was found to be equivalent to 7.983PSI. Adding this figure to the previously calculated 1.087PSI fittings losses resulted in a total pressure drop of 9.071PSI attributed to 3m of pipework, two 90^0 elbows and a plug valve.

3.4.5 VERIFICATION OF VALVE CALIBRATION RESULTS

It was essential that the calibration curve obtained was verified as being within tolerance to expected results. First, the friction coefficient, k_L (PSI/gpm^2) is calculated via (13) [34]. This accounts for the effect of the line, fittings and equipment on friction.

$$k_L = \frac{\Delta\overline{p_L}}{G_f \bar{f}^2} \tag{13}$$

Δp_L is the pressure drop across the line and fittings (8.8822PSI), G_f is the specific gravity of water at 20^{o}C (0.9982) and f^2 is the flow through the valve (1.85gpm) squared. It was found that the friction coefficient, k_L was 2.602PSI/gpm^2.

The valve capacity coefficient, C_v was calculated through a process of calculations. First the metric capacity coefficient, K_v was calculated using (14) [17].

$$K_v = q\sqrt{\frac{G_f}{\Delta p}} \tag{14}$$

Where q is volumetric flow rate (m^3/h), G_f is the specific gravity of the liquid relative to water at 60^{o}F (dimensionless) and Δp is pressure drop across the valve (bar). From measured values of 0.42m^3/h, 0.9982 and 0.612bar respectively, K_v was calculated to be 0.538 (m3/h)/(bar)$^{1/2}$. This was then converted to a value of 0.62 (gpm)/(PSI) $^{1/2}$ for the required value of C_v via (15) [17].

$$C_v = \frac{K_v}{0.865} \tag{15}$$

As the existing choice of valve C_v was either 0.45 or 1.5, it was clear that the larger valve with a C_v of 1.5 was more appropriate. This is because when sizing a valve for an application, the valve employed needs to exhibit a larger C_v than the theoretical requirement. In order to ensure the calibration curve obtained for this valve was correct, (16) [34], was utilised. Here, Δp_o is the total pressure drop across the line, fittings and valve in PSI.

$$F = \frac{C_v}{\sqrt{1 + k_L C_v^2}} \sqrt{\frac{\Delta p_o}{G_f}} \tag{16}$$

This equation was then applied to calculate expected flow at each relevant percentage valve opening. Figure 11 shows a plot of these theoretical flow results compared with field calibration test results for the modified equal percentage control valve.

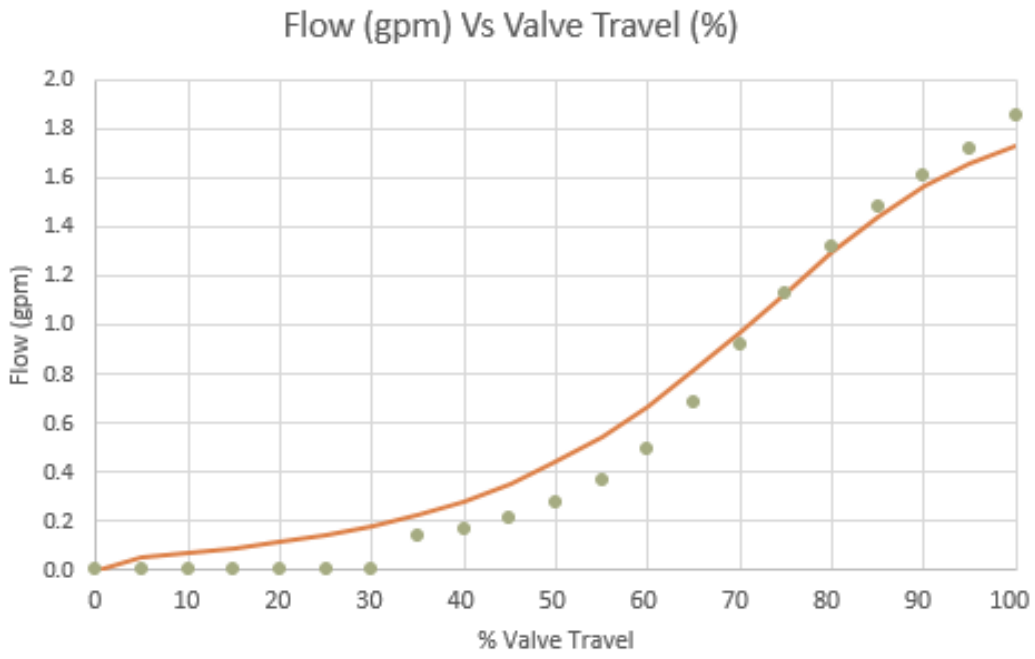

FIGURE 11 RAW WATER FLOW VALVE CALIBRATION VERIFICATION

3.5 FLOW TRANSMITTERS

The existing flow transmitter on the outlet of the product pump was retained to measure process flow from CSTR 3 to the holding tank arrangement. Two further transmitters were sourced to measure the flow from the holding tank arrangement and the flow of raw water entering it. Although magnetic flowmeters were almost exclusively used to measure flow throughout the EPP, differential pressure type flowmeters with an integral orifice have been sourced and installed as part of this scope. This is for two main reasons:

- Magnetic flowmeters (magflow meters) are more expensive than other alternatives [17];
- The flow meters previously implemented in the plant require a 240V supply.

Two Yokogawa EJX115A-FMS4G differential pressure transmitters were chosen for this application. This Yokogawa transmitter possesses an integral orifice. As this type of flow meter is commonly applied to pilot plants, it was considered appropriate for this application. The chosen model supports Foundation Fieldbus bi-directional digital communication. The digital signal output corresponds to the measured flow. The sensor features Fieldbus function blocks, alarm functions and self-diagnostic capabilities [35, 36].

3.5.1 MEASUREMENT PRINCIPLE

Differential pressure transmitters with an integral orifice are ideal for low flow measurement scenarios. By introducing a restriction of known size into the flow path of a tube, the cross-sectional area of the tube is reduced to a known dimension. The result is an increase in flow velocity and a corresponding decrease in pressure just after the orifice plate. This occurs in an area of the flow path denoted the vena contracta [37]. A visual depiction of this phenomenon is shown in Figure 12.

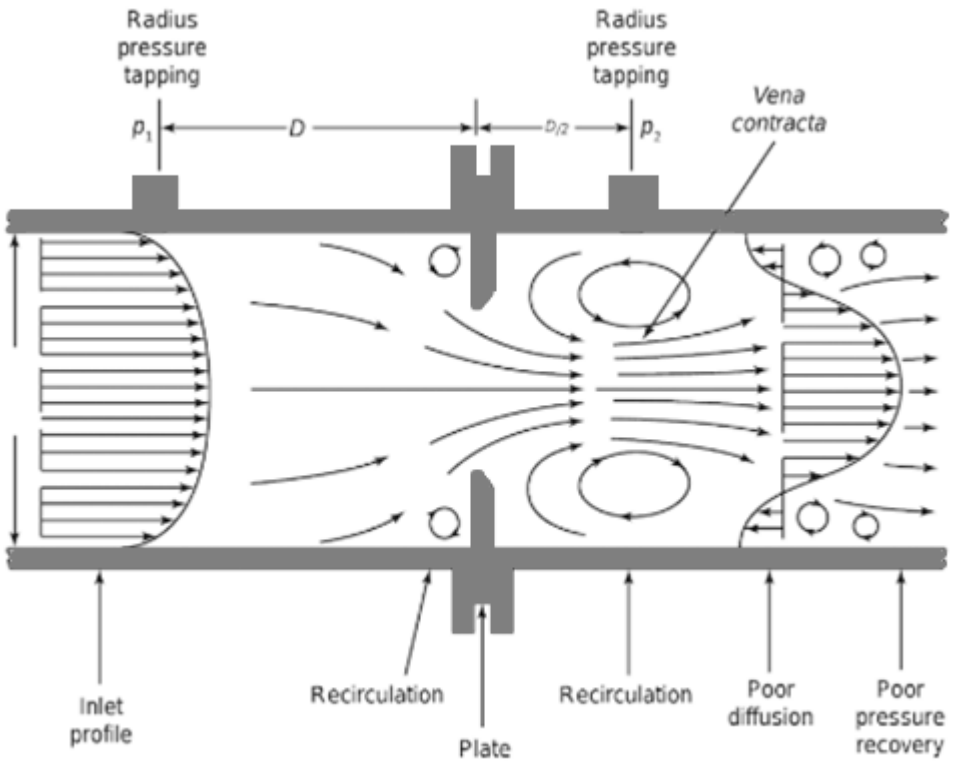

FIGURE 12 FLOW PATHS WITHIN AN ORIFICE PLATE FLOWMETER – ADAPTED FROM [38]

The proportional relationship between the square root of the pressure across the restriction and flow rate can then be used to calculate the mass flow rate of fluid passing through the restriction. (17) [37], derived from Bernoulli's Theorem displays this relationship.

$$W = kA\sqrt{h\rho} \quad \textbf{(17)}$$

Where W is mass flow rate, A is cross-sectional area of the pipe, h is differential pressure between points of measurement, ρ is the density of the flowing fluid and k is a proportionality constant.

3.6 24V SOLENOID VALVES

One flow transmitter will measure the flow rate of product from the holding tank arrangement. This will be directed to only one of three possible destinations. For this reason, only solenoid on/off type valves were required to direct flow to a choice of the storage tanks, CSTRs or drain. Honeywell SA Lucifer 24V AC 50Hz solenoids controlling 2 way ¼ inch valves are currently implemented in the EPP for on/off control of the process. For this reason, the same valves and solenoids were ordered for this application.

3.6.1 PRINCIPLE OF OPERATION

There are three major components that constitute a solenoid valve shown in Figure 13. The first is an electromagnet. This comprises of copper windings (solenoid) and a magnetic yoke. The yoke is a metallic case surrounding the coil. The second component is a moveable plunger or pilot. In some cases this is directly responsible for open and closing the valve. The third component is the valve body. This contains an orifice that is opened or closed by the plunger to enable or prevent process flow [39].

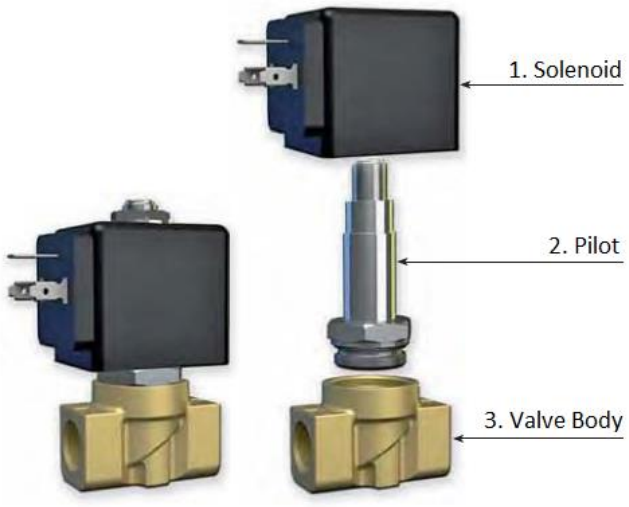

FIGURE 13 EXPLODED VIEW OF A SOLENOID - ADAPTED FROM [39]

The magnetic coil consists of copper wire wound on a reel as shown in Figure 14. When the coil has an electric current applied to it, a magnetic field is created. These are concentrated at the centre of the coil. The magnetic fields raise the movable plunger within the coil until the plunger makes contact with the pole piece. This creates an opening in the valve body orifice below. This enables process flow through the valve body. When the coil is de-energised, a return spring allows the plunger to move back to its original closed position within the valve body. This restricts any process flow through the valve [39].

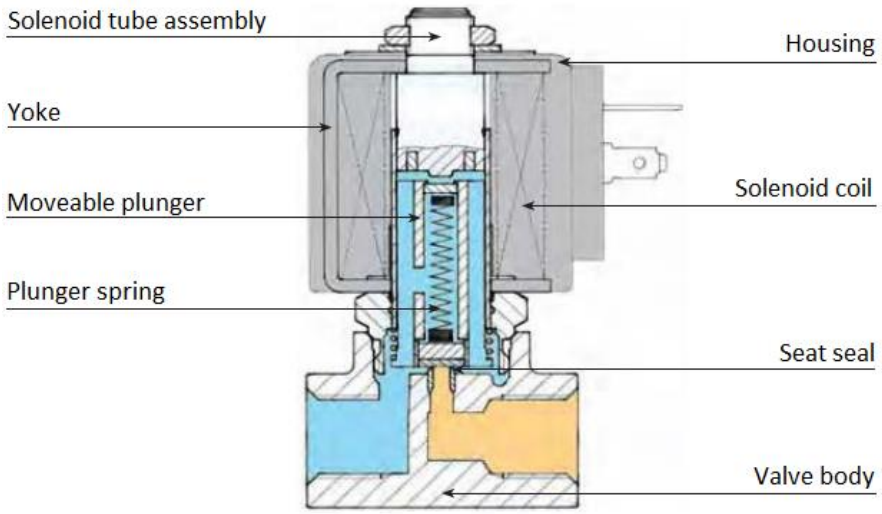

FIGURE 14 SOLENOID VALVE DIAGRAM – ADAPTED FROM [39]

3.7 POSITIVE DISPLACEMENT PUMP

After extensive consultation with project supervision and EPP technical staff, it was decided that the most suitable pump for this application was identical to the previously implemented product pump, PP-681. This positive displacement gear pump moves product from CSTR 3 to drain. Concerns about other types of pumps being able to process high-temperature water was the main reason for this decision. Pump capacity was also crucial to ensure the holding tank level could be adequately controlled. After an inventory of spare pilot plant parts was complete, it was found that an identical pump, shown in Figure 15, was available for application. Thus, the pump selected was a Liquiflo H7F heavy duty industrial sealed long-coupled external gear pump. This has a permissible operating temperature range between -40^{o}C and 260^{o}C. This pump possesses a maximum flow rate of 40.5L/min and a maximum speed of 1750RPM [40].

FIGURE 15 LIQUIFLO HF7 HEAVY DUTY EXTERNAL GEAR PUMP

3.7.1 HOW EXTERNAL GEAR PUMPS WORK

Gear pumps belong to the positive displacement rotary pump family. Figure 16 illustrates the principle of operation. Construction comprises two gears enclosed in a close-fitting housing. The gears are external to each other. This differentiates it from an internal gear pump which contains one gear positioned inside the other. A motor shaft is mechanically coupled to the pump drive shaft. This causes the drive gear to rotate. This, in turn, rotates the idler gear through the meshing of the teeth between the two gears. A vacuum is caused when a tooth is pulled from the space between two teeth from the other gear. As the housing forms a seal around the gears, liquid from the pumps suction port enters this area. It is then trapped in place by the housing until it exits via the discharge side of the pump as the gears rotate [41] [42].

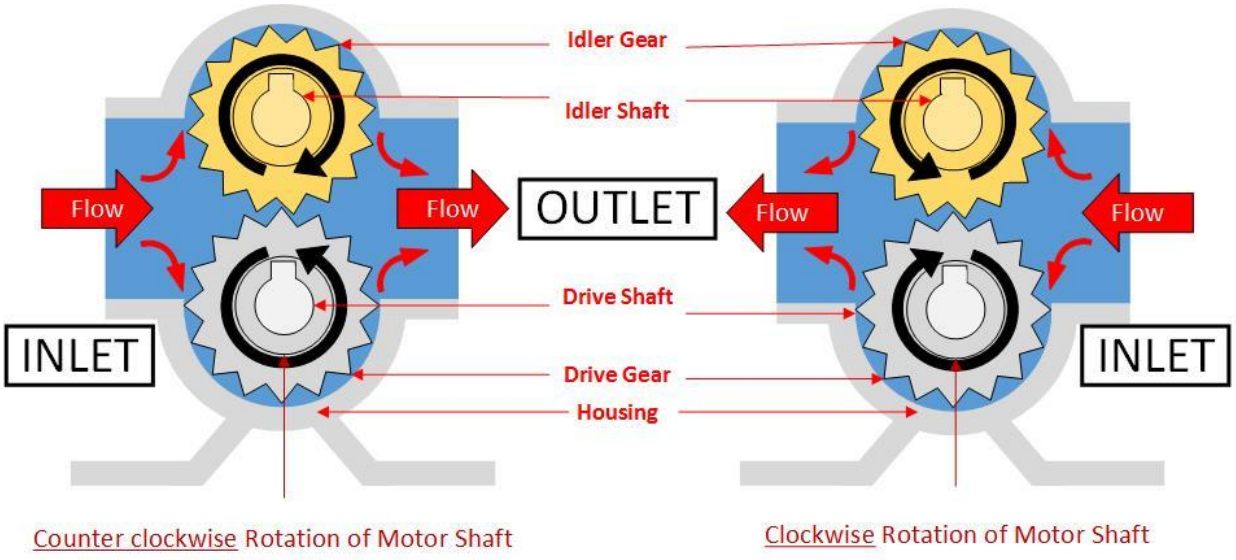

FIGURE 16 GEAR PUMP OPERATION – ADAPTED FROM [43]

3.7.2 VARIABLE SPEED DRIVE CONTROL

A Danfoss VLT HVAC Drive FC 102 Variable Speed Drive (VSD) was selected to control the speed of the pump coupled to the new holding tank outflow pump. This is designed for control of Heating, Ventilation and Air Conditioning (HVAC) applications. It is also useful in applications with pumps. The VLT HVAC drive comprises of a compact design and a heat management system to manage waste heat. This made it the ideal choice for applications where drive space is restricted [44]. This was the case in the existing EPP electrical control cabinet where the other VSDs were situated. Identical model VSDs control the speed of the other pumps across the EPP. For this reason, the same model was deemed appropriate.

3.7.2.1 OPERATION PRINCIPLE OF A VARIABLE SPEED DRIVE

Variable speed drives allow the user to change the speed of a motor by varying the frequency of the supply to it [45]. Figure 17 shows a block diagram of the components found within a VSD.

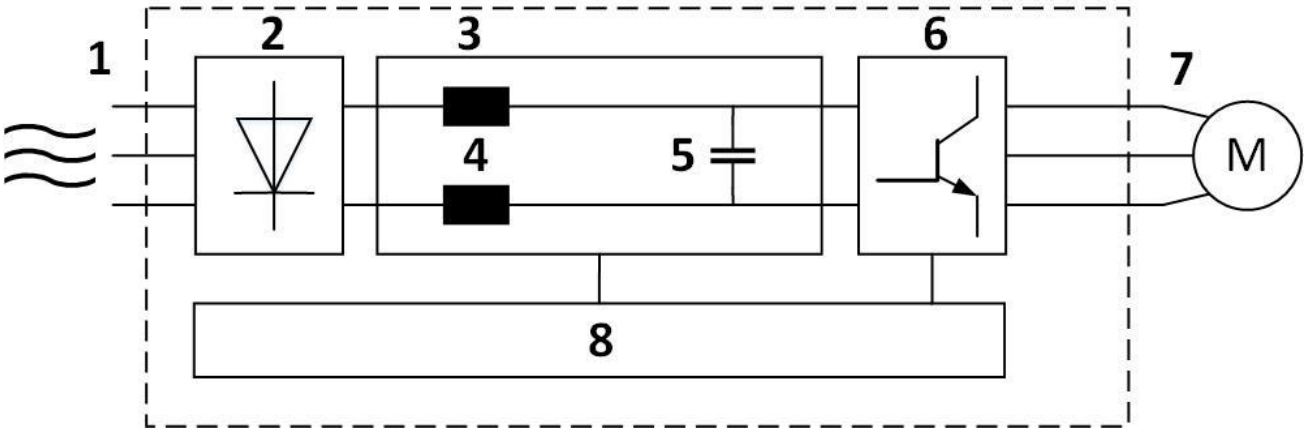

FIGURE 17 FREQUENCY CONVERTER BLOCK DIAGRAM – ADAPTED FROM [45]

First, the three-phase AC mains power supply is fed to the frequency converter (1). Next, the rectifier bridge (2) converts the AC waveform to DC supplying the inverter. The intermediate DC-bus circuit (3) handles the direct current. Within this circuit, inductors (4) filter the DC circuit voltage, provide line transient protection and reduce harmonics from the AC input. The capacitor bank (5) then stores the DC charge. The inverter (6) converts the DC signal into a controlled pulse width modulated (PWM) three phase AC waveform as a controlled variable output to the motor (7). Internal control circuitry (8) provides user interface and monitoring capabilities [45].

3.8 FOUNDATION FIELDBUS COMMUNICATIONS

Foundation Fieldbus (FF) is a bi-directional, digital, multi-drop communication protocol. It is a Local Area Network (LAN) for compatible field devices over a digital bus network. FF was developed for process control and automation. It consists of two distinct communication protocols: H1 and High Speed Ethernet (HSE). H1 transmits data at 31.25 Kb/s and is utilised in the interconnection of field devices. HSE makes use of 10/100 Mbps Ethernet to provide high-speed support for the network [46].

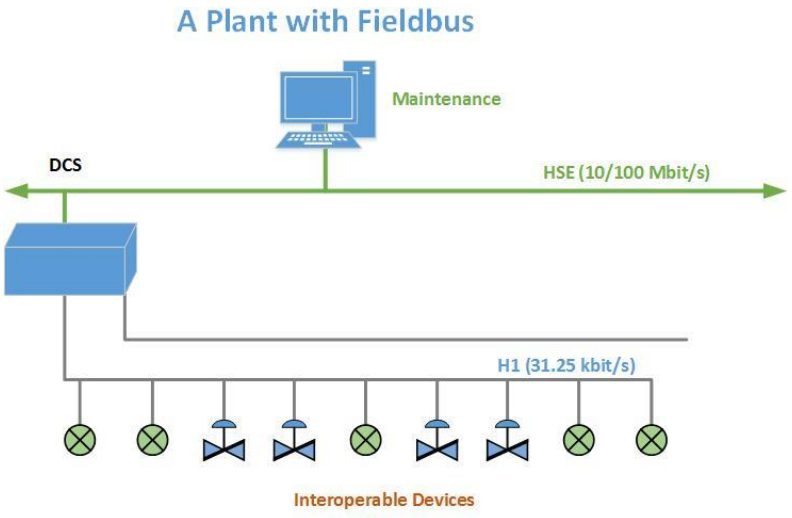

FIGURE 18 TYPICAL FIELDBUS NETWORK – ADAPTED FROM [47]

FF operates as a peer to peer protocol. Field device instruments and Human Machine Interfaces (HMIs) on the bus have the capability to communicate with each other in the absence of a host. Communication can occur between field devices without any centralised command present. An example of this is the transmission of an alarm when a field device experiences a problem [48] [49]. In the current iteration of the EPP, Honeywell's Experion PKS C300 controller allows Fieldbus integration via a Fieldbus Interface Module (FIM 4 or 8). This was not implemented prior to this project, but would allow for system-wide integration of data access and control, diagnostics and alarms within the C300 controller. This is achieved by integration into a database using Control Builder (CB) [50].

3.8.1 SYSTEM ARCHITECTURE

FF is based on the International Standards Organisation (ISO) Open Systems Interconnect (OSI) seven layer communications model. It comprises of a physical layer, the communication stack and a user layer. The OSI model does not define the user layer as shown below in Figure 19. FF does not implement layers three through six. This is because they are not required in process control applications [46].

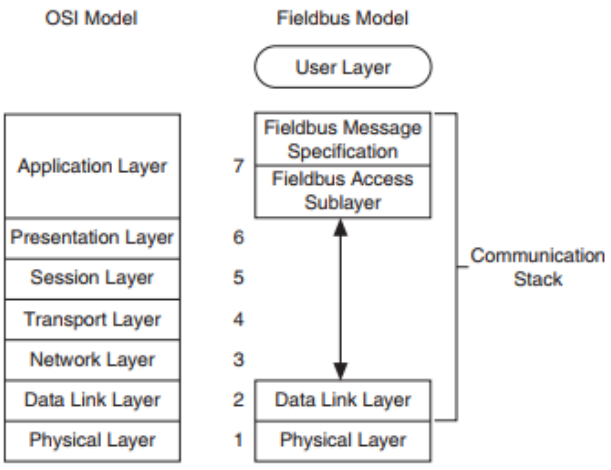

FIGURE 19 FIELDBUS MODEL AND OSI 7 LAYER COMMUNICATIONS MODEL – ADAPTED FROM [46]

The physical layer converts digital Fieldbus messages from the communication stack into physical signals on the bus and vice versa. The communication stack performs the tasks required to interface between the user and physical layers. This is achieved by encoding and decoding user layer messages and ensuring message transfer efficiency and accuracy. The communication stack consists of [46]:

- Fieldbus Message Specification (FMS);
- Fieldbus Access Sublayer (FAS);
- Data Link Layer (DLL).

3.8.1.1 FIELDBUS MESSAGE SPECIFICATION

The Fieldbus Message Specification (FMS) defines the model for applications to interact with each other over the bus. This model comprises of an object dictionary and virtual field device. This dictionary is a structure within a FF device that describes data that can be communicated over the bus. It provides information about a value, e.g. its data type that can then be written to or read from a field device. The virtual field device is a model that allows for remote viewing of data described within the object dictionary [46].

3.8.1.2 FIELDBUS ACCESS SUBLAYER

The Fieldbus Access Sublayer (FAS) is responsible for providing an essential interface between the Data Link and FMS layers. The FAS enables communication services such as event distribution, publisher/subscriber and client/server [46].

3.8.1.3 DATA LINK LAYER

The Data Link Layer (DLL) controls access to the bus through the Link Active Scheduler. This is achieved by splitting data into frames to send over the physical layer. The scheduler also receives acknowledgement frames and retransmits them if there are any errors in transmission. An important additional feature of this layer is error checking [46].

3.8.1.4 USER APPLICATION LAYER

The User Application Layer is based on blocks. Each block represents a different type of application function. Figure 20 displays each variant of block used within this layer [51].

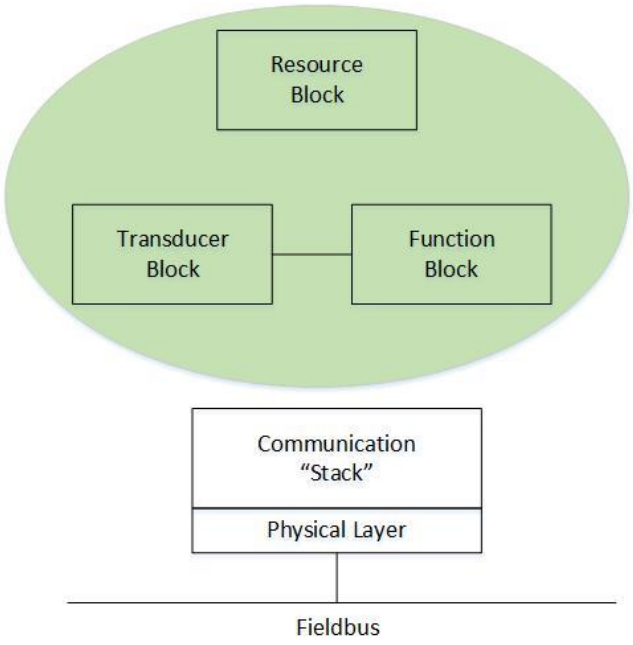

FIGURE 20 USER APPLICATION BLOCKS – ADAPTED FROM [51]

The Resource Block describes the Fieldbus device characteristics. These include its device name, serial number and manufacturer. There is one Resource Block per device. Function Blocks provide the behaviour of the control system. The execution of each of these blocks is accurately scheduled. There can be multiple Function Blocks within a single User Application. There are several standard Function Blocks for basic control. Ten of these are listed below in Table 1 [51].

TABLE 1 FOUNDATION FIELDBUS FUNCTION BLOCKS [51]

Function Block Name	Symbol
Analogue Input	**AI**
Analogue Output	**AO**
Bias/Gain	**BG**
Control Selector	**CS**
Discrete Input	**DI**
Discrete Output	**DO**
Manual Loader	**ML**
Proportional/Derivative	**PD**
Proportional/Integral/Derivative	**PID**
Ratio	**RA**

Transducer Blocks contain crucial information such as sensor type and associated calibration date. They decouple Function Blocks from the local I/O functions required to read these sensors and provide commands to output hardware [51].

3.8.2 PHYSICAL LAYER - SIGNALS

Devices on a Fieldbus network transmit signals digitally over the same twisted pair cables that power the devices. All devices on a segment within the network receive each transmission. The Link Active Scheduler selects which single device can transmit at a time. This is done by sending a special frame to each device in turn. This frame could be a request for the device to transmit data, data broadcasted by another device or an error condition being reported by a device on the network. When a device is not transmitting, it draws device power from the bus for operation. When transmitting a high signal, the device draws 10mA less current than normal. This results in a voltage increase between the wires. When a device transmits a low signal, it draws 10mA extra current. This results in a voltage decrease [51].

The resulting digital data (ones and zeroes) is represented as Manchester code. A positive signal transition is represented by a zero while a negative transition is represented by a one in the middle of a bit cell. Each bit cell is 32 microseconds long. This is because data is transmitted at 31.25kbits/second on an H1 network. The voltage change across the signal is generally 750mV peak to peak. The transition, rather than the size of the signal is used for communication. An example sequence of Manchester-encoded ones and zeroes is shown in Figure 21 [51].

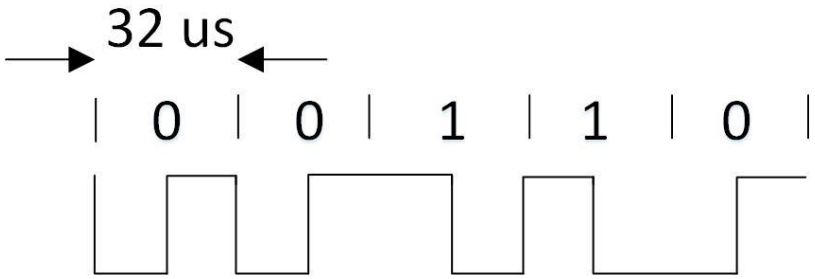

FIGURE 21 MANCHESTER CODE EXAMPLE – ADAPTED FROM [51]

When a device transmits, the data frame shown in Figure 22 consists of several different components. The first component is called the preamble. This allows receiving devices to synchronize their internal clock with the incoming Fieldbus signal. Next, a start delimiter denotes the start of the Fieldbus message [51]. The data portion of the frame (Data Link Layer Protocol Data Unit) contains the intended device address, frame type identification and measures values amongst other information. This frame can be up to 266 bytes long. The Frame Check Sequence is the last portion of the data section of the data frame. This allows for the detection of data corruption by noise. This feature makes Fieldbus more robust than other types of control networks. The last component of the frame is an end delimiter containing N+ and N- signals denoting the end of the Fieldbus message [52].

FIGURE 22 FIELDBUS DATA PACKET STRUCTURE – ADAPTED FROM [51]

3.8.3 FIELDBUS INTERFACE MODULE

The Series C Fieldbus Interface Module (FIM4/8) acts as an interface between the Experion Control Execution Environment (CEE) and the Fieldbus control functions. It complements both the C300 controller and supports Fault Tolerant Ethernet (FTE) communications. The module provides support for both publish/subscribe and client/server communication methods employed when communicating with FF function blocks. The module supports up to four or eight H1 links respectively. A spare CC-PFB401 FIM4 device was located in pilot plant storage and utilised. This was mounted directly onto a non-redundant Input/Output Termination Assembly (IOTA) [53]. Several implementation challenges were overcome by updating the firmware associated with the device. Detailed procedures for how to implement a FIM4 module into Experion and how to upgrade FIM4 firmware can be found in Appendix B FIM4 Experion Guides.

3.8.4 FIELDBUS POWER SUPPLY

Standard DC power supplies are an insufficient means of providing the necessary field power to the bus-powered devices on each of the four H1 links on the FIM4 device. This is because they do not possess the required isolation, current limiting and power conditioning qualities required for this application. A block diagram of a standard Fieldbus supply is depicted in Figure 23. Common DC power supplies are grounded in industrial applications. By contrast, Fieldbus supplies isolate the Fieldbus signal from the ground. This reduces possible interference from noise [52].

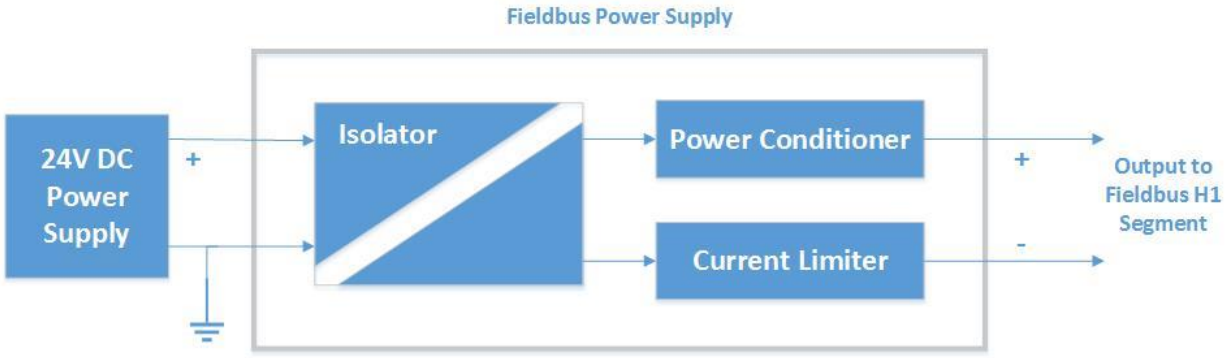

FIGURE 23 FIELDBUS POWER SUPPLY BLOCK DIAGRAM – ADAPTED FROM [52]

Regular DC power supplies will absorb any digital signals that a FF device would attempt to transmit across the network. Power conditioning capabilities inherent in a Fieldbus supply act like a one-way valve. Power is supplied to the Fieldbus, while blocking digital communication signals from the Fieldbus from flowing to the isolator or power supply. Fieldbus supplies also offer current limiting characteristics to prevent damage from a short-circuit or over-load condition [52].

An additional power conditioner was required to implement a functional H1 segment. For this application, a KLD2-FBPS-1.25.360 Fieldbus power supply available from vendor Pepperl+Fuchs was installed. This unit is designed to provide power for a single Foundation Fieldbus H1 segment. It incorporates galvanic isolation capabilities, power conditioning and segment termination within a compact design. Power output is suited explicately to long cable lengths and high device counts. LED indicators display the current component status to the user. A mobile Advanced Diagnostic Module connects directly to tests sockets on plug-in terminals for additional diagnostic capability. When paired with a segment protector, this power conditioner provides a H1 network with all necessary components [54].

3.8.5 4-20MA TO FOUNDATION FIELDBUS CONVERSION

Most of the instrumentation sourced or repurposed for this scope provides a 4-20mA output. A solution was required that would act as an interfacing device between the 4-20mA signal from the devices to the FF network. Two Smar IF302 4-20mA to FB converter devices were found in storage and set aside for this project. The digital technology embedded within this device enables a single unit to process three separate 4-20mA signal inputs. Each input has a common ground and is protected from reverse polarity signals. In order to enable correct operation, all inputs should be connected as shown in Figure 24 [55].

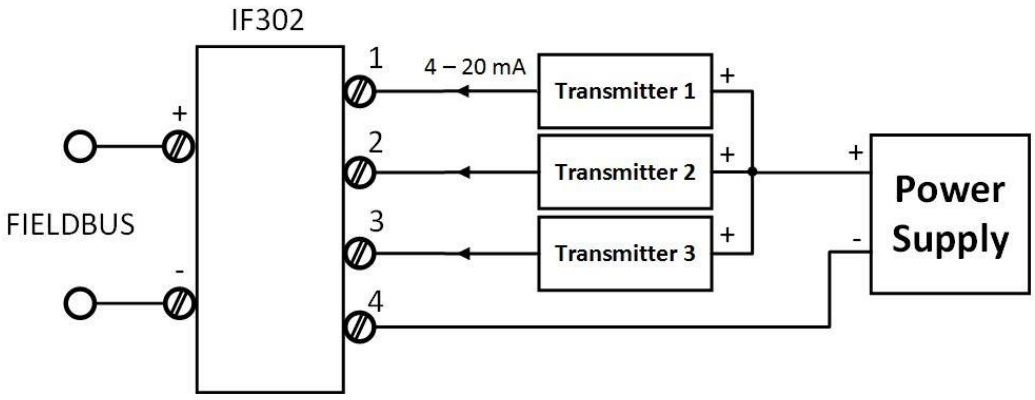

FIGURE 24 SMAR IF302 INPUT WIRING – ADAPTED FROM [55]

3.8.5.1 PRINCIPLE OF OPERATION

Figure 25 depicts a block diagram of the Smar IF302 4-20mA to FF converter. Starting from the right, the MUX multiplexes the input terminals. This means that multiple input signals are combined into one output signal [56]. This ensures that all of the input channels reach the analogue/digital (A/D) converter. This then converts the analogue signal to digital for processing by the central processing unit (CPU). This data signal is electrically isolated from the CPU for protective purposes. This means there is no direct electrical connection present [57]. The CPU is the brains of the Smar converter. It is responsible for the operation and management of block execution, communications and self-diagnosis. Flash memory stores the program while Random Access Memory (RAM) temporarily stores non-critical data. Electrically Erasable Programmable Read-Only Memory (EEPROM) is used for storage of critical data. Examples of this include calibration and configuration data [55].

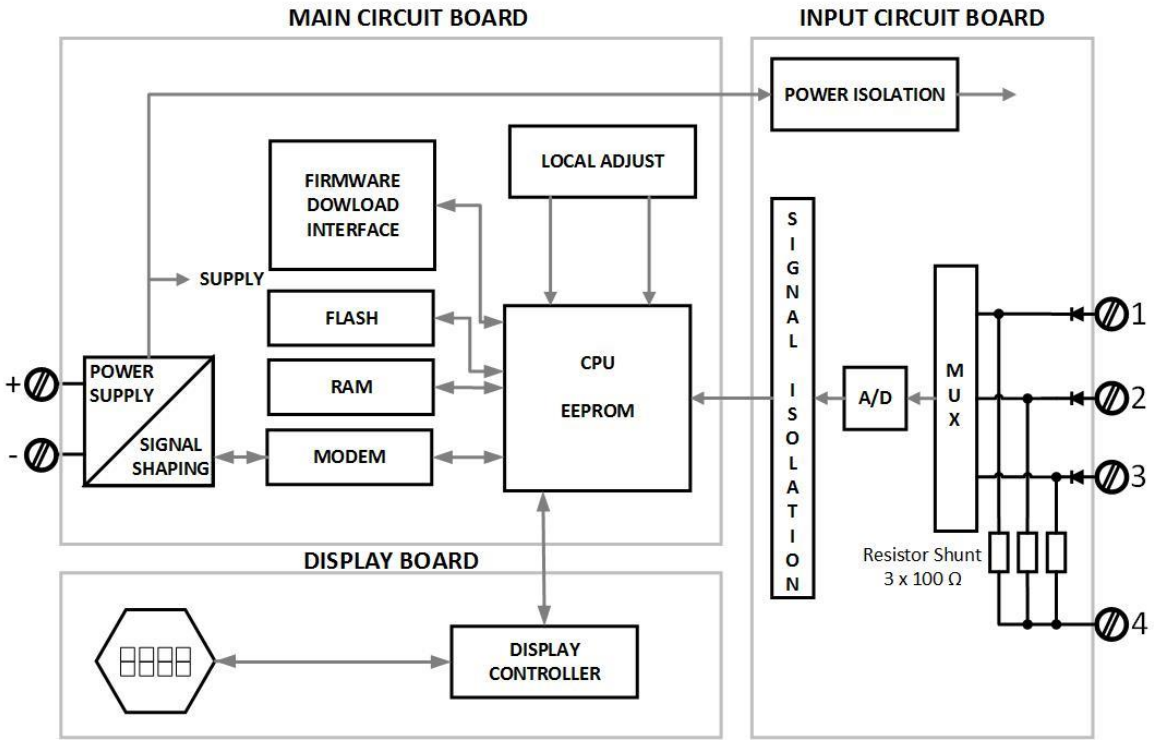

FIGURE 25 SMAR IF302 BLOCK DIAGRAM – ADAPTED FROM [55]

The communication controller performs signal shaping duties for the device. This includes the monitoring of line activity, modulation and demodulation of the signal for the network. The power supply uses loop power from the incoming supply to power the internal circuitry. Similar to what occurs on incoming signals at the inputs, the power to the inputs must also have electrical isolation. This is provided by the power isolation module. The display controller manages the Liquid Crystal Display (LCD) screen and displays relevant data from the CPU. Local adjustment is also possible via two magnetically activated switches. This negates the need for mechanical or electrical contact [55].

3.9 HONEYWELL EXPERION PKS

The Honeywell Experion PKS DCS is currently implemented for plant control purposes within the Murdoch University South Street Campus EPP. A DCS is an automated control system comprising of distributed control elements across a plant or control area. An example DCS network is shown in Figure 26. Each process element, machine or group of machines is controlled by a dedicated controller. These controllers are all interconnected by a high-speed digital communication network. A range of different communication protocols can be employed for this task. Distributed Control Systems are capable of handling a large number of control loops within a process [58]. Experion PKS provides a unified architecture. This allows for total integration of all process control, application software and safety systems. The platform is capable of continuous, sequence and batch control. It is also capable of safety, security, electrical, SCADA and asset management [59].

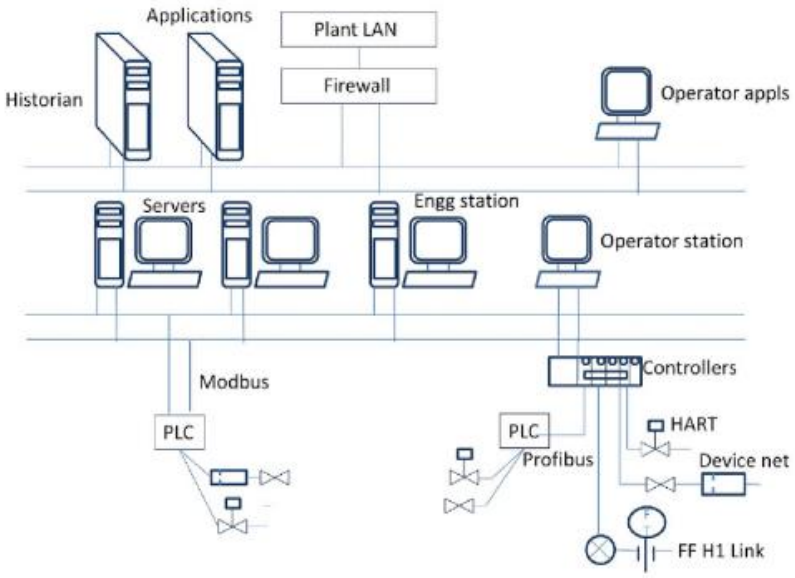

FIGURE 26 ARCHITECTURE OF A BASIC DISTRIBUTED CONTROL SYSTEM – ADAPTED FROM [58]

3.9.1 CONTROL EXECUTION ENVIRONMENT, C300 CONTROLLER AND I/O MODULES

The Honeywell Control Execution Environment (CEE) provides the platform for Experion CEE-based control processors. The CEE is configured using the Honeywell Control Builder Environment. In the EPP, the CEE is hosted on the C300 controller. The C300 controller provides an interface from the I/O modules to the EPP instrumentation within the pilot plant. These I/O modules acquire plant data from instrumentation as either a digital 0-24V signal or an analogue 4-20mA signal. This is then communicated to the C300 controller. A FIM was utilised to enable Foundation Fieldbus integration [60]. The current I/O includes:

- 2x Digital Input 24V;
- 2x Digital Output 24V;
- 2x HART Analogue Input;
- 1x Hart Analogue Output.

3.9.2 CONFIGURATION STUDIO

Configuration Studio (CS), shown in Figure 27, is a software application from Honeywell. It provides all of the required tools to configure, check status and access information within an Experion system. CS enables the management of all aspects of the system configuration. This includes hardware configuration, history, controllers and field devices amongst other features. Other useful programs in the Experion environment including Control Builder and HMIWeb Display Builder are accessible from this program [61].

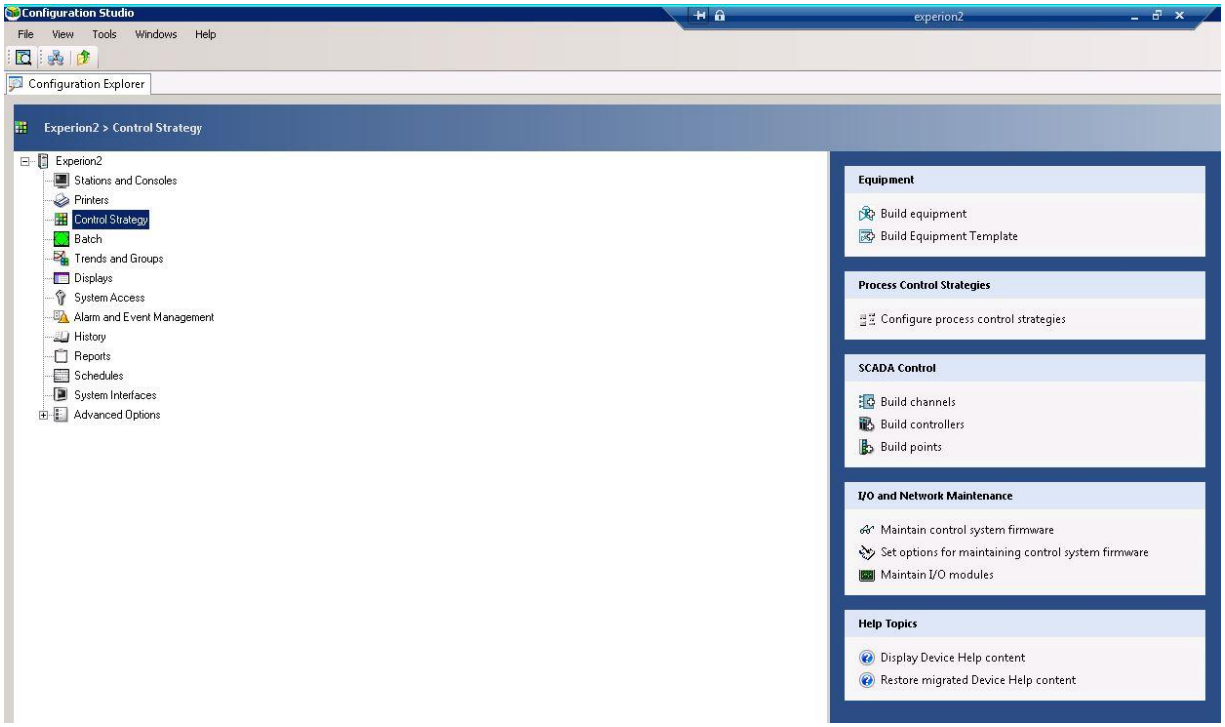

FIGURE 27 EXAMPLE CONFIGURATION STUDIO SCREEN

3.9.3 CONTROL BUILDER

Control Builder (CB), shown in Figure 28, is a graphical configuration tool utilised in configuration of Experion system components and control strategies for the C300 controller. This particular example shows some function block style code for a component within the EPP. CB provides two different working environments. Project is for use offline. This environment allows the user to create and modify all system configuration without disturbing the current (on-line) configuration. Monitor mode is for use on-line. This allows the user to observe the entire control scheme as a live environment. Only minor changes (limits, constraints etc) are allowed in this mode. This allows for an effective software environment enabling the user to create or modify the configuration in the background while monitoring the actual configuration in the foreground [60].

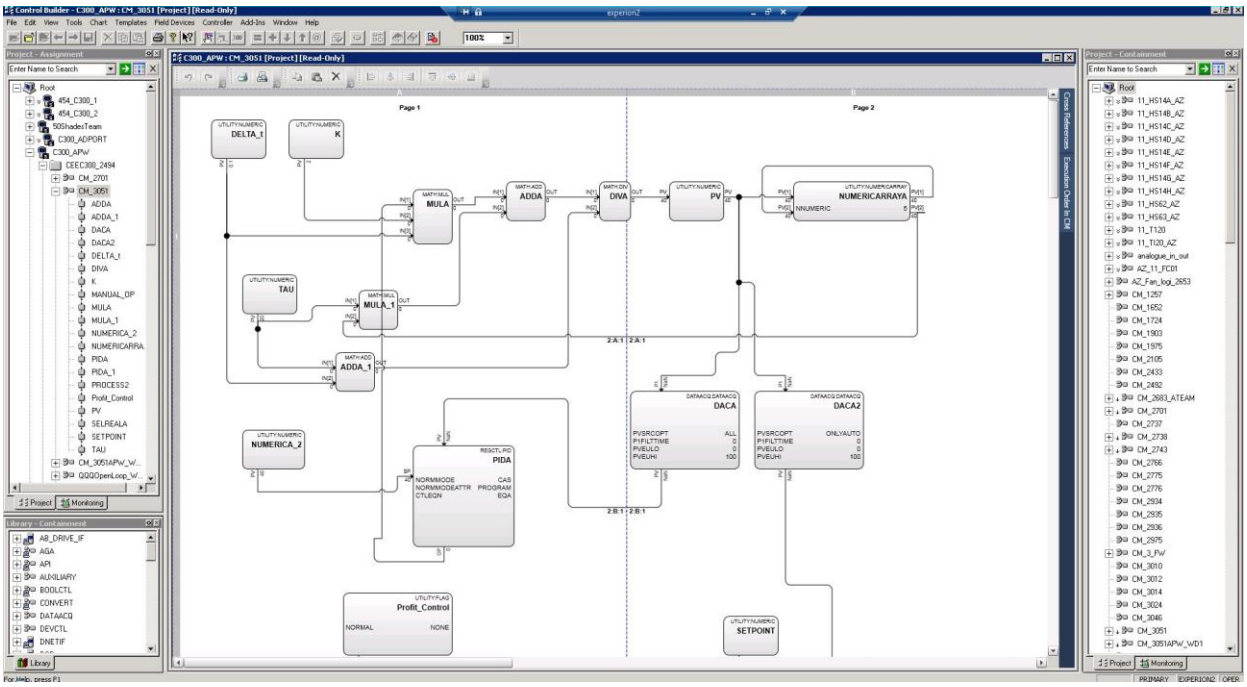

FIGURE 28 EXAMPLE CONTROL BUILDER SCREEN

3.9.4 HMIWEB DISPLAY BUILDER

HMIWeb Display Builder, shown in Figure 29, is a drawing application. This particular example shows a feature that allows the programmer to create custom animations through the use of several different static images. HMIWeb Display Builder enables the user to create their own displays. These displays allow the user to present information in an appropriate layout that is both user-friendly and intuitive. Well-designed displays allow plant operators (students at Murdoch University) to visualise the process they are attempting to control. This also aids greatly in reducing the probability of operator error [62].

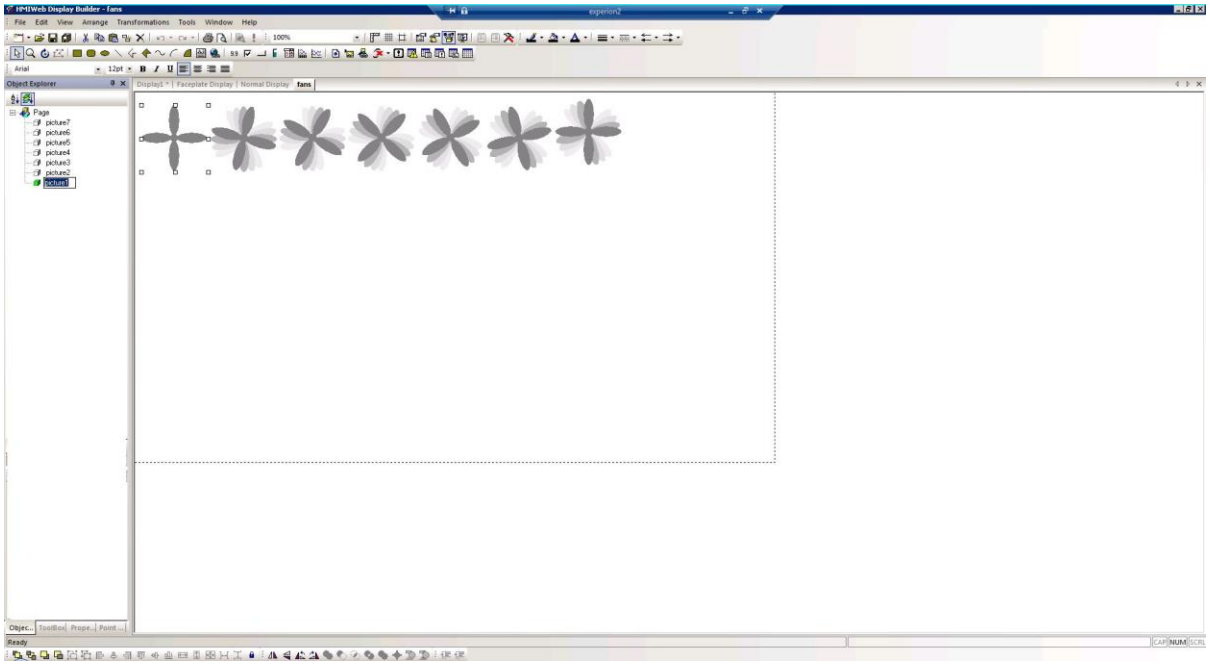

FIGURE 29 EXAMPLE HMIWEB DISPLAY BUILDER SCREEN

3.9.5 STATION

Station is the software necessary to view HMI pages created within HMIWeb Display Builder. It can be utilised for various functions. These include operation, monitoring, maintenance and engineering. Two variants of station are supported by Experion; Direct Station and Flex Station. In this instance, Flex Station is being utilised. A client-server relationship is used to present process data to the user [63]. Figure 30 shows a HMI screen displaying reat time status information about the process in the EPP. This HMI screen allows the user to interact with the pilot plant by changing pre-determined input variables.

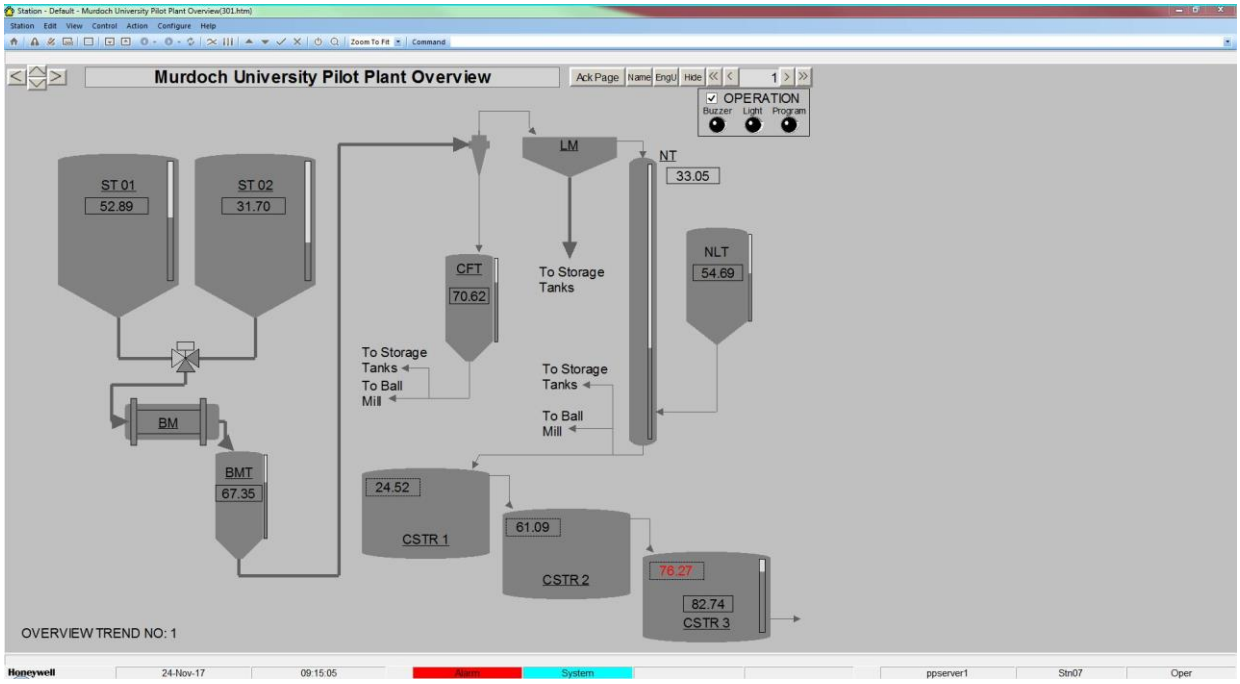

FIGURE 30 EPP STATION HMI SCREEN

4 IMPLEMENTATION

A solid understanding of the fundamentals of Foundation Fieldbus communication and networks, instrumentation and desired control methods had been established at this point. Due to budgeting and time constraints along with limited EPP technical staff availability, it was decided that a sample FF network would be established. This would ensure working communications from FF and 4-20mA field instruments back to the Honeywell Experion PKS DCS. A model of the desired recycle and dilution section of the pilot plant was also derived. From this model, data was obtained and analysed allowing the development of appropriate simulations and control strategies. This would allow for easy implementation at a later stage when the overall design is implemented.

4.1 SYSTEM ANALYSIS AND MODELLING

In order to understand the type of system that required process control in this scenario, system analysis was required. First, a diagram was constructed to reflect the proposed tank arrangement with all relevant system variables. Variables used in this model (shown in red) reflect those used within the balances performed once calibration curves were obtained for all relevant control elements. This is displayed in Figure 31.

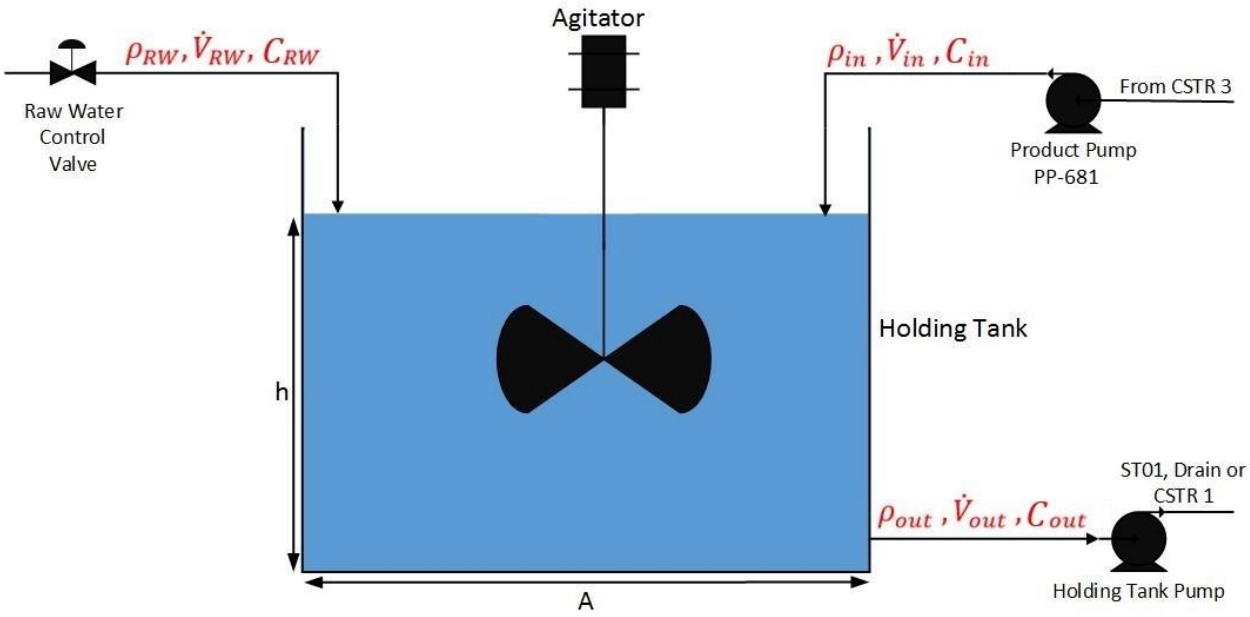

FIGURE 31 SYSTEM DIAGRAM

The input stream on the left side of the holding tank in is representative of the raw water supply input into the holding tank. This will be controlled by the raw water control valve. The input stream on the right side of the holding tank shows the product being supplied to the holding tank via the product pump, PP-681. This pump is typically utilised to control the product level within CSTR 3. The output stream on the bottom right of the holding tank indicates the output stream. This is controlled via the holding tank pump.

Next, appropriate loop pairings were chosen. The intention of the fresh water stream is to dilute the saline solution being supplied to the holding tank arrangement. For this reason, the fresh water control valve was chosen as manipulated variable (MV) 1 to control process variable (PV) 1 being the holding tank solution conductivity. As the product pump, PP-681 is always chosen as the manipulated variable to control the level in CSTR 3, the holding tank pump is the only remaining MV. This makes the product pump a disturbance in this scenario. For this reason, the holding tank pump (MV) is used to control the holding tank height (PV 2). Loop pairings are shown in Table 2.

TABLE 2 CONTROL LOOP PAIRINGS

Manipulated Variable	Process Variable
Fresh Water Control Valve	Holding Tank Conductivity
Holding Tank Pump	Holding Tank Level

4.1.1 CALIBRATION CURVES

To obtain an accurate model of the process, flow calibration curves were obtained for the pumps and control valves requiring future implementation. Temporary tubing and wiring installed by pilot plant technical staff allowed for this testing to take place. For consistency, it was assumed the fresh water stream and product pump would have to overcome one metre of head pressure to enter the top of the holding tank arrangement. As an identical pump will be used to pump product from the holding tank arrangement up to the same head height, this curve was used for both pumps to be modelled. The temporary testing arrangement for valve calibration is shown in Figure 32. This involved the use of a Fluke 744 Documenting Process Calibrator to read values output from the control valve during testing and provide 24 VDC loop power to the control loop.

FIGURE 32 CALIBRATION TESTING APPARATUS

Calibrations curves were obtained from readings taken at 5% increment increases in either valve % opening or pump % operation across the entire operational range (0 – 100% and 0 - 40%). These results were then plotted using Microsoft Excel. From here, trend lines of polynomial of varying order equations were applied to obtain characteristic equations. These equations provide a model of the static behaviour of the pumps and control valve. The derived equations are shown in Table 3. Microsoft Excel has built-in linear regression capabilities for data analysis. The goal of this analysis is to calculate coefficient values for the best fit characteristic equations that minimise the sum of error (vertical) between the line of fit and the observed data points [64]. The associated R^2 value for each fit (coefficient of determination) is a measure of the proportion of variance between the line of fit and the observed data points. This is a value between zero and one. The closer the R^2 value is to one, the better the fit [65] [66].

TABLE 3 CALIBRATION CURVES

MV	Characteristic Equation	Coefficient of Determination
Product pump	$-3.92*10^{-8}x^2 + 5.07*10^{-6}x$	0.9948
Holding tank pump	$-3.92*10^{-8}x^2 + 5.07*10^{-6}x$	0.9948
Fresh water control valve	$-5.72*10^{-12}x^4 + 1.04*10^{-9}x^3$ $-3.98*10^{-8}x^2 + 4.71*10^{-7}x$	0.9971

Figure 33 represents results obtained during flow calibration testing of the raw water valve flow characteristics. This is indicative of its modified equal percentage type operation. It was found that for this valve a sigmoidal type curve was most appropriate. As the trend line function within Microsoft Excel does not offer this type of fit, a fourth order polynomial with accuracy 99.71% was utilised instead.

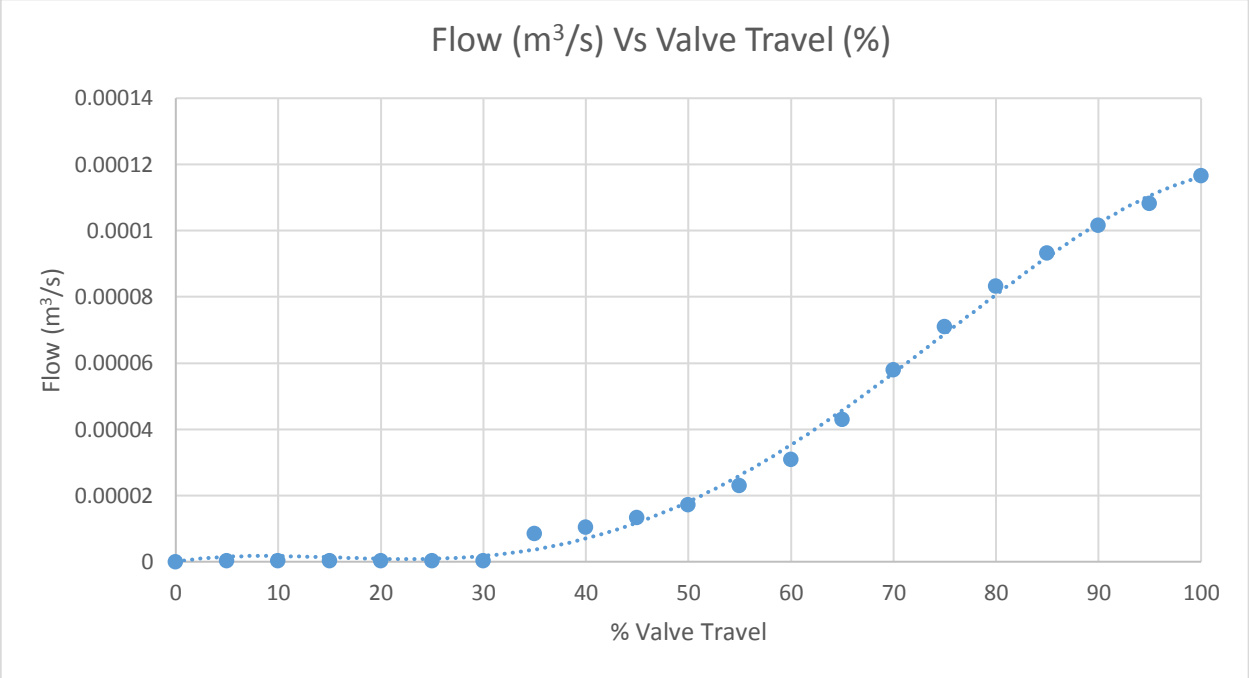

FIGURE 33 RAW WATER VALVE CALIBRATION CURVE

Figure 34 displays the results from calibration tests for the existing product pump. These results were obtained while pumping out up to one metre of head pressure. The qualitative nature of the response indicates that the pump is exhibiting a polynomial response to user input. For this reason, a second order polynomial trend line was utilised to obtain the best fit line with Microsoft Excel.

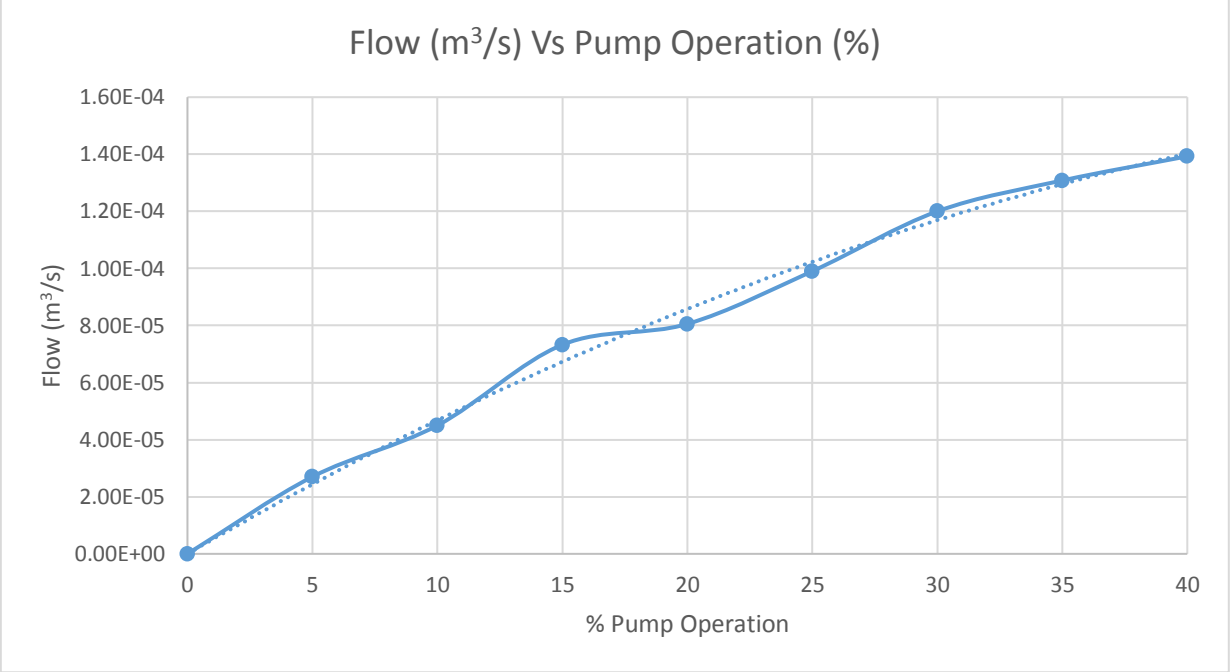

FIGURE 34 PUMP CALIBRATION CURVE

4.1.2 MASS BALANCE

For the purposes of level control within the holding tank arrangement, an overall mass balance, (18) was performed. A perfectly mixed tank arrangement with no concentration fluctuations was assumed. As a result, the density of the process medium within and exiting the tank are considered equal:

$$\frac{d(\rho_{out}V)}{dt} = \rho_{RW}\dot{V}_{RW} + \rho_{in}\dot{V}_{in} + \rho_{out}\dot{V}_{out} \quad \textbf{(18)}$$

Where ρ is fluid density (kg/m^3) and $\dot{V}$ is the volumetric flow rate (m^3/s). The density of a table salt and water solution will increase relative to increases in concentration [67]. This suggests that the resultant holding tank solution density is subject to change. The height of the solution within the tank is also a dynamic value. The volume of the holding tank is equal to the height, h multiplied by the cross-sectional area, A. The mass balance can be further simplified by dividing through the mass balance by the holding tank cross-sectional area which is a constant value of 0.748m^2 to arrive at (19).

$$\frac{d(\rho_{out}h)}{dt} = \frac{\rho_{RW}\dot{V}_{RW} + \rho_{in}\dot{V}_{in} - \rho_{out}\dot{V}_{out}}{A} \quad \textbf{(19)}$$

Next, the product rule, shown in (20) [68], is used to find the derivative of the product of the two functions within the mass balance; ρ_{out} and h [68]. This rule takes the form:

$$\frac{d}{dx}(uv) = v\frac{du}{dx} + u\frac{dv}{dx} \quad \textbf{(20)}$$

Applying the product rule to the differential term of the mass balance equation produces (21):

$$\frac{d(\rho_{out}h)}{dt} = h\frac{d\rho_{out}}{dt} + \rho_{out}\frac{dh}{dt} \quad \textbf{(21)}$$

Substitutinig (21) into (19) gives:

$$h\frac{d\rho_{out}}{dt} + \rho_{out}\frac{dh}{dt} = \frac{\rho_{RW}\dot{V}_{RW} + \rho_{in}\dot{V}_{in} - \rho_{out}\dot{V}_{out}}{A} \quad \textbf{(22)}$$

4.1.3 COMPONENT MASS BALANCE

To control the amount of table salt (NaCl) concentration within the holding tank arrangement, a component mass balance for NaCl is performed:

$$\frac{d(C_{out}V)}{dt} = C_{RW}\dot{V}_{RW} + C_{in}\dot{V}_{in} - C_{out}\dot{V}_{out} \quad \textbf{(23)}$$

Where C is the concentration of NaCl in kg/m^3. The component balance, (23) is divided through by the constant holding tank area, A:

$$\frac{d(C_{out}h)}{dt} = \frac{C_{RW}\dot{V}_{RW} + C_{in}\dot{V}_{in} - C_{out}\dot{V}_{out}}{A} \quad \textbf{(24)}$$

Again, the product rule, shown in (20), is used to expand the right-hand side of (24). This will find the derivative of the product of two different functions within the component mass balance; C_{out} and h. The application of the product rule to the derivative within (24) gives:

$$\frac{d(C_{out}h)}{dt} = h\frac{dC_{out}}{dt} + C_{out}\frac{dh}{dt} \quad \textbf{(25)}$$

Substituting (25) into (24) results in:

$$h\frac{dC_{out}}{dt} + C_{out}\frac{dh}{dt} = \frac{C_{RW}\dot{V}_{RW} + C_{in}\dot{V}_{in} - C_{out}\dot{V}_{out}}{A} \quad \textbf{(26)}$$

4.1.4 RELATING DENSITY TO CONCENTRATION

The density of pure water at 20°C is 998.2kg/m^3 [18]. The density of an electrolytic solution comprising of water and salt (NaCl) at 20°C for concentrations ranging from 20408.16 to 351351.4mg/L is 1012 to 1199kg/m^3. Literature results are plotted in Figure 35. If the solution temperature increases, this density value will decrease [67]. This effect is beyond the scope of this project and was not explored further. The solubility of salt in water is 35.88g salt per 100g water at 20°C. This is a concentration of 26.41% [69]. Above this concentration, the aqueous solution is saturated allowing no further salt to dissolve [70].

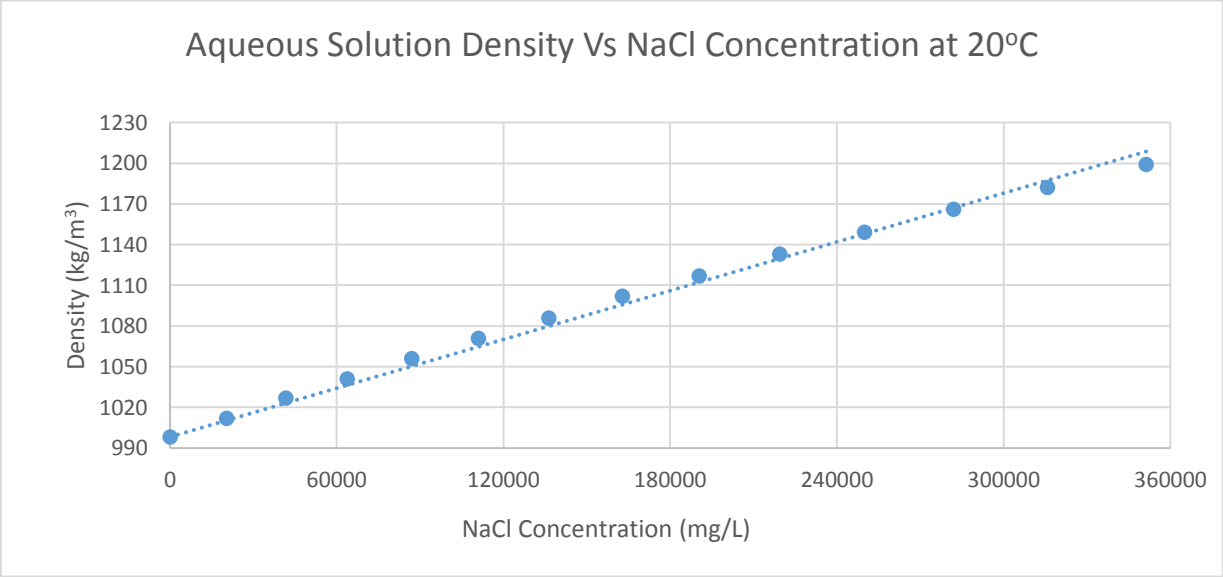

FIGURE 35 AQUEOUS SOLUTION DENSITY VS NACL CONCENTRATION AT 20°C

Detailed tables of these literature obtained test results are shown in Table 13 and Table 14 within Appendix C Density of an Aqueous Solution with NaCl. A plot of these results at 20°C is shown in Figure 35. As the density displayed a linear response to changes in concentration, a first order line of best fit was applied to the results via the Microsoft Excel plotting function. This resulted in an equation with a coefficient of determination value of 0.9937:

$$\rho(C) = 0.0006C + 998.2 \quad \textbf{(27)}$$

(27) enables density, ρ to be replaced by mass concentration, C in the mass balance performed earlier. The aim of the scope, however, is to measure and control the conductivity of an aqueous solution.

4.1.5 RELATING CONDUCTIVITY TO CONCENTRATION

The literature states that pure water exhibits minimal levels of conductivity. At 20°C, this has been found experimentally to be 0.04194μS/cm [71]. A plot of literature lab results at 20°C is shown in Figure 36.

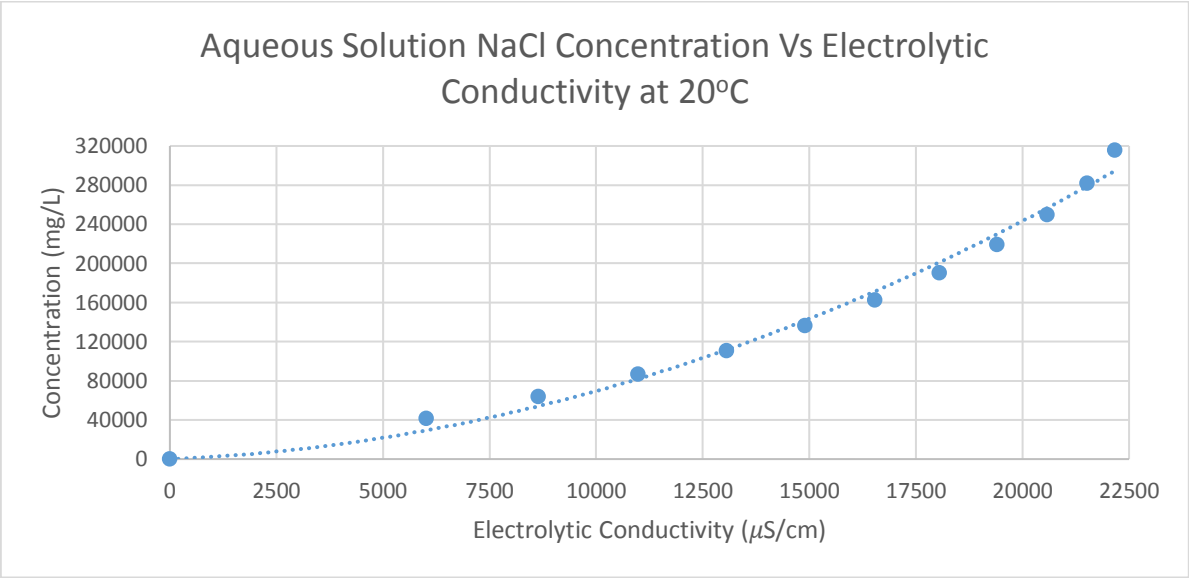

FIGURE 36 AQUEOUS SOLUTION NACL CONCENTRATION VS ELECTROLYTIC CONDUCTIVITY AT 20°C

The conductivity, κ of an aqueous solution comprising both water and salt (NaCl) at 20°C for concentrations ranging from 41666.67 to 315789.5 mg/L is 6018.7 to 22172.8 μS/cm. Increases in solution temperature will lead to a corresponding increase in conductivity [67]. These full laboratory literature results are shown in Table 15 and Table 16 within Appendix D Conductivity of an Aqueous Solution with NaCl. The effects of temperature are deemed outside of this thesis scope. As the existing conductivity sensors measure conductivity in μS/cm and the results of the experiments were in S/m, each

result was multiplied by 1000. Concentration exhibited a 2nd order curve response to changes in conductivity and for this reason, a 2nd order polynomial line of fit was used. This had an associated coefficient of determination value of 0.9899:

$$C(\kappa) = 0.0005\kappa^2 + 1.7558\kappa \quad \textbf{(28)}$$

It was also necessary to find a relationship that defined conductivity as a function of concentration. Referring to laboratory test literature in this area, results were plotted as shown in Figure 37 [67].

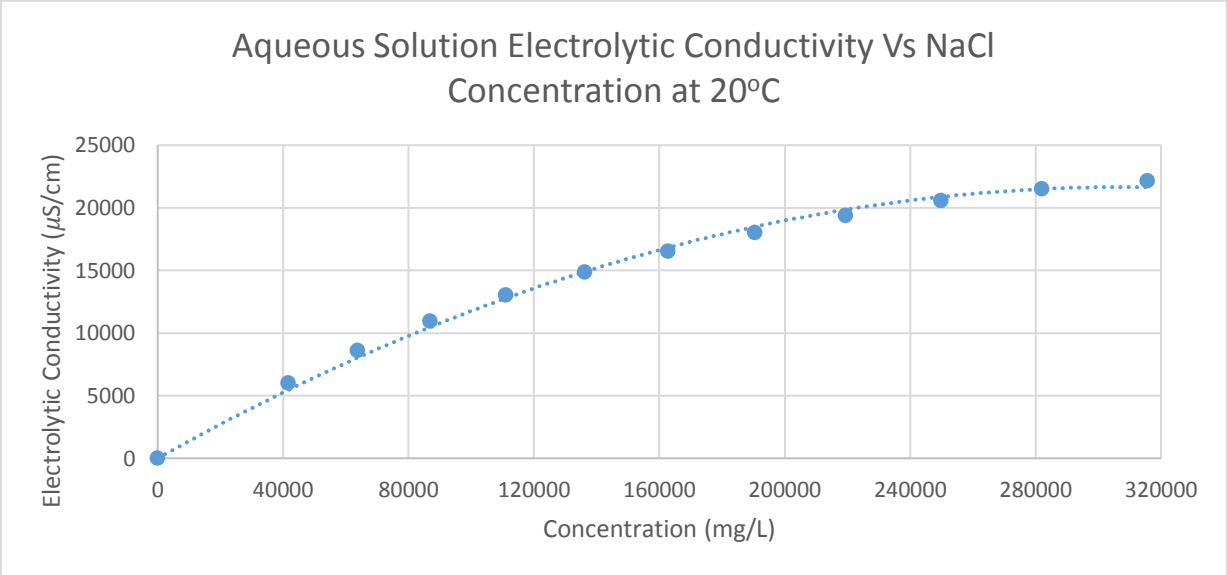

FIGURE 37 AQUEOUS SOLUTION ELECTROLYTIC CONDUCTIVITY VS NACL CONCENTRATION AT 20°C

A trend line was applied to this plot via Microsoft Excel to obtain the required function. This had a coefficient of determination value of 0.9964:

$$\kappa(C) = -2 \times 10^{-7}C^2 + 0.1404C + 0.0419 \quad \textbf{(29)}$$

4.1.6 REARRANGEMENT OF BALANCES IN TERMS OF H AND C

Returning to the resulting mass balance previously found in (22) and substituting density, ρ as a function of concentration, C derived earlier via (27) along with C_{RW} as 998.2 kg/m^3 gives:

$$h\frac{d[0.0006C_{out}+998.2]}{dt}+[0.0006C_{out}+998.2]\frac{dh}{dt} = \frac{998.2\dot{V}_{RW}+[0.0006C_{in}+998.2]\dot{V}_{in}-[0.0006C_{out}+998.2]\dot{V}_{out}}{A} \quad (30)$$

Next, the derivative term containing the variable, C_{out} is differentiated with respect to time, t. This results in:

$$0.0006h\frac{dC_{out}}{dt}+[0.0006C_{out}+998.2]\frac{dh}{dt} = \frac{998.2\dot{V}_{RW}+[0.0006C_{in}+998.2]\dot{V}_{in}-[0.0006C_{out}+998.2]\dot{V}_{out}}{A} \quad (31)$$

In a similar fashion to above, returning to the resulting component (NaCl) mass balance previously derived in (26) and rearranging this for $(hC_{out})/dt$ and cancelling out the $C_{out}V_{RW}$ term (the concentration of salt in raw water is assumed to be zero percent) yields:

$$h\frac{dC_{out}}{dt}=\frac{C_{in}\dot{V}_{in}-C_{out}\dot{V}_{out}}{A}-C_{out}\frac{dh}{dt} \quad (32)$$

(32) is then substituted into (31). This results in:

$$0.0006\left(\frac{C_{in}\dot{V}_{in} - C_{out}\dot{V}_{out}}{A} - C_{out}\frac{dh}{dt}\right) + [0.0006C_{out} + 998.2]\frac{dh}{dt} = \frac{998.2\dot{V}_{RW} + [0.0006C_{in} + 998.2]\dot{V}_{in} - [0.0006C_{out} + 998.2]\dot{V}_{out}}{A} \quad \textbf{(33)}$$

Expanding the brackets on the left hand side of (33) produces:

$$0.0006\frac{C_{in}\dot{V}_{in}}{A} - 0.0006\frac{C_{out}\dot{V}_{out}}{A} - 0.0006C_{out}\frac{dh}{dt} + 0.0006C_{out}\frac{dh}{dt} + 998.2\frac{dh}{dt} = \frac{998.2\dot{V}_{RW} + 0.0006C_{in}\dot{V}_{in} + 998.2\dot{V}_{in} - 0.0006C_{out}\dot{V}_{out} - 998.2\dot{V}_{out}}{A} \quad \textbf{(34)}$$

Removing terms that cancel to zero within (34) gives:

$$998.2\frac{dh}{dt} = \frac{998.2\dot{V}_{RW} + 998.2\dot{V}_{in} - 998.2\dot{V}_{out}}{A} \quad \textbf{(35)}$$

Dividing through both sides of (35) by 998.2 yields an equation for the change in holding tank height:

$$\frac{dh}{dt} = \frac{\dot{V}_{RW} + \dot{V}_{in} - \dot{V}_{out}}{A} \quad \textbf{(36)}$$

Now that there is an equation to solve for the change in holding tank process fluid height with respect to time, (36) is then substituted into (32):

$$h\frac{dC_{out}}{dt} = \frac{C_{in}\dot{V}_{in} - C_{out}\dot{V}_{out}}{A} - C_{out}\frac{\dot{V}_{RW} + \dot{V}_{in} - \dot{V}_{out}}{A} \quad \textbf{(37)}$$

Expanding out this equation, grouping like terms and rearranging for dC_{out}/dt yields:

$$\frac{dC_{out}}{dt} = \frac{C_{in}\dot{V}_{in} - C_{out}\dot{V}_{out} - C_{out}\dot{V}_{RW} - C_{out}\dot{V}_{in} + C_{out}\dot{V}_{out}}{Ah} \quad \textbf{(38)}$$

Removing terms that cancel to zero and grouping like terms results in an equation for the change in holding tank salt concentration:

$$\frac{dC_{out}}{dt} = \frac{(C_{in} - C_{out})\dot{V}_{in} - C_{out}\dot{V}_{RW}}{Ah} \quad \textbf{(39)}$$

This results in two equations that would allow for solving for either the change in height or concentration within the holding tank arrangement.

4.1.7 SIMULATION OF SYSTEM

With differential equation models obtained that track the change in both desired process variables within the system and appropriate measurements of the holding tank arrangement, a simulation of this system was created through the Mathworks Simulink program. This software package allows users to efficiently model the dynamics of a plant. It also affords users to tools to design and tune feedback loops and controllers for testing purposes. This is a graphical type simulation environment [72]. A screenshot of the fully implemented system model can be located in Appendix E Simulink System Model.

4.1.8 MODEL VALIDATION

When a model of a system is derived, validation of this model is required. This validation provides evidence that the model is a sufficiently accurate representation of the system it is intended to represent. This usually involves comparing open loop system responses to the same manipulated variable inputs for both the real system and the associated model. If these are found to be within an acceptable tolerance, the model is said to be satisfactory in predicting system response for controller implementation and calibration.

Unfortunately for this thesis scope, this action was not possible. This is because the physical system (tanks, instrumentation, tubing, wiring etc.) were not able to be implemented within the scope timeframe due to several budget and labour restrictions. Instead, the system model derived from fundamental principles acted as a guide for the potential proposed system yet to be implemented.

4.2 DERIVATION OF SYSTEM CONTROLLERS

Once a feasible model of both the holding tank height and conductivity was created, suitable controllers were then derived to control both of the desired process variables: level and conductivity.

4.2.1 SYSTEM IDENTIFICATION AND CONTROLLER TUNING

Both holding tank level and conductivity controller agorithms were created using the method of direct synthesis. This method of controller design is based on two main components: a process model and a desired closed loop transfer function. Depending on the type of system, this can result in a Proportional (P), Proportional and Integral (PI) or Proportional, Integral and Derivative (PID) type controller [73].

This controller takes the form [30],

$$g_c = \frac{1}{g}\left(\frac{q}{1-q}\right) \quad (40)$$

where g_c is the controller equation, g is the process transfer function and q is the desired closed loop reference trajectory transfer function. In order to obtain a transfer function model of the system, the system identification toolbox feature within Matlab was utilised. This toolbox utilises measured input and output data to construct mathematical models of dynamic systems. This includes the use of time or frequency domain input and output data [74].

Data from the Simulink model after both positive and negative unit step inputs to both manipulated variables were sent to the Matlab workspace allowing it to be interrogated by the system identification toolbox. This was achieved through the use of the “To Workspace” block shown in Figure 38.

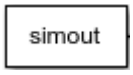

FIGURE 38 SIMULINK "TO WORKSPACE" BLOCK

This then allows for data from the Simulink simulation to be obtained from within the general Matlab program user window as shown in Figure 39.

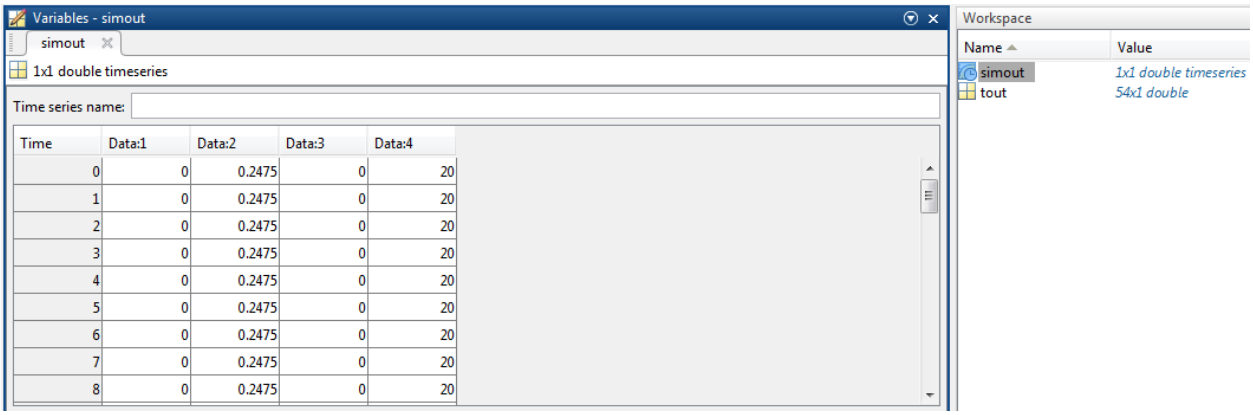

FIGURE 39 MATLAB WORKSPACE SIMULINK DATA COLLECTION

This information then entered into a Microsoft Excel spreadsheet in the form of deviation variables. Deviation variables are variables that show the amount of deviation from the steady-state value of a variable. This is found by deducting the attributed steady state value from each result for each variable [30]. The Simulink simulation time interval was one second. This information was then imported back into Matlab via the import data button available on the home screen. The required information was then exported back to the Matlab workspace as column vectors. This allowed multiple columns of data to be selected and exported at the same time.

The system identification toolbox within Matlab was then pivotal in identifying the nature of each attributed system. Starting with a change in holding tank height, time domain data was imported into the toolbox as shown in Figure 40.

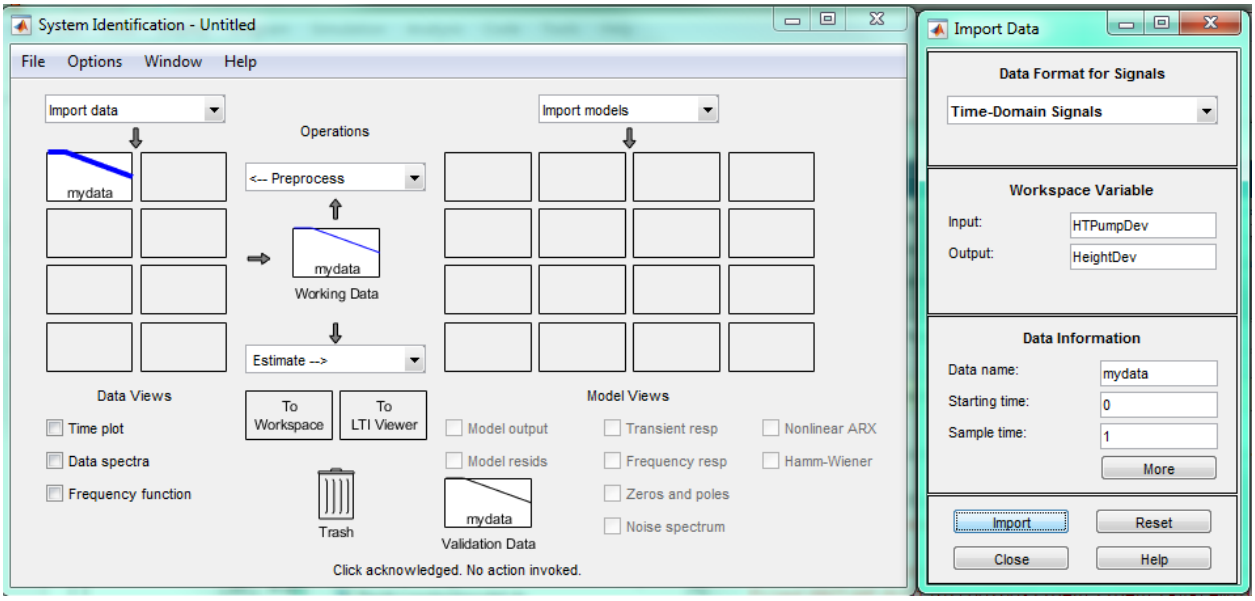

FIGURE 40 SYSTEM IDENTIFICATION TOOLBOX IMPORT DATA WINDOW

The holding tank height is referred to as a purely capacitive system. This is because should the outlet pump be turned off, and the inlet pump be turned on, the tank will fill to capacity and then overflow without input from the outlet pump. Once the data was imported into the toolbox, the process model option under the estimate menu was selected. This allowed for customisation of the desired type of model the toolbox should try to fit. Figure 41 shows the particular options selected and corresponding identified transfer function for the tank height system model. A gain or K value of $-4.630*10^{-6}$ and $-4.735*10^{-6}$ was identified for positive and negative unit steps applied respectively to the holding tank pump. An average of these two values was then taken to obtain an appropriate transfer function.

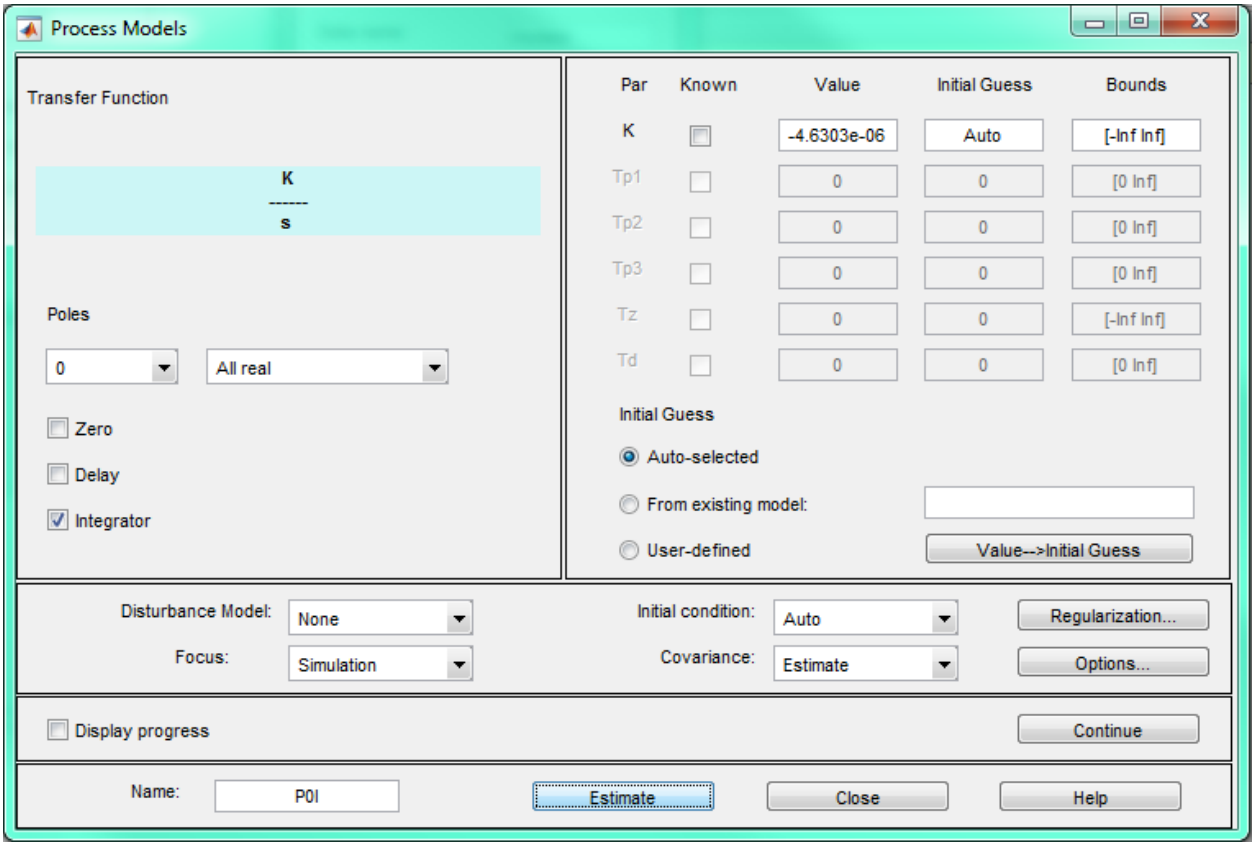

FIGURE 41 SYSTEM IDENTIFICATION TOOLBOX PROCESS MODEL FOR HOLDING TANK HEIGHT

The identified holding tank height system model in transfer function form found via this method was:

$$g_h = \frac{-4.6827 \times 10^{-6}}{s} \tag{41}$$

The gain is a measure of how much the process output will change in response to a change in process input [30]. It is the negative term on the top half of the transfer function in (41). This negative gain indicates an increase in the associated manipulated variable will result in a decrease in the process variable and vice versa. This is expected as the manipulated variable controlling tank height is the holding tank (outflow) pump operating percentage.

Next, the desired response, q is required. A first-order response with an appropriate time constant, τ was desired. The time constant is a measure of how fast the process output will react to a change in process input. The smaller the value of τ, the faster the process response and conversely, the larger this value, the slower the process response. A first order process will reach 99.7% of the final value within approximately 5τ [30]. For holding tank height control, a time constant of 5 seconds was chosen. This is a compromise between fast controller action response by the system and minimal wear on the corresponding control element.

$$q_h = \frac{1}{5s+1} \tag{42}$$

Substituting both g_h and q_h into (40) and solving for the holding tank height controller:

$$\begin{aligned} g_c &= \frac{1}{\frac{-4.6827 \times 10^{-6}}{s}} \left(\frac{\frac{1}{5s+1}}{1 - \frac{1}{5s+1}} \right) \\ g_c &= \frac{s}{-4.6827 \times 10^{-6}} \left(\frac{\frac{1}{5s+1}}{1 - \frac{1}{5s+1}} \right) \times \frac{5s+1}{5s+1} \\ g_c &= -\frac{s}{4.6827 \times 10^{-6}} \left(\frac{1}{5s} \right) \\ g_c &= -\frac{1}{5 \times 4.6827 \times 10^{-6}} \\ g_c &= -\frac{1}{23.414 \times 10^{-6}} \end{aligned} \tag{43}$$

This yields the required tuning parameter, K_c for the holding tank level controller, g_c as follows:

$$g_c(s) = K_c \quad where \quad K_c = -\frac{1}{23.414 \times 10^{-6}} = -42710.40212 \tag{44}$$

An identical method was used to identify an appropriate model of the conductivity system response regarding both positive and negative unit step inputs from the raw water valve. These resulted in a gain or K value of -0.070505 and $-9.1876*10^{-6}$ respectively. The identified holding tank conductivity average system model in transfer function form found via this method was:

$$g_{Con} = \frac{-0.035257}{s} \tag{45}$$

This, similar to the holding tank height, is a capacity type system. As before, the desired response for the conductivity within the holding tank was required. In this instance, a longer time constant of 15 seconds was chosen as tank height is a faster activing system. The desired system response transfer function for conductivity was:

$$q_C = \frac{1}{15s + 1} \tag{46}$$

This desired system response transfer function, along with the system transfer function were substituted into (40) to derive the required system controller:

$$\begin{gathered} g_c = \frac{1}{\frac{-0.035257}{s}} \left(\frac{\frac{1}{15s+1}}{1 - \frac{1}{15s+1}} \right) \\ g_c = -\frac{s}{0.035257} \left(\frac{\frac{1}{15s+1}}{1 - \frac{1}{15s+1}} \right) \times \frac{15s+1}{15s+1} \\ g_c = -\frac{s}{0.035257} \left(\frac{1}{15s} \right) \\ g_c = -\frac{1}{15 \times 0.035257} \\ g_c = -\frac{1}{0.52886} \end{gathered} \tag{47}$$

The required tuning parameter, K_c for the holding tank conductivity controller, g_c was as follows:

$$g_c(s) = K_c \quad where \quad K_c = -\frac{1}{0.52886} = -1.89087 \tag{48}$$

4.2.1.1 ALTERNATIVE CONTROLLER TUNING

Given a first-order reference trajectory for each controller discussed above, the result was a gain only controller in both instances. Once implemented, these controllers exhibited a slight offset. This is explored in more detail later in this report. This could be eliminated with the introduction of an integral term into the control scheme structure. The purpose of the integral term, τ_I in a controller, is to eliminate any steady state offset resultant from closed loop response. This offset occurs in the absence of integral action [30]. The form of a standard Proportional and Integral (PI) controller is [30]:

$$g_c(s) = K_c\left(1 + \frac{1}{\tau_I s}\right) \tag{49}$$

The introduction of an integral term into the desired PI controllers was achieved by selecting a second order reference trajectory for the direct synthesis controller design. This takes the form [30]:

$$q(s) = \frac{1}{\tau^2 s^2 + 2\tau\zeta s + 1} \tag{50}$$

Where K is the steady state gain. This is represented by 1 on the numerator in this instance. Tau, τ is the natural period and zeta, ζ is the damping coefficient [30].

Selection of different values for the damping coefficient results in vastly differing process responses to step inputs. These fall into three ranges [30]:

- $0 < \zeta < 1$;
- $\zeta = 1$;
- $\zeta > 1$.

The first case results in an oscillatory response. This is often said to be underdamped. This result reaches the final value the fastest, however, takes a period to settle. The second case is said to be critically damped. This case offers the fastest approach to a final value, AK without oscillations. The third case is termed overdamped and exhibits a sluggish or slow response taking a long time, t to approach its final intended value [30]. Figure 42 shows these differences.

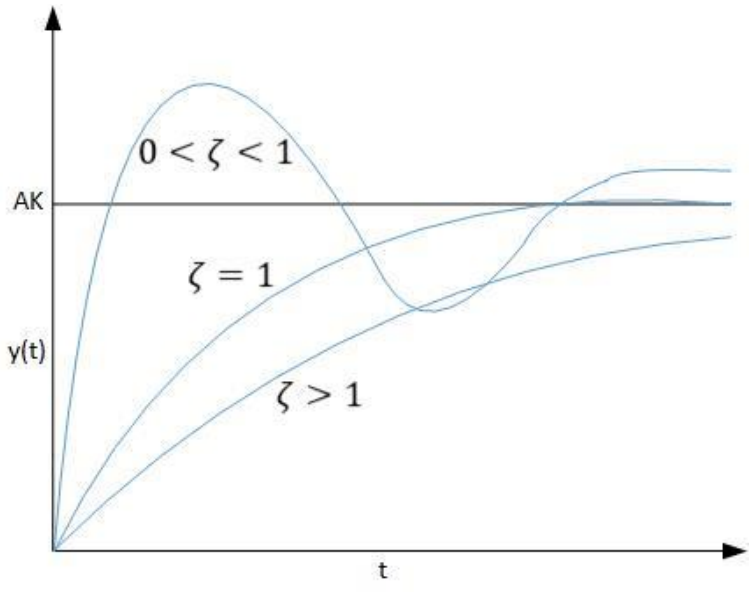

FIGURE 42 STEP RESPONSES OF A SECOND ORDER SYSTEM – ADAPTED FROM [30]

The chosen reference trajectory equation shown in (51) for the height PI controller utilised the same τ value as that used for the P only height controller derivation. This was 5 seconds. A damping coefficient value of 0.1 was chosen as this would result in the fastest system response. The holding tank height desired system response under PI control is:

$$q_h = \frac{1}{25s^2 + s + 1} \tag{51}$$

Substituting both the system model derived earlier and the desired system response into (40) and solving for the holding tank height PI controller:

$$g_c = \frac{1}{\frac{-4.6827 \times 10^{-6}}{s}} \left(\frac{\frac{1}{25s^2 + s + 1}}{1 - \frac{1}{25s^2 + s + 1}} \right)$$

$$g_c = \frac{s}{-4.6827 \times 10^{-6}} \left(\frac{\frac{1}{25s^2 + s + 1}}{1 - \frac{1}{25s^2 + s + 1}} \right) \times \frac{25s^2 + s + 1}{25s^2 + s + 1}$$

$$g_c = -\frac{s}{4.6827 \times 10^{-6}} \left(\frac{1}{25s^2 + s} \right)$$

$$g_c = -\frac{1}{4.6827 \times 10^{-6}} \left(\frac{1}{25s + 1} \right) \tag{52}$$

$$g_c = -\left(\frac{1}{11.7086 \times 10^{-5} s + 4.6827 \times 10^{-6}} \right)$$

$$g_c = -\frac{1}{4.6827 \times 10^{-5}} \left(1 + 0.04 \frac{1}{s} \right)$$

$$g_c = -21355.20106 \left(1 + 0.04 \frac{1}{s} \right)$$

This yielded the required tuning parameters, gain, K_c and integral time, τ_i for the holding tank level PI controller, g_c as follows:

$$K_c = -\frac{1}{4.6827 \times 10^{-6}} = -213552.0106 \quad (53)$$

$$\tau_i = \frac{1}{\frac{11.7086 \times 10^{-5}}{4.6827 \times 10^{-6}}} = \frac{1}{25} = 0.04 \quad (54)$$

This process was again repeated for the conductivity PI controller. For this controller, a τ value of 15 seconds, the same utilised for the P only conductivity controller derivation was chosen. A damping coefficient value of 0.1 was again chosen on this occasion. The holding tank conductivity desired system response under PI control is:

$$q_h = \frac{1}{225s^2 + 3s + 1} \quad (55)$$

Solving for the holding tank conductivity PI controller:

$$g_c = \frac{1}{\frac{-0.035257}{s}} \left(\frac{\frac{1}{225s^2 + 3s + 1}}{1 - \frac{1}{225s^2 + 3s + 1}} \right)$$

$$g_c = \frac{1}{\frac{-0.035257}{s}} \left(\frac{\frac{1}{225s^2 + 3s + 1}}{1 - \frac{1}{225s^2 + 3s + 1}} \right) \times \frac{225s^2 + 3s + 1}{225s^2 + 3s + 1}$$

$$g_c = -\frac{s}{0.035257} \left(\frac{1}{225s^2 + 3s} \right) \quad (56)$$

$$g_c = -\frac{1}{0.035257} \left(\frac{1}{225s + 3} \right)$$

$$g_c = -\left(\frac{1}{7.932825s + 0.10577} \right)$$

$$g_c = -\frac{1}{0.10577}\left(1 + 0.013333\frac{1}{s}\right)$$

$$g_c = -9.45439\left(1 + 0.013333\frac{1}{s}\right)$$

The resultant tuning parameters, gain, K_c and integral time, τ_i for the holding tank conductivity PI controller, g_c were as follows:

$$K_c = -\frac{1}{0.10577} = -9.45439 \quad \textbf{(57)}$$

$$\tau_i = \frac{1}{\frac{7.932825}{0.10577}} = \frac{1}{75} = 0.013333 \quad \textbf{(58)}$$

4.2.2 CONTROLLER IMPLEMENTATION

Both P and PI controllers were implemented within Simulink. This involved the addition of the PID controller block. P and PI only control were selected respectively. The block was put in an ideal form to enable correct operation. To minimise error associated with these controllers, the Simulink program has been constructed to operate with deviation variables of both of their associated manipulated and process variables. A screenshot of the associated Simulink code for both types of controllers can be located in Appendix F Simulink System Model with Control.

4.3 CONTROLLER PERFORMANCE MEASURES

Quantitative performance measures of each implemented controller were explored. These measures can best be classified within two distinct categories:

- Statistical process control;
- Error based criteria.

4.3.1 STATISTICAL PROCESS CONTROL

Statistical process control monitors and controls a process though the use of statistical methods. It is a method of quality control [75]. Two typical applications were explored to assess the suitability of both types of implemented controllers. These fall under the Shewhart control chart and the Cumulative sum (CUSUM) chart.

4.3.1.1 SHEWHART CONTROL CHARTS

Shewhart control charts allow the user to confirm the process stability when under an implemented control strategy [76]. Sample data is obtained from the process at steady state. The standard deviation, σ of this data set from the mean, $\bar{x}$ is next obtained. The smaller the standard deviation of a data set while at steady state, the more stable the process is. Finally, an upper control limit (UCL) and lower control limit (LCL) is applied to the data set. The same UCL and LCL are then applied to the mean of each steady state and disturbance rejection dataset discussed below. These are calculated as three standard deviations (3σ) above and below the mean of the collected data. This represents the maximum expected deviations in the process [77]. This is because it is known that 99.73% of a data set will fall within these limits [12]. The Shewhart chart is an effective tool in identifying large deviations from the mean of a data set.

4.3.1.1.1 LEVEL CONTROLLERS

Simulink simulation data was obtained and then plotted with Microsoft Excel. A set point change from 0.2475m to 0.3m was applied at 10 s. The desired set point was achieved before 600s into each simulation. For each plot, a 400 second sample time with interval 1 second, was taken from 600s to 1000s. The mean, standard deviation, UCL and LCL were calculated and applied accordingly. Table 4 summarises the findings.

TABLE 4 SHEWHART CHART DATA - HEIGHT CONTROLLERS

Controller	Mean ($\bar{x}$)	Standard Deviation (σ)	UCL	LCL
P	0.30094 m	$5.57*10^{-16}$m	$\bar{x} + 1.67*10^{-15}$m	$\bar{x} - 1.67*10^{-15}$m
PI	0.30032 m	$4.11*10^{-7}$m	$\bar{x} + 1.23*10^{-7}$m	$\bar{x} - 1.23*10^{-7}$m

It was interesting to note from the observed results, that the P only controller exhibited a persistent offset of $9.37*10^{-4}$m from set-point. This was unexpected as the tank is a capacity system and has inherent integrating characteristics. These characteristics should remove any offset when tracking a set point. This offset could be attributed somewhat to the obtained system model. This was derived from an average of both positive and negative step inputs applied during system identification. As this was an average, the applied P only controller could be expected to exhibit a degree of offset as there would be a minor element of error in controller derivation. A biasing term could be introduced to the controller to eliminate this offset.

By contrast, the introduction of an integral term in the PI controller was able to reduce any offset from set point dramatically. The offset observed in this instance was $3.19*10^{-4}$m. This was an offset reduction in the magnitude of 2.94 times that displayed by the P controller. From these obtained results, it was evident that the PI controller performed better when tasked with tracking a desired set point.

It was also observed that the P controller exhibited a lower standard deviation, σ ($5.57*10^{-16}$m) than that exhibited by the PI controller ($4.11*10^{-7}$m). This would suggest that the gain only controller provided more stability when maintaining set point. Closer analysis of the PI height controller steady state data shown in Figure 43 shows that the standard deviation observed was due to the presence of the integral term. The integral continued trying to reduce the error present and as such, displayed a more substantial standard deviation. By Shewhart chart analysis criteria, the PI height controller was deemed most appropriate as there was minimal set point deviation while still displaying appropriate process stability.

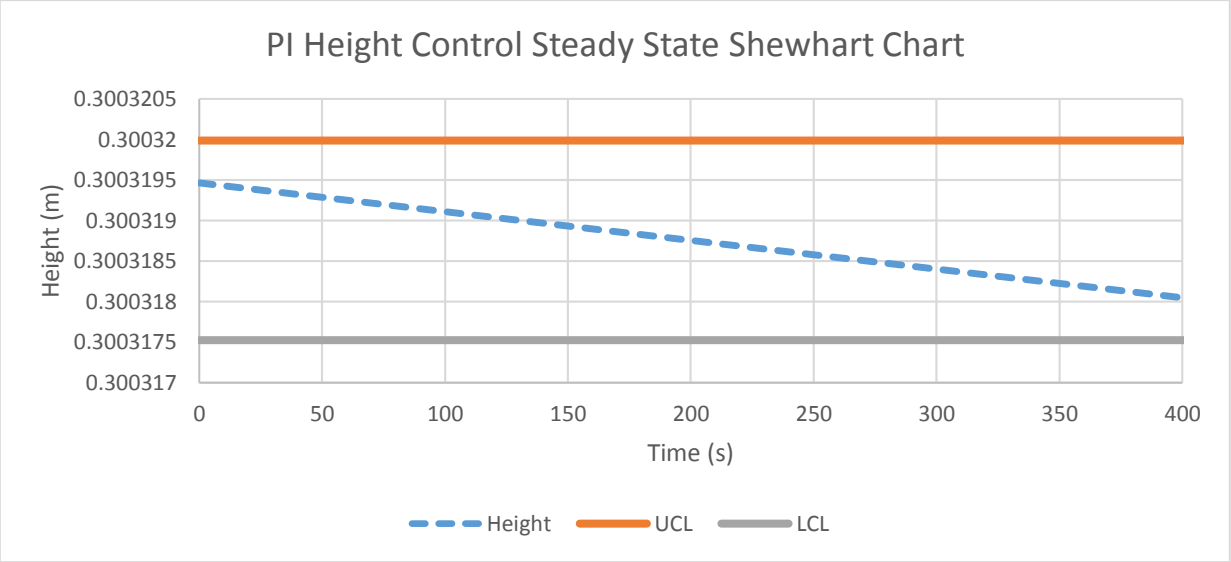

FIGURE 43 PI HEIGHT CONTROL STEADY STATE SHEWHART CHART

At 500s into the second set of simulations, a set point change was applied (15488μS/cm down to 15000μS/cm) to the conductivity set point causing the raw water valve to operate. This fed fresh water to the holding tank. As this occurred, it was observed that there was a disturbance in the process variable under both P and PI control. Results are shown in Figure 44 and Figure 45 over a 500s sample with 1 second interval. It is evident from these plots, disturbance rejection capabilities present in either controller were poor. PI control took longer to return to a steady state value, but exhibited less offset.

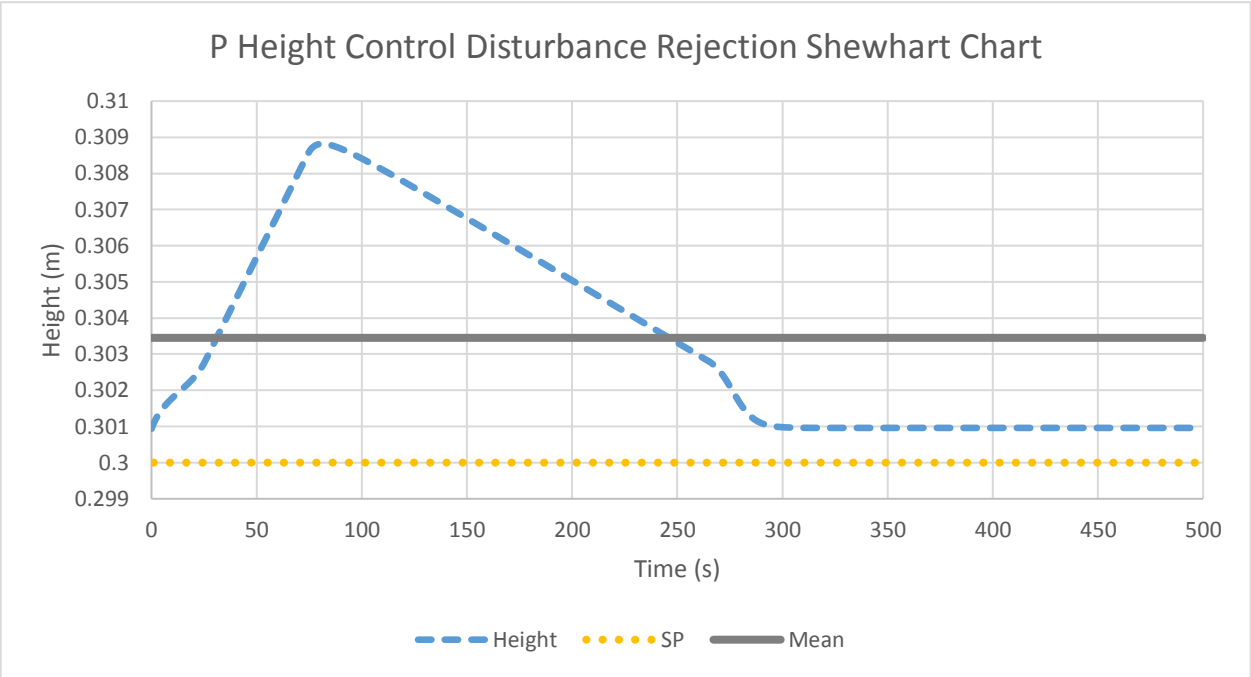

FIGURE 44 P CONTROL HEIGHT SHEWHART CHART

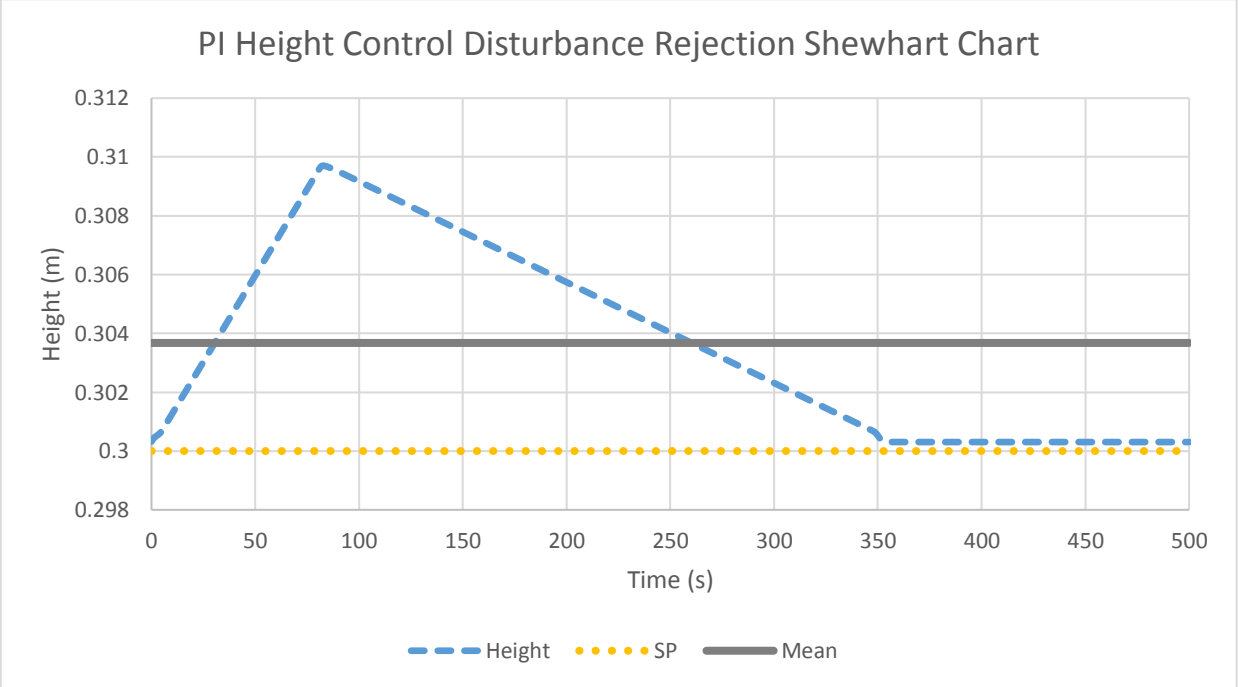

FIGURE 45 PI HEIGHT CONTROL SHEWHART CHART

4.3.1.1.2 CONDUCTIVITY CONTROLLERS

New simulations were run in Simulink and plotted in Microsoft Excel for the conductivity controllers. For this simulation, a set point change from 15488μS/cm to 15000μS/cm was applied to the simulation at 10s. As with the height controllers previously discussed, the set point or new steady state value was reached before 600s. For each plot, a 400 second sample time with interval 1 second, was taken from 600s to 1000s. The mean, standard deviation, UCL and LCL were calculated and applied. Table 5 summarises the observed results.

TABLE 5 SHEWHART CHART DATA - CONDUCTIVITY CONTROLLERS

Controller	Mean ($\bar{x}$)	Standard Deviation (σ)	UCL	LCL
P	15018.3 μS/cm	$3.82*10^{-11}$ μS/cm	$\bar{x} + 1.15*10^{-10}$ μS/cm	$\bar{x} - 1.15*10^{-10}$ μS/cm
PI	15003.6 μS/cm	$1.55*10^{-3}$ μS/cm	$\bar{x} + 4.65*10^{-3}$ μS/cm	$\bar{x} - 4.65*10^{-3}$ μS/cm

The P only controller persistent offset of 18.3μS/cm from set-point. This can be attributed to model design and implementation. As the equations used to relate conductivity to concentration and vice versa were not exactly the same, there were minor errors present in the implemented system model. With this is mind, the applied P only controller could be expected to exhibit a degree of offset as there would be a minor amount of error present in the model for conductivity. As a result, there would also be error present in the associated controller derivation.

As with height control, the introduction of an integral term in the PI controller significantly reduced any offset from a set point substantially. The offset observed for this controller was 3.61μS/cm. This was an offset reduction in the magnitude of 5.07 times that displayed by the P controller. The PI controller was observed to have performed much better when tasked with tracking a desired set point by the user.

It was again noted that the P controller exhibited a lower standard deviation, σ ($3.82*10^{-11}\mu$S/cm) than the PI controller ($1.55*10^{-3}\mu$S/cm). This would suggest better controller performance related to system stability. Closer analysis of the PI conductivity controller steady state data shown in Figure 46 was again required. As was the case with height controllers, this chart the integral continued trying to reduce the error present and as such displayed a larger standard deviation. The PI height controller exhibited minimal set point deviation whilst still displaying acceptable process stability. For this reason, it was deemed the most appropriate controller for holding tank conductivity.

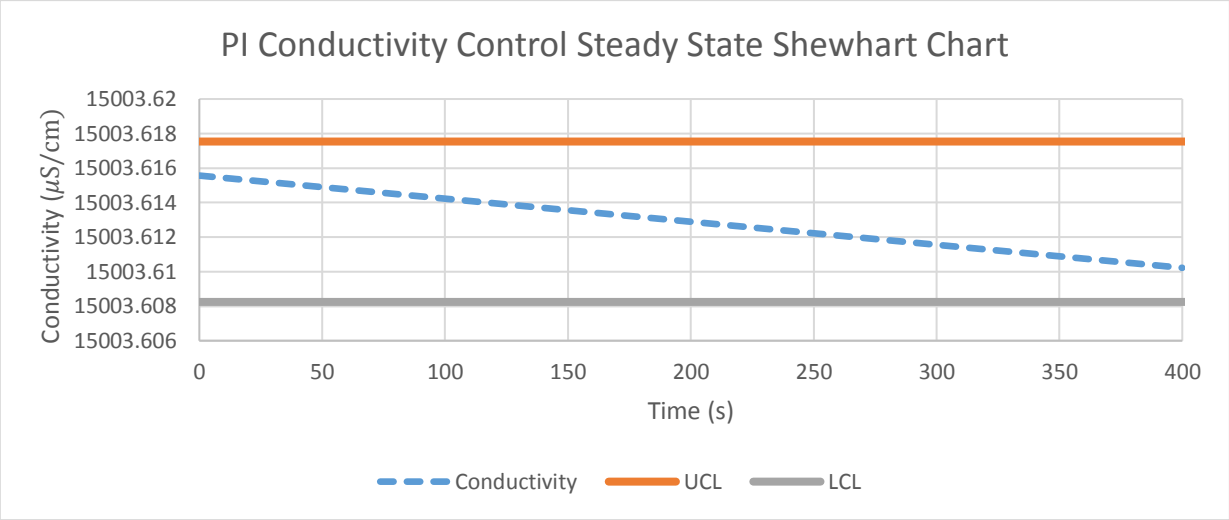

FIGURE 46 PI CONDUCTIVITY CONTROL STEADY STATE SHEWHART CHART

At 500s into the simulation, a disturbance was introduced to the process. The concentration of the stream from CSTR3 into the holding tank was increased from 14895.2 to 16000μS/cm. A 500s sample of data was then taken for simulation time 500 – 1000s and observed. A disturbance in the process variable under both P and PI control was again observed. Results are shown in Figure 47 and Figure 48 over a 500s sample with 1 second interval. Set point is not shown due to amount of offset. It was again noted that disturbance rejection capabilities present in either controller was average. PI control took longer to return to a steady state value, but exhibited less offset as with the case of height control.

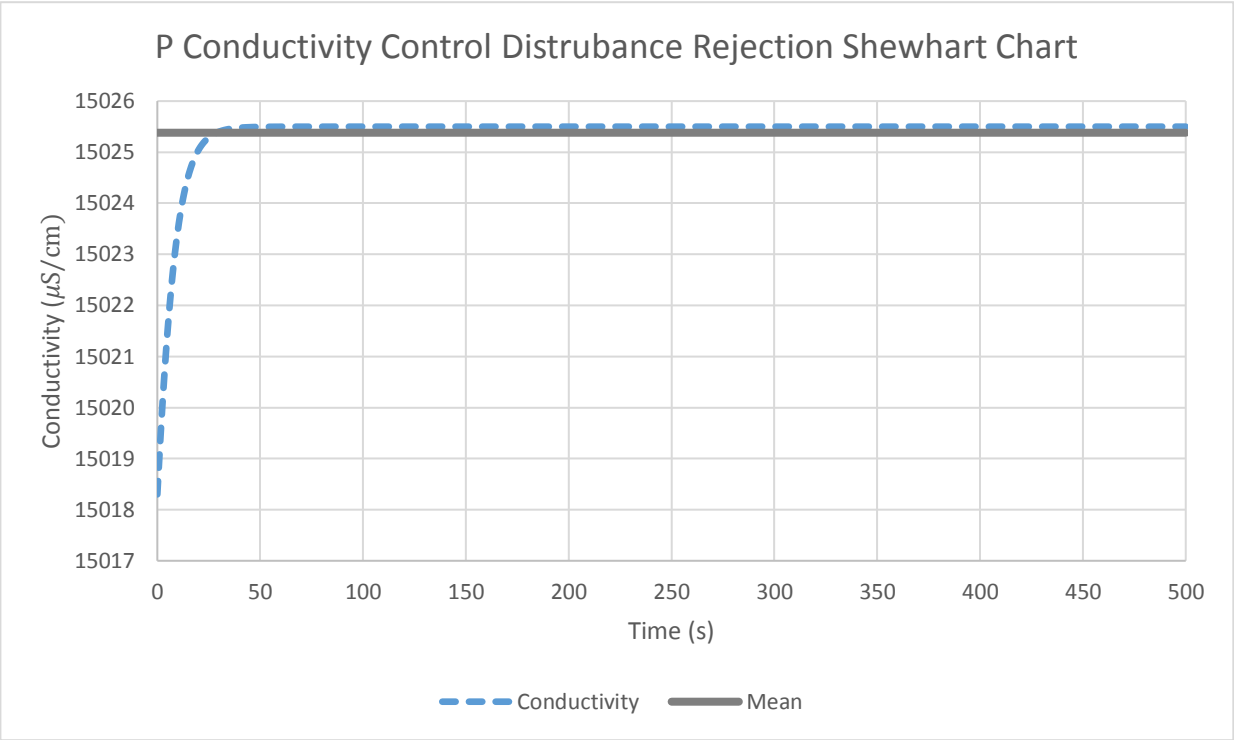

FIGURE 47 P CONDUCTIVITY CONTROL DISTURBANCE REJECTION SHEWHART CHART

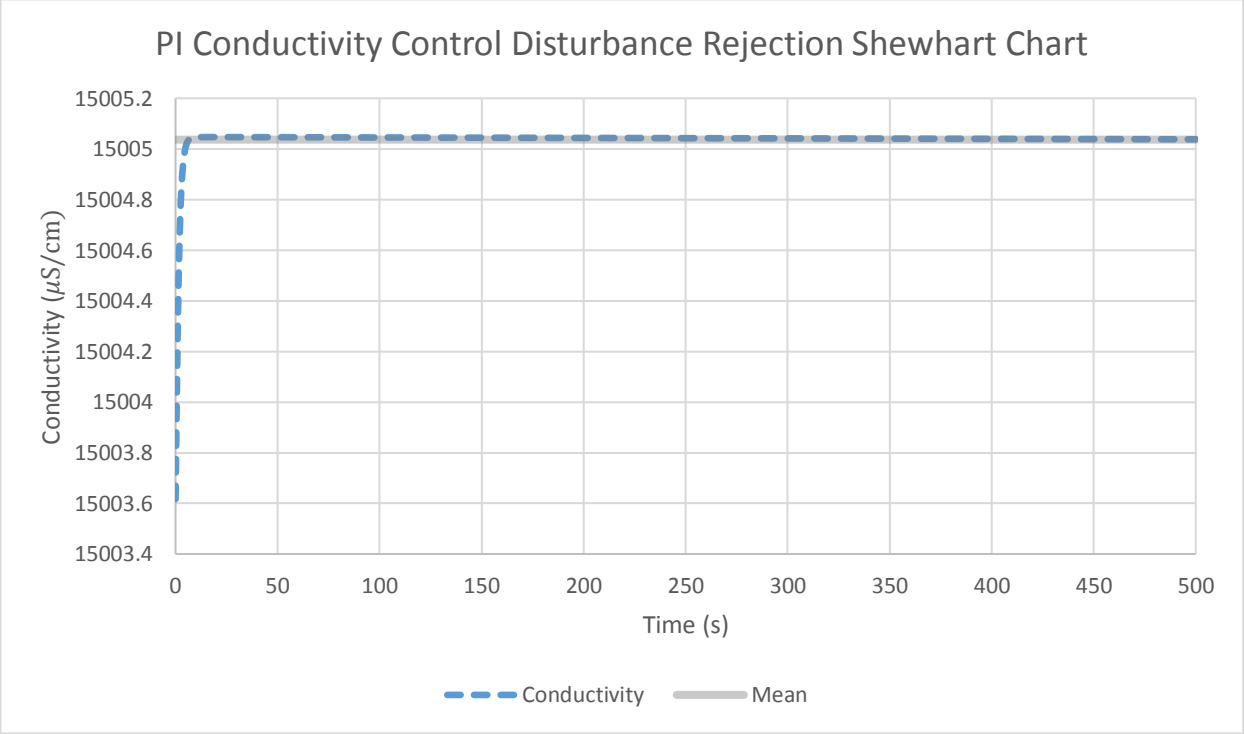

FIGURE 48 PI CONDUCTIVITY CONTROL SHEWHART CHART

4.3.1.2 CUMULATIVE SUM CHARTS

Cumulative Sum (CUSUM) charts are often useful for detecting small, persistent deviations of 1.5σ from the mean of a chosen data set. Shewhart charts are ineffective in this area. CUSUM is defined as a running summation of the process variable deviations from its desired set point such that [73]:

$$S_{(k)} = \sum_{i=1}^{k} \bar{x}_{(i)} - t = \sum_{i=1}^{k} e_{(i)} \quad \textbf{(59)}$$

Where S is the CUSUM score, $\bar{x}$ is the mean of a data set, t is the target value and e is mean error of a data set. During normal process operation, the score, S will vary around zero. If there is either a positive or negative persistent error, the CUSUM score will display a positive or negative trend away from zero respectively. The CUSUM chart can therefore either be employed to generate a signal when a persistent slope is detected, or employ upper and lower control limits to send a signal when the limits are exceeded. An unintended change in the process mean can be discovered and investigated as a result [73].

A variation of the CUSUM method which was utilised for controller analysis distinguishes between the positive and negative cumulative error. This is achieved by employing a recursive calculation of the values; C+ and C- such that [73]:

$$C^{+} = \max[0, e_k - K + {C^{+}}_{k-1}], \qquad C^{-} = \max[0, -e_k - K + {C^{-}}_{k-1}] \quad \textbf{(60)}$$

Where K is a slack parameter. C+ and C-, the sums for high and low directions, will only sum upwards when the error is larger than the slack parameter. A specified control limit or threshold, H was chosen and once either C+ or C- reaches this value a signal is output and the value is reset to zero. Typically, K and H are chosen as multiples of the standard deviation of a representative data set so that the number of signals received over a time frame can be interpreted according to the expected number of signals [73]

In this instance, K was chosen to be half the standard deviation and H was chosen to be five times the standard deviation. Table 6 outlines the number of expected signals for various standard deviations from the target value for the process variable. As the slack parameter chosen was half the standard deviation, σ, there was 13-14 expected signals for assessment purposes over a 500s time frame.

TABLE 6 CUSUM AVERAGE RUN LENGTH AND EXPECTED RESULTANT SIGNALS [73]

Shift from target (in multiples of σ)	Average Run Length H = 5σ	Signals over 500 s period
0	465	0-1
0.25	139	1-2
0.5	38	13-14
0.75	17	19-30
1	10.4	48-49
2	4.01	124-125
3	2.57	194-195

4.3.1.2.1 HEIGHT CONTROLLERS

To more appropriately measure height controller performance at steady state, CUSUM charts were employed. Figure 49 and Figure 50 show the resultant plots for both the P and PI controllers for holding tank height. It is evident from the CUSUM charts, that there is a persistent offset present for both controllers in the positive direction. It is also clear that the magnitude of the offset is larger for the P controller than it is for the PI controller. Table 7 shows that both controllers performed relatively poorly under these criteria. More advanced control schemes would fare better here.

TABLE 7 HEIGHT CONTROLLER CUSUM RESULTS

Controller	K	H	C- Signals	C+ Signals	Total	Expected
P	2.78E-16	2.78E-15	50	201	251	13-14
PI	2.05E-7	2.05E-6	0	200	200	13-14

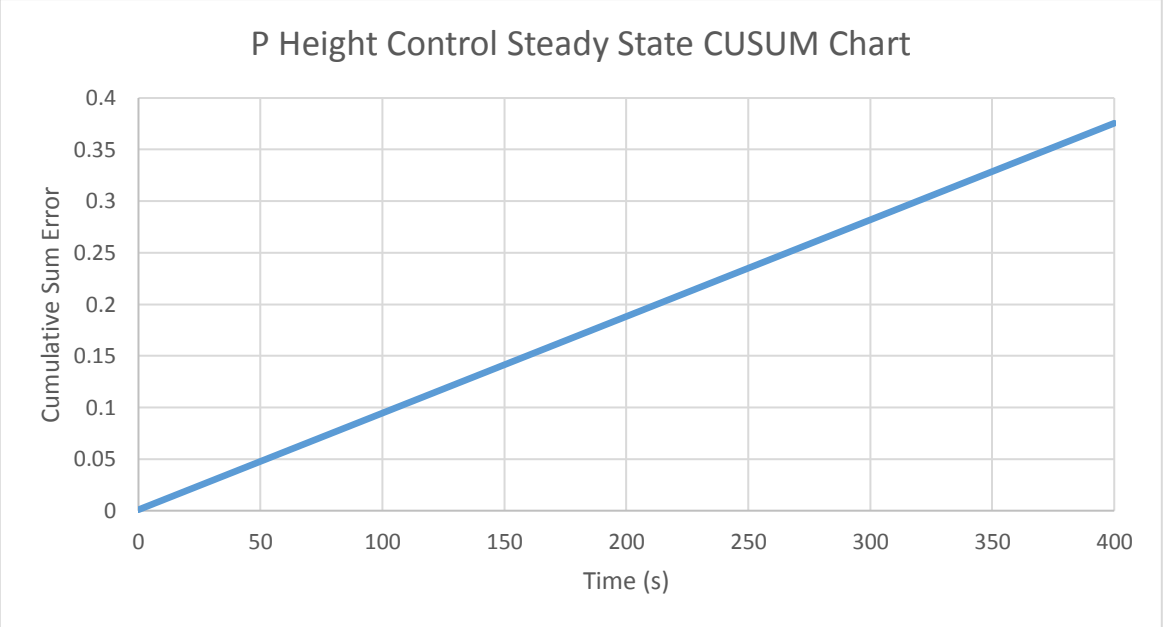

FIGURE 49 P HEIGHT CONTROL STEADY STATE CUSUM CHART

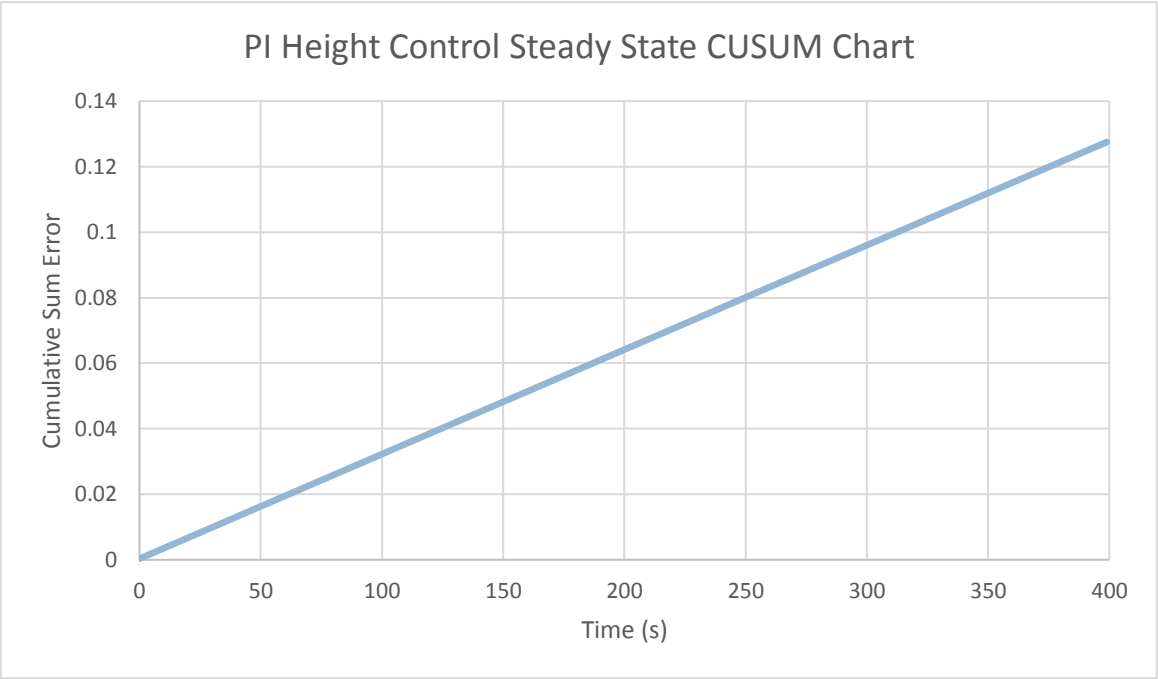

FIGURE 50 PI HEIGHT CONTROL STEADY STATE CUSUM CHART

4.3.1.2.2 CONDUCTIVITY CONTROLLERS

CUSUM charts were also utilised to assess the performance of each conductivity controller at steady state. Both the P and PI controllers for holding tank conductivity results are shown in Figure 51 and Figure 52. Again, as with the height controllers, there was a persistent offset present for both controllers. As with the height controllers, the P controller exhibited a larger offset than the PI controller. Table 8 shows that both controllers performed fairly poorly under these criteria.

TABLE 8 CONDUCTIVITY CONTROLLER CUSUM RESULTS

Controller	K	H	C- Signals	C+ Signals	Total	Expected
P	$1.91*10^{-11}$	$1.91*10^{-10}$	0	200	200	13-14
PI	$7.74*10^{-4}$	$7.74*10^{-3}$	0	200	200	13-14

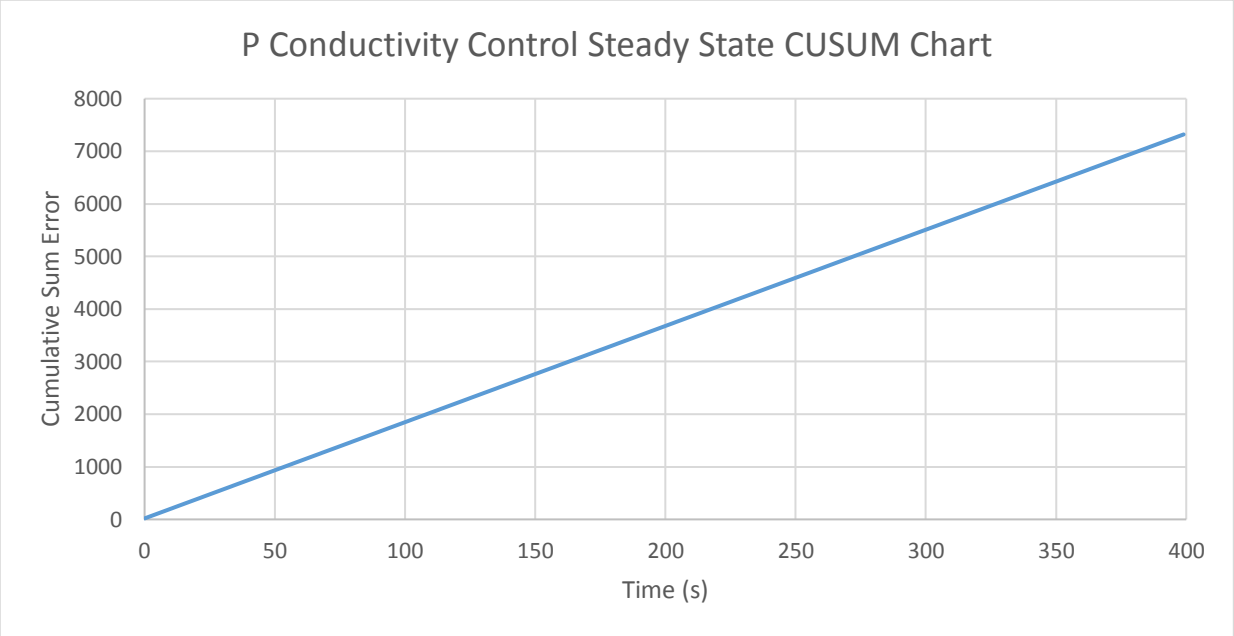

FIGURE 51 P CONDUCTIVITY CONTROL STEADY STATE CUSUM CHART

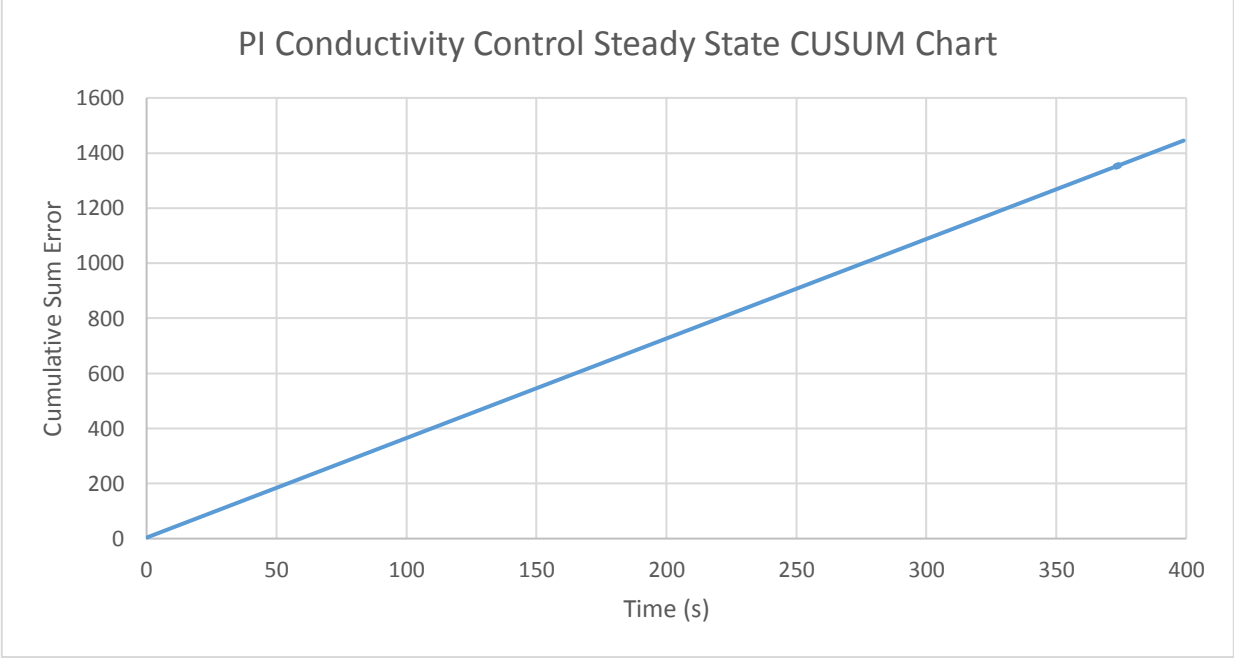

FIGURE 52 PI CONDUCTIVITY CONTROL STEADY STATE CUSUM CHART

4.3.2 ERROR BASED CRITERIA

Error based criteria are a measure of control system performance over a given period. For a closed-loop system response, the error can be defined as [12]:

$$e(t) = y_{sp}(t) - y(t) \tag{61}$$

Time integral error criteria quantify this error over time. This error can be identified for [12]:

- Set point tracking;
- Disturbance rejection.

Four methods commonly applied include:

- Integral of the Absolute value of the Error (IAE) [12];

$$IAE = \int_o^t |e(t)|dt \tag{62}$$

- Integral of the Squared Error (ISE) [12];

$$ISE = \int_0^t e(t)^2 dt \tag{63}$$

- Integral of the Time-Weighted Absolute Error (ITAE) [12];

$$ITAE = \int_o^t t|e(t)|dt \tag{64}$$

- Integral of the Time-Weighted Squared Error (ITSE) [78];

$$ITSE = \int_o^t te(t)^2 dt \tag{65}$$

ISE penalises large deviations from the set point. More aggressive control schemes score well under this error criterion. By contrast, ITAE and ITSE heavily penalise deviations that persist over time. Conservative control schemes score well under ITAE and ITSE. Typically, ITAE is used over ITSE as ITAE is more likely to punish small deviations over extended periods [78]. IAE does not place a higher importance on either type of control scheme. Therefore, IAE favours control schemes between those favoured by ISE and ITAE [73]. It is evident, therefore to select controller settings such that they are satisfactory for the set point tracking and disturbance rejection scenarios.

4.3.2.1 HEIGHT CONTROLLERS

The performance of each height controller was assessed using integral error criteria. This is discussed in more detail below.

4.3.2.1.1 SET POINT TRACKING

Each simulation was run for a period of 1000 seconds with a 1 second time interval. A set point change was implemented 10 seconds into the simulation to change the height set point from 0.2475m (steady state) to 0.3m. The results for each controller response are shown on one plot in Figure 53. Integral error criteria was applied to the performance of each controller for set point tracking during this set point change. These results are tabulated in Table 9.

TABLE 9 HEIGHT CONTROLLER SET POINT TRACKING INTEGRAL ERROR RESULTS

Controller	IAE	ISE	ITAE	ITSE
P	12.129	0.402	$2.113*10^3$	45.611
PI	12.081	0.415	$1.939*10^3$	47.542

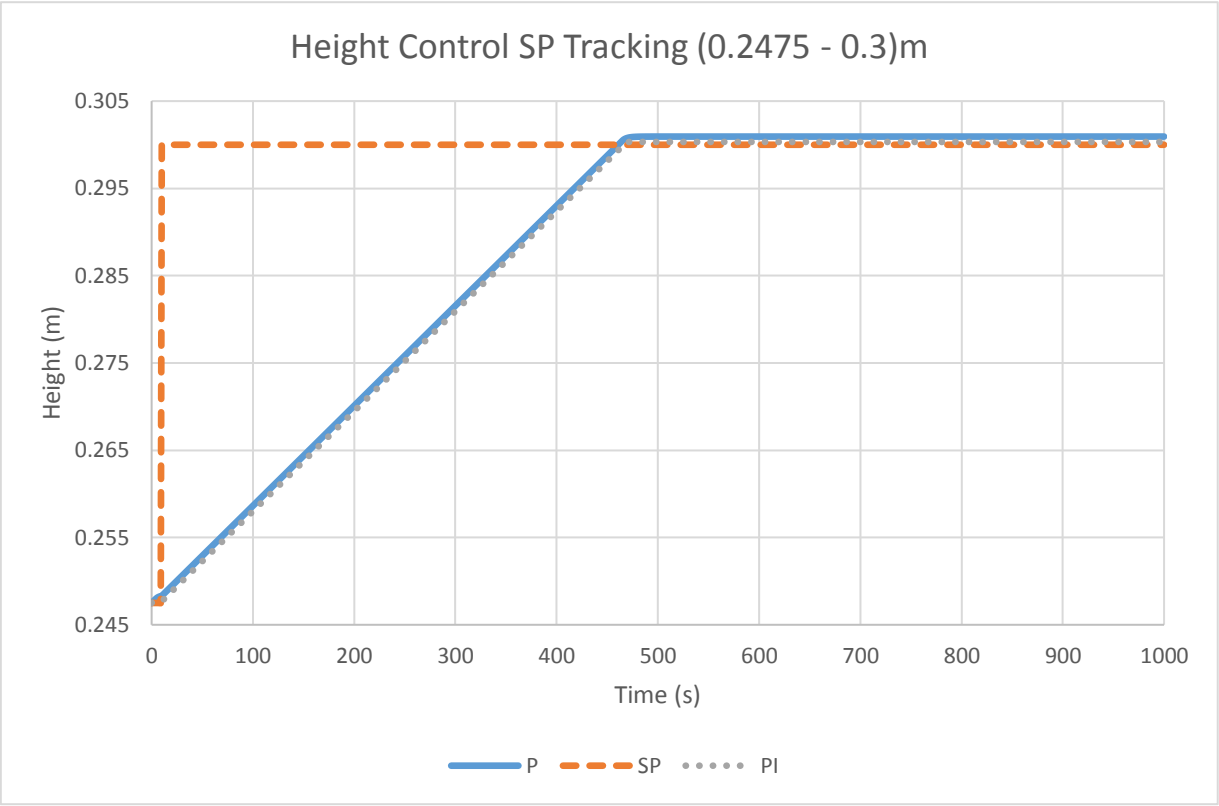

FIGURE 53 P AND PI HEIGHT CONTROL SP TRACKING

Interpretation of the tabulated integral error results showed that the P height controller exhibited a larger persistent offset than that exhibited by the PI height controller. This is evident in a higher ITAE result for the P controller. The P controller was deemed more aggressive as shown by a lower integral of squared error score. The PI controller had a more desired response. This is supported by the lower score in the integral of absolute value of error field. For set point tracking the PI controller exhibited the most desired response and was deemed most suitable.

4.3.2.1.2 DISTURBANCE REJECTION

For this test, the same data used for the Shewhart chart analysis was used. Figure 44 and Figure 45 shown earlier, display the plotted results of these simulations. These were run over 500 seconds with a one second time interval. A relevant disturbance was applied once the desired set point was reached as described earlier. Integral error criteria was applied to the performance of each controller for disturbance rejection during this simulation.

TABLE 10 HEIGHT CONTROLLER DISTURBANCE REJECTION INTEGRAL ERROR RESULTS

Controller	IAE	ISE	ITAE	ITSE
P	1.714	0.010	267.9	1.167
PI	1.833	0.012	268.7	1.446

By interpreting the integral error results tabulated in Table 10, it was found that the PI controller was less favourable in terms of disturbance rejection. The PI height controller performed worse in each integral error criteria category in this circumstance. This is somewhat expected as the PI controller has a lower associated gain, making it less aggressive. The introduction of the integral term also means controller response is slower than that exhibited by the P height controller.

4.3.2.2 CONDUCTIVITY CONTROLLERS

Integral error criteria was used to assess the performance of each conductivity controller implemented in the simulation. This is discussed in more detail below.

4.3.2.2.1 SET POINT TRACKING

Each simulation was again run for a period of 1000 seconds with a 1 second time interval. A set point change was again implemented 10 seconds into the simulation to change the conductivity set point from 15488μS/cm (steady state) to 15000μS/cm. The results of each controller response are shown on one plot in Figure 54. Integral error criteria was again applied to the performance of each controller for set point tracking during this set point change. These results are tabulated in Table 11.

TABLE 11 CONDUCTIVITY CONTROLLER SET POINT TRACKING INTEGRAL ERROR RESULTS

Controller	IAE	ISE	ITAE	ITSE
P	$33.34*10^3$	$5.543*10^6$	$9.323*10^6$	$254.53*10^6$
PI	$19.60*10^3$	$5.231*10^6$	$2.139*10^6$	$96.64*10^6$

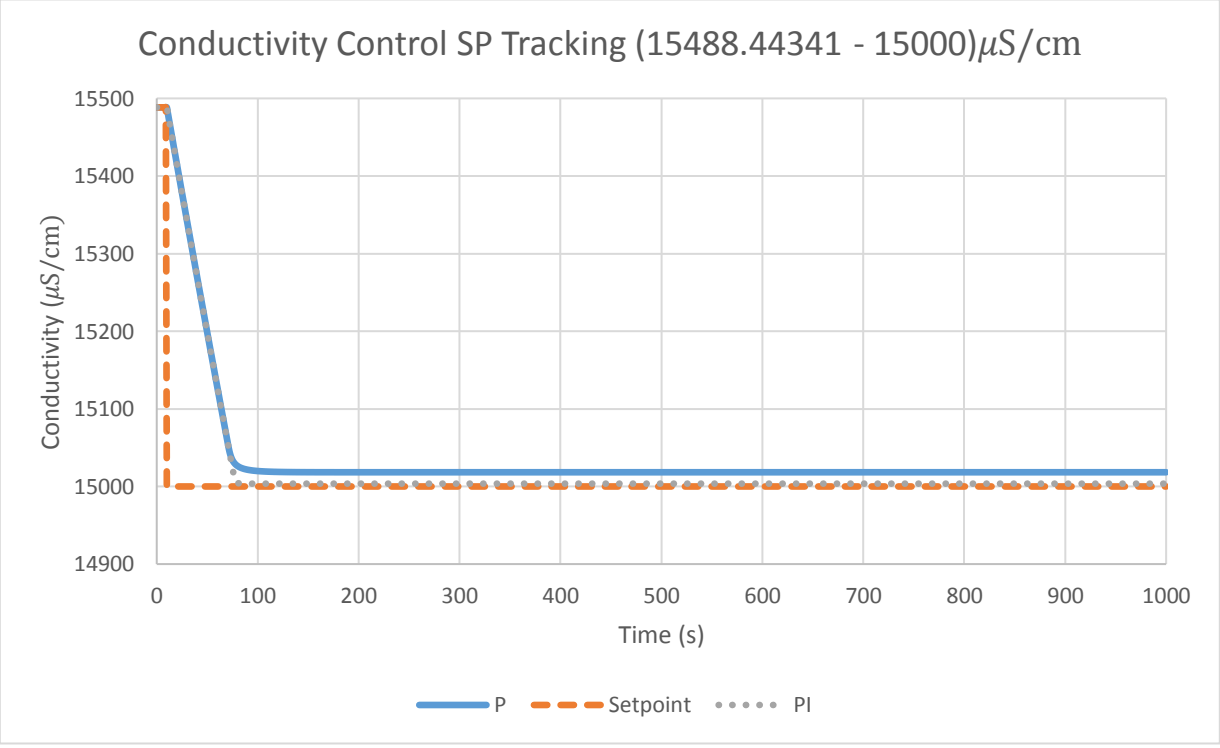

FIGURE 54 P AND PI CONDUCTIVITY CONTROL SP TRACKING

Interpretation of the tabulated integral error results showed that the P height controller again exhibited a larger persistent offset than that exhibited by the PI height controller. This is evident in a higher integral of time-weighted error result for the P controller. The P controller was deemed to have displayed a higher offset. This is supported by a higher integral of squared error score. The PI controller was found to exhibit a more desired response. This is supported by the lower score in all the integral error fields. For set point tracking the PI controller exhibited the most desired response and was deemed most suitable.

4.3.2.2.2 DISTURBANCE REJECTION

For this test, the same data used for the Shewhart chart analysis discussed earlier was again utilised. Figure 47 and Figure 48 show the plotted results of these simulations. This was again over a period of 500 seconds with a one second time interval. A relevant disturbance was applied once the desired set point was reached as described earlier. Integral error criteria was applied to the performance of each controller for disturbance rejection during this simulation.

TABLE 12 CONDUCTIVITY CONTROLLER DISTURBANCE REJECTION INTEGRAL ERROR RESULTS

Controller	IAE	ISE	ITAE	ITSE
P	$1.248*10^{3}$	$317.969*10^{3}$	$3.067*10^{6}$	$78.212*10^{6}$
PI	$6.152*10^{6}$	$92.312*10^{9}$	$17.564*10^{9}$	$2.6361*10^{13}$

By interpreting the integral error results tabulated in Table 12, it was again found that the PI controller was less favourable in terms of disturbance rejection. The PI height controller performed worse in each integral error criteria category. This is somewhat expected as the PI controller has a lower associated gain, making it less aggressive. The introduction of the integral term also means controller response is slower than that exhibited by the P height controller. It was found that overall the performance of the PI controller in both scenarios made it the more appropriate controller for both process variables.

4.4 FOUNDATION FIELDBUS H1 NETWORK IMPLEMENTATION

A Foundation Fieldbus H1 network required implementation in the pilot plant as part of this project scope. How this was achieved is outlined below.

4.4.1 NETWORK TOPOLOGY

Foundation Fieldbus (FF) networks operate on a trunk and spur topology. For this type of wiring scheme, a trunk cable acts as a bridge between a DCS or appropriate interfacing module and field instrumentation or devices. If there are multiple field devices, these can be connected via a spur cable with the aid of a segment or device coupler. These segment couplers can be located either in a control room or within the plant in a junction box. Terminators are required at each end of a trunk cable within a FF network. This is to prevent signal reflections causing distortion. Terminators are often built into FF power supplies and segment couplers. They can also be separate devices [52]. An example FF network is shown in Figure 55 (For simplicity, wire pairs are denoted as a single line in this figure).

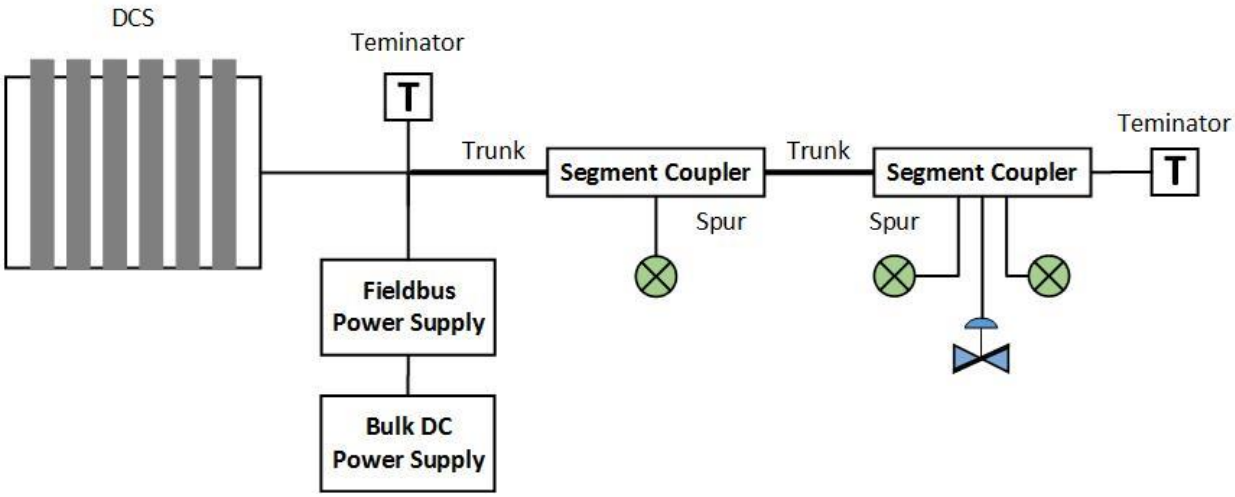

FIGURE 55 COMMON FIELDBUS SEGMENT CONFIGURATION – ADAPTED FROM [52]

4.4.2 CABLING SELECTION AND INSTALLATION

Correct Fieldbus network implementation requires the use of cabling compliant with the FF-844 standard. This standard ensures that cable rated for high temperatures and harsh conditions is selected. The cable comprises of twisted pair wires. This reduces the effects of external noise. A foil shield over the twisted pair reduces this effect further. Further cabling considerations beyond the standard include the use of 16 American Wire Gauge (AWG) (1.5mm^2) cable for trunks and 18 AWG (0.75mm^2) cable for spurs. Trunk cabling is usually longer, while spur cabling is shorter [52]. Existing field instrument wiring from the 4-20 mA field instrument was able to be repurposed for the purposes of implementation of a sample FF H1 network. This is possible because the wiring requirements were met by the existing instrument wiring.

4.4.3 CONNECTION OF DEVICES

Segment couplers are the standard method of connecting field devices to a Fieldbus segment. Compliance with the FF-846 standard for device couplers created by the Fieldbus Foundation ensures that minimum conditions are met. These include input impedance and voltage drop amongst others. A major advantage introduced by segment couplers is the introduction of current limiting capability. This prevents a short circuit on a spur connection rendering the entire segment out of service [52].

For this project, a F2-SP-IC04 Fieldbus Segment Coupler from vendor Pepperl+Fuchs was sourced and installed. This segment coupler is fully enclosed and able to be field mounted. A coupler with 4 spur connections was chosen to allow for expansion of the implemented FF network in future. This unit has status lights, diagnostics and an integrated Fieldbus terminator selectable via a jumper. The short circuit current limitation can also be adjusted [79].

4.4.4 FIELDBUS SEGMENT DESIGN

There are several factors that have a direct influence on Foundation Fieldbus segment design [52]:

- Power Distribution;
- Distance;
- Control System;
- Process Criticality;
- Area Classification.

All of these areas were taken into consideration when designing the implemented FF H1 network within the EPP.

4.4.4.1 POWER DISTRIBUTION

The Fieldbus power supply voltage, the resistance of the cable wiring and device current draw all contribute to limiting the number of devices that can be added to a FF H1 segment. These calculations can become quite complicated when adding multiple devices to a segment at different places. For this reason, online calculators available from Fieldbus power supply vendors can be utilised. An example of such a calculator is that available from the Pepperl+Fuchs website [80]. Device characteristics, the type of power supply, cable type and lengths are entered into the calculator. The program will advise the health of the segment: good, marginal or bad [52].

4.4.4.2 DISTANCE

Distance limitations on the network are dictated by the Fieldbus standard. A maximum allowable spur length of 120m must be considered. Additionally, the total length of the segment wiring (trunk length and spur lengths) must be less than 1900 m [52].

4.4.4.3 CONTROL SYSTEM

Although rarely the limiting factor when determining the maximum number of devices allowable of a Fieldbus segment, most control systems support a maximum of 16 devices per Fieldbus I/O card [52]. This also happens to be the device limit per H1 segment for the FIM4 device implemented in the current Honeywell Experion PKS DCS in the EPP [81].

4.4.4.4 PROCESS CRITICALITY

Plant-specific design requirements limit the number of devices and control elements per H1 segment. This can also have a contributing factor to the number of permissible devices. [52]

4.4.4.5 AREA CLASSIFICATION

Implementation of a H1 network in an area classified as hazardous can limit permissible cable lengths and the number of devices per H1 segment [52]. Hazardous area classification and its application to segment design are considered beyond the scope of this thesis as the EPP is considered a safe area with no hazardous area concerns.

4.4.5 H1 NETWORK INSTALLATION

With assistance from EPP technical staff, a sample FF H1 network was successfully implemented within the EPP. There were several challenges with this implementation as the single segment power conditioner utilised did not have clear wiring instructions for how this was to connect to the FIM4 module power supply 16 pin J6 connection point [53]. It was eventually found that pins 2 and 4 of the J6 connection on the FIM4 IOTA respectively were to be the positive and negative conditioned power connections for H1 Link 1. A diagram of the wiring connections used to implement the network can be located in Appendix H EPP Foundation Fieldbus H1 Network Wiring Diagram for reference.

4.4.6 IMPLEMENTATION INTO EXPERION

Once the physical layer wiring required for the H1 segment was implemented, Experion implementation could commence. A complete guide for how this was achieved can be viewed via Appendix G Foundation Fieldbus Device Addition Guide for Experion. This guide details what to expect within Experion Control Builder once the network is up and running after the installation and how to commission a new un-commissioned device.

5 FUTURE WORKS

As much of the work completed during this thesis scope revolved around design and planning, the implementation of the proposed design is left to future thesis students. It is recommended that this thesis act as a starting point for any future students intending to implement this proposed design or add devices onto the Fieldbus network in future.

The following tasks are awaiting action from future students:

- Install all required plant and instrumentation (outlined at beginning of report)
- Install all interconnecting cabling and tubing between instruments and DCS
- Several instruments can be made to communicate with Foundation Fieldbus communications while others can utilise 4-20mA communications
- New Instrumentation will need to be programmed into Experion via Control Builder
- HMI Web Builder will need to be utilised to update user HMIs
- The new section of the plant can be run and system models obtained
- These can be compared to the model derived from base principles
- More complex control strategies can be implemented

6 CONCLUSION

There were many challenges met during the planning and design stage of this project. Budget limitations, labour availability, and a continually changing thesis focus were three significant factors limiting the implementation stage. Working within these limitations, a proposed design solution was incepted. All of the required instrumentation and plant was next identified. Extensive research was undertaken during this phase, to ensure the right equipment was chosen for the proposed design.

A process model was then created from fundamental principles through the use of differential equations derived from both a total and salt component mass balance. This model was then simulated in Simulink. Both P and PI controllers were created via means of direct synthesis. The performance of these controllers was then analysed in depth in regards to steady state stability, set point tracking and disturbance rejection. PI control was deemed to be the most appropriate control scheme for control of both the holding tank height and conductivity.

A Foundation Fieldbus network was successfully implemented within the pilot plant. The purpose of this was to provide a new communications network for future plant and instrumentation in the plant to communicate back to the existing Honeywell Experion DCS. As there was only one Fieldbus device available, a Honeywell pressure differential transmitter was installed on this network. This instrument was then commissioned via the Experion Control Builder software for future implementation in pilot plant code. Three remaining spur connections on this network were left available for future Foundation Fieldbus compatible instrumentation.

7 REFERENCES

[1] C. Schmitz, Handbook of Aluminium Recycling, Germany: Vulkan-Verlag GmbH, 2006.

[2] Honeywell, "Experion PKS," 2017. [Online]. Available: https://www.honeywellprocess.com/en-US/explore/products/control-monitoring-and-safety-systems/integrated-control-and-safety-systems/experion-pks/Pages/default.aspx. [Accessed 6 August 2017].

[3] Honeywell, "Experion C300 Controller," [Online]. Available: https://www.honeywellprocess.com/library/marketing/notes/exp_c300_pin.pdf. [Accessed 11 August 2017].

[4] Murdoch University, "School of Engineering and Information Technology. The Bayer Pilot Plant," 2106. [Online]. Available: http://www.murdoch.edu.au/School-of-Engineering-and-Information-Technology/Facilities/The-Bayer-Pilot-Plant/. [Accessed 9 August 2017].

[5] Murdoch University, "ENG322 Process Control Engineering II Unit Overview and Prerequisities," 2016. [Online]. Available: https://moodleprod.murdoch.edu.au/mod/page/view.php?id=599625. [Accessed 8 August 2017].

[6] Murdoch University, "Instrumentation and Control Systems Design (ENG445)," 2016. [Online]. Available: http://handbook.murdoch.edu.au/units/details/?unit=ENG445. [Accessed 1 August 2018].

[7] A. Punch, "Implementation of Advanced Control Technology in the Murdoch University Pilot Plant," Murdoch University, Perth, 2009.

[8] S. Mackay, "Development of Murdoch University Pilot Plant Maintenance & Demonstration Programs," Murdoch University, Perth, 2012.

[9] J. Dring, "Pilot Plant Automation," Murdoch University, Perth, 2012.

[10] T. Meiri, "Experion Simulation and Pilot Plant Maintenance," Murdoch University, Perth, 2015.

[11] D. Pol, "Implementation of Conductivity Sensors in the Murdoch University Pilot Plant," Murdoch University, Perth, 2016.

[12] J. A. Romagnoli and A. Palazoglu, Introduction to Process Control, Boca Raton: CRC Press, 2012.

[13] N. Ghasem and R. Henda, Principles of Chemical Engineering Processes: Material and Energy Balances, Second Edition, Boca Raton: CRC Press, 2014.

[14] Water Corporation, "Trade Waste," [Online]. Available: https://www.watercorporation.com.au/home/business/trade-waste. [Accessed 5 November 2017].

[15] Water Corporation, “Acceptance criteria for trade waste - Information sheet 6,” [Online]. Available: https://www.watercorporation.com.au/-/media/files/business/trade-waste/applying-to-discharge/acceptance-criteria.pdf. [Accessed 10 August 2017].

[16] T. Andersson and P. Pucar, “Estimation of residence time in continuous flow systems with dynamics,” *University of Linkoping, Department of Electrical Engineering,* Vols. S-581, no. 83, 1995.

[17] B. G. Liptak, Ed., Instrument Engineers' Handbook: Process Control, 3rd ed., Florida: CRC Press LLC, 1999.

[18] R. P. Singh and D. R. Heldman, Introduction to Food Engineering Fourth Edition, London: Academic Press, 2009.

[19] Lightnin, “Lightnin MIxers General Overview,” 28 April 2014. [Online]. Available: http://www.spxflow.com/en/assets/pdf/B-937%20LIGHTNIN%20General%20Brochure%20US.5.20.14_tcm11-9420.pdf. [Accessed 30 July 2018].

[20] Butterworth-Heinemann, Instrumentation Reference Book, vol. IV, W. Boyes, Ed., London: Elsevier Science & Technology, 2009.

[21] R. L. Miller, W. L. Bradford and N. E. Peters, “Specific Conductance: Theoretical Considerations and Application to Analytical Quality Control,” *United States Geological Survey Water Supply Paper 2311,* 1982.

[22] Endress+Hauser, “Operating Instructions Liqiuline CM442/CM444/CM448,” 30 May 2018. [Online]. Available: https://portal.endress.com/wa001/dla/5000301/8271/000/10/BA00444CEN_2318.pdf. [Accessed 8 August 2018].

[23] Endress+Hauser, “Technical Information Liquiline CM442/CM444/CM448,” 13 June 2018. [Online]. Available: https://portal.endress.com/wa001/dla/5000299/4131/000/09/TI00444CEN_2118.pdf. [Accessed 8 August 2018].

[24] Endress+Hauser, “Digital conductivity sensor Indumax CLS50D,” 2016. [Online]. Available: https://www.au.endress.com/en/Field-instruments-overview/liquid-analysis-product-overview/conductivity-toroidal-sensor-cls50d. [Accessed 8 August 2018].

[25] Endress+Hauser, “Technical Information Indumax CLS50D/DLS50,” 2015. [Online]. Available: https://portal.endress.com/wa001/dla/5000557/6415/000/07/TI00182CEN_1615.pdf. [Accessed 7 August 2018].

[26] Honeywell, “Technical Information ST 3000 SMart Pressure Transmitter Series 900 Differential Pressure Models,” January 2013. [Online]. Available: https://www.honeywellprocess.com/library/marketing/tech-specs/34-ST-03-65.pdf. [Accessed 1 August 2018].

[27] D. R. Gillum, Industrial Pressure, Level and Density Measurement, North Carolina: International Society of Automation, 2009.

[28] Emerson, “Baumann 51000 High-Pressure, Low-Flow Control Valve Product Bulletin,” September 2017. [Online]. Available: http://www.emerson.com/documents/automation/product-bulletin-baumann-51000-high-pressure-low-flow-control-valve-en-122776.pdf. [Accessed 8 August 2018].

[29] S. Ebnesajjad, Expanded PTFE Applications Handbook: Technology, Manufacturing and Applications, New York: Elsevier, 2016.

[30] O. A. Babatunde and R. W. Harmon, Process Dynamics, Modeling and Control, New York: Oxford University Press, 1994.

[31] R. Darby, Chemical Engineering Fluid Mechanics 2nd edition, New York: Marcel Dekker Inc., 2001.

[32] W. S. Janna, Introduction to Fluid Mechanics Fifth Edition, New York: CRC Press, 2015.

[33] International Organization for Standardization, *ISO/TR 3666:1998 Viscosity of water 2nd Edition,* Geneva: International Organization for Standardization, 1998.

[34] A. B. Corripio and C. A. Smith, Principles and Practice of Automatic Process Control, New York: John Wiley & Sons Inc., 1997.

[35] Yokogawa Electric Coporation, “General Specifications EJX115A Low Flow Transmitter,” June 2017. [Online]. Available: https://web-material3.yokogawa.com/GS01C25K01-01EN.pdf?_ga=2.236914312.80403291.1536627233-694305752.1536206823. [Accessed 7 September 2018].

[36] Yokogawa Electric Corporation, “General Specifications EJX Series Foundation Fieldbus Communication,” June 2017. [Online]. Available: https://web-material3.yokogawa.com/GS01C25T02-01EN.pdf?_ga=2.12020468.1940564394.1537335072-694305752.1536206823. [Accessed 7 September 2018].

[37] B. G. Liptak, Ed., Flow Measurement, Radnor, Pennsylvania: Chilton Book Company, 1993.

[38] R. C. Baker, Flow Measurement Handbook: Industrial Designs, Operating Principles, Performance, and Applications 2nd Edition, New York: Cambridge University Press, 2016.

[39] Parker Hannifin Corporation, “A Complete Range of Solenoid Valves for Fluid Control: General Catalogue,” August 2014. [Online]. Available: http://www.parker.com/Literature/Fluid%20Control%20Division%20Europe/English%20Catalogues/FCDE%200110UK.pdf. [Accessed 10 July 2018].

[40] Liquiflo Chemical Processing Pumps, “Model H7F Heavy Duty Industrial Gear Pump,” [Online]. Available: http://www.liquiflo.com/v2/gears/h/h7f.htm. [Accessed 2018 July 15].

[41] L. Nelik, Centrifugal & Rotary Pumps: Fundamentals With Applications, London: CRC Press, 1999.

[42] Liquiflo, “H-Series & 3-Series Sealed Gear Pumps Installation, Operation & Mantenance Manual,” February 2015. [Online]. Available: http://www.liquiflo.com/v2/manual/IOM-3&H-Sealed-Small.pdf. [Accessed 25 July 2018].

[43] Liquiflo, “External gear pump principle of operation & advantages,” 2015. [Online]. Available: http://www.liquiflo.com/v2/files/pdf/Gear_Pump_Basics.pdf. [Accessed 1 August 2018].

[44] Danfoss Drives, “VLT HVAC Drive FC 102,” 2018. [Online]. Available: http://drives.danfoss.com.au/products/vlt/low-voltage-drives/vlt-hvac-drive-fc-102/#/. [Accessed 7 September 2018].

[45] Danfoss, “Operating Instructions VLT HVAC DRive FC 102 1.1-90kW,” 25 February 2014. [Online]. Available: http://drives.danfoss.com.au/knowledge-center/technical-documentation/#/. [Accessed 5 September 2018].

[46] National Instruments, “Fieldbus: Foundation Fieldbus Overview,” August 2011. [Online]. Available: http://www.ni.com/pdf/manuals/370729c.pdf. [Accessed 5 November 2017].

[47] Emerson Exchange, “Fieldbus Tutorial - Part 11 HSE Fieldbus,” 11 November 2010. [Online]. Available: https://www.slideshare.net/EmersonExchange/fieldbus-tutorial-part-11-hse-fieldbus. [Accessed 25 October 2017].

[48] I. Verhappen and A. Pereira, Foundation Fieldbus, USA: ISA, 2008.

[49] Emerson Process Management, “FOUNDATION fieldbus H1 or Profibus PA?,” 2002. [Online]. Available: http://www2.emersonprocess.com/siteadmincenter/PM%20Central%20Web%20Documents/Eng%20Sch%20-%20Buses%20301.pdf. [Accessed 20 October 2017].

[50] Honeywell, “FOUNDATION Fieldbus Integration,” 2017. [Online]. Available: https://www.honeywellprocess.com/en-US/explore/products/control-monitoring-and-safety-systems/integrated-control-and-safety-systems/experion-pks/open-protocol-integration/Pages/foundation-fieldbus-integration.aspx. [Accessed 1 November 2017].

[51] Fieldbus Foundation, “Technical Overview Foudation Fieldbus,” 2003. [Online]. Available: http://www.fieldbus.org/images/stories/technology/developmentresources/development_resources/documents/techoverview.pdf. [Accessed 10 September 2018].

[52] Relcom Inc., “Fieldbus Wiring Guide 4th Edition,” 2011. [Online]. Available: http://www.relcominc.com/pdf/501-123%20Fieldbus%20Wiring%20Guide.pdf. [Accessed 9 September 2018].

[53] Honeywell, “Experion PKS Series C Fieldbus Interface Module User's Guide,” February 2018. [Online]. Available: https://www.honeywellprocess.com/library/support/Public/Documents/Series-C-Fieldbus-Interface-Module-Users-Guide-EPDOC-X125-en-431.pdf. [Accessed 20 July 2018].

[54] Pepperl+Fuchs, “KLD2-FBPS-1.25.360 Fieldbus Power Supply Data Sheet,” 30 June 2016. [Online]. Available: https://files.pepperl-fuchs.com/webcat/navi/productInfo/edb/189514_eng.pdf?v=20181109000110. [Accessed 1 September 2018].

[55] smar, “smar - IF302 Triple Channel Current to Fieldbus Converter Operation & Maintenance Instructions Manual,” July 2016. [Online]. Available:

http://www.smar.com/en/product/if302-if302-triple-channel-current-to-foundationtm-fieldbus-converter. [Accessed 1 August 2018].

[56] M. Cvijetic, Optical Transmission Systems Engineering, Boston: Artech House, 2004.

[57] C. K. Alexander and M. N. O. Sadiku, Fundamentals of Electric Circuits 3rd Edition, New York: McGraw-Hill Higher Education, 2007.

[58] B. R. Mehta and Y. J. Reddy, Industrial Process Automation Systems: Design and Implementation, Amsterdam: Elsevier, 2015.

[59] Honeywell, "EXPERION PKS OVERVIEW," 2016. [Online]. Available: https://www.honeywellprocess.com/library/marketing/brochures/Experion-Brochure-2016.pdf. [Accessed 3 November 2017].

[60] Honeywell, "Experion CEE-based Controllers and I/O Overview," July 2010. [Online]. Available: http://www.izoformltd.com.tr/upload/files/Kontrol_Cihazlari/2180b_EP03-CEE-IO-Ovr-R400V1-eop.pdf. [Accessed 10 November 2017].

[61] Honeywell International Sàrl, "Experion Configuration Studio Overview Guide," February 2014. [Online]. Available: https://www.honeywellprocess.com/library/support/Public/Documents/Configuration_Studio_Overview_Guide_EXDOC-X113-en-110.pdf. [Accessed 10 November 2017].

[62] Honeywell International Sàrl, "Experion HMIWeb Display Building Guide," February 2014. [Online]. Available: https://www.honeywellprocess.com/library/support/Public/Documents/HMIWeb_Display_Building_Guide_EXDOC-XX54-en-110.pdf. [Accessed 12 November 2017].

[63] Honeywell, "Experion Station Specification," February 2015. [Online]. Available: http://www.lesman.com/unleashd/catalog/control/Honeywell-Experion-LX/HW-Experion-LX-station-ds-LX03-210-120-V1-2015-02.pdf. [Accessed 3 November 2017].

[64] G. S. Linoff, Data Analysis Using SQL and Excel, Indianapolis, Indiana: John Wiley & Sons, 2015.

[65] K. D. Lawrence, R. K. Klimberg and S. M. Lawrence, Fundamentals of Forecasting Using Excel, New York: Industrial Press Inc., 2009.

[66] S. C. Albright, W. Winston and C. Zappe, Data Analysis and Decision Making with Microsoft Excel, Revised, USA: Cengage Learning, 2008.

[67] I. D. Zaytsev and G. G. Aseyev, Properties of Aqueous Solutions of Electrolytes, London: CRC Press, 1992.

[68] J. Stewart, Calculus 7E, Belmont, CA: Cengage Learning, 2011.

[69] D. R. Lide and T. J. Bruno, CRC Handbook of Chemistry and Physics 95th Edition, New York: Bukupedia, 2014.

[70] A. D. McNaught and A. Wilkinson, Compendium of Chemical Terminology, Oxford: Blackwell Science Ltd, 1997.

[71] IC Controls, "Conductivity measurement in high purity water samples below 10 microSiemens/cm," 2012. [Online]. Available: https://iccontrols.com/wp-

content/uploads/art-4-2_conductivity_measurement_in_high_purity_water.pdf. [Accessed 10 October 2018].

[72] Mathworks, "Simulink," 2018. [Online]. Available: https://au.mathworks.com/products/simulink.html. [Accessed 15 August 2018].

[73] D. E. Seborg, T. F. Edgar, D. A. Mellichamp and F. J. Doyle III, Process Dynamics and Control, New Jersey: John WIley & Sons Inc, 2010.

[74] Mathworks, "System Identification Toolbox Product Description," 2018. [Online]. Available: https://au.mathworks.com/help/ident/gs/product-description.html. [Accessed 2 October 2018].

[75] R. E. Barlow and T. Z. Irony, "Foundations of Statistical Quality Control," *Current Issues in Statistical Inference: Essays in Honor of D. Basu,* vol. 17, pp. 99-112, 1992.

[76] P. Qiu, Introduction to Statistical Process Control, Boca Raton, FL: CRC Press, 2014.

[77] E. R. Ott, E. G. Schilling and D. V. Neubauer, Process Quality Control: Troubleshooting and Interpretation of Data, Michigan: McGraw-Hill, 2000.

[78] A. R. Rao, Process Control Engineering, Amsterdam: CRC Press, 1993.

[79] Pepperl+Fuchs, "Fieldbus Segment Protector F2-SP-IC Data Sheet," 25 January 2017. [Online]. Available: https://files.pepperl-fuchs.com/webcat/navi/productInfo/edb/t157545_eng.pdf?v=20180608101735. [Accessed 1 November 2018].

[80] Pepperl+Fuchs, "Pepperl+Fuchs Segment Checker," 2018. [Online]. Available: https://www.pepperl-fuchs.com/australia/en/segmentchecker.htm. [Accessed 10 October 2018].

[81] Honeywell, "Experion FOUNDATION Fieldbus Integration Product Information Note," September 2012. [Online]. Available: https://www.honeywellprocess.com/library/marketing/notes/Exp_Foundation_Fieldbus_PIN.pdf. [Accessed 15 August 2018].

[82] L. T. Vu, P. A. Bahri and G. R. Cole, "The use of the pilot plant facility in teaching process control engineering at Murdoch University," Murdoch University, Perth, 2010.

[83] C. E. Spergeon, Ethernet: The Definitive Guide, Sebastopol, CA: O'Reilly Media, Inc., 2000.

[84] Rockwell Automation, "Enhanced and Ethernet PLC-5 Programmable Controllers User Manual," July 2015. [Online]. Available: http://literature.rockwellautomation.com/idc/groups/literature/documents/um/1785-um012_-en-p.pdf. [Accessed 15 October 2017].

[85] Control and Thermal Engineering, "Case Study 13 Refining Process Pilot Plant for Murdoch University," [Online]. Available: http://www.cte.com.au/html/pdf/CASE13.PDF. [Accessed 25 September 2017].

[86] Danfoss, "Danfoss VLT® 5000 Instruction Manual," [Online]. Available: drives.danfoss.us/workarea/downloadasset.aspx?id=17179911542. [Accessed 10 October 2017].

[87] Badger Meter, “Reasearch Control Valves; Small Control Valve Type 808,” [Online]. Available: https://www.badgermeter.com/resources/4921cce2-6196-4a8f-baf4-7b8a8e61b98a/small%20control%20valve%20type%20808%20product%20data%20sheet%20rcv-ds-00569-en.pdf/. [Accessed 31 October 2017].

[88] B. Nesbitt, “Handbook of Valves and Actuators: Valves Manual International,” Butterworth-Heinemann, Great Britain, 2011.

[89] marshbellofram.com, “Type 1000 I/P & E/P Transducers,” [Online]. Available: https://www.marshbellofram.com/industrial/belloframindustrial/wp-content/uploads/2012/07/Type-1000-LT70201.pdf. [Accessed 29 October 2017].

[90] D. W. Spitzer, “Variable Speed Drives: Principles and Applications for Energy Cost Savings, Fourth Edition,” Momentum Press, New York, 2012.

[91] Danfoss, “Enhanced VLT® HVAC Drive FC 102,” [Online]. Available: http://drives.danfoss.com/products/vlt/low-voltage-drives/vlt-hvac-drive-fc-102/#/. [Accessed 8 August 2017].

[92] S. Mackay, E. Wright, J. Park and D. Reynders, Practical Industrial Data Networks: Design, Installation and Troubleshooting, Britain: Newnes, 2004.

[93] E. Hopkinson, “Murdoch University Pilot Plant Advanced Control Technology Upgrade,” Murdoch University, Perth, 2010.

[94] N. P. Mahalik, Fieldbus Technology: Industrial Network Standards for Real-Time Distributed Control, New York: Springer Science & Business Media, 2013.

[95] E. H. H. Lum, “Honeywell Experion System for Teaching Purposes,” Murdoch University, Perth, 2011.

[96] K. L. S. Sharma, Overview of Industrial Process Automation, Saint Louis: Elsevier Science, 2016.

[97] R. Bitter, T. Mohiuddin and M. Nawrocki, LabView: Advanced Programming Techniques, Second Edition, Boca Raton, FL: CRC Press, 2006.

[98] Honeywell, “Experion PKS Control Hardware and I/O Modules Firmware Upgrade Guide,” May 2018. [Online]. Available: https://www.honeywellprocess.com/library/support/Public/Documents/Control-Hardware-and-IO-Modules-Firmware-Upgrade-Guide-EPDOC-X150-en-500.pdf. [Accessed 1 August 2018].

[99] Encylopaedia Britannica Inc, “Alumina,” 2017. [Online]. Available: https://www.britannica.com/science/alumina#ref148550. [Accessed 27 September 2017].

[100] J. George and R. Vacca, “Murdoch University Pilot Plant,” Murdoch University, Perth, 2016.

[101] S. Godfrey, “Honeywell Experion System: Configuration, Simulation and Process Control Software Interoperability,” Murdoch University, Perth, 2016.

[102] Emerson Automation Solutions, “Control Valve Handbook Fifth Edition,” 2017. [Online]. Available: http://www.emerson.com/documents/automation/control-valve-handbook-en-3661206.pdf. [Accessed 7 August 2018].

[103] COOPER Crouse-Hinds, “F660A technical datasheet,” 9 April 2010. [Online]. Available: https://www.mtl-inst.com/images/uploads/datasheets/fieldbus/F660A.pdf. [Accessed 9 August 2018].

[104] MTL, “Technical Data MTL Fiedlbus Networks: F101/102 Low-power fieldbus power supply,” January 2016. [Online]. Available: https://www.mtl-inst.com/images/uploads/datasheets/fieldbus/EPS_F10x_5.pdf. [Accessed 10 September 2018].

[105] Australian Government; National Health and Medical Research Council, “National Water Quality Management Strategy: Australian Drinking Water Guidelines 6 2011 Version 3.5,” August 2018. [Online]. Available: https://nhmrc.gov.au/about-us/publications/australian-drinking-water-guidelines#block-views-block-file-attachments-content-block-1. [Accessed 15 September 2018].

APPENDICES

APPENDIX A DETAILED ENGINEERING PILOT PLANT OVERVIEW

The Bayer process EPP was first unveiled at Murdoch University in 1998 after extensive industry collaboration. Initially, an inert solid material and water was used to simulate a part of the Bayer process. For automation purposes, a high level Supervisory, Control And Data Acquisition (SCADA) system, SCAN3000 was implemented through collaboration with Honeywell. The associated software was run on a Windows server [82].

A Programmable Logic Controller (PLC), specifically an Allen-Bradley PLC5/20E was utilised to communicate with the SCAN3000 SCADA sever through Ethernet. Ethernet is a network protocol that controls the transmission of data over a Local Area Network (LAN) [83]. This PLC made use of ladder logic code style programming which is representative of relay logic [84]. This server then communicated to four operator workstations [85] [82].

The PLC had a generous Input/Output (I/O) capability supported on board. This included [86]:

- 48 digital inputs
- 41 digital outputs
- 59 analogue inputs
- 20 analogue outputs.

These 20 separate analogue outputs were connected to 10 pneumatic control valves and 10 Danfoss VLT5000 Variable Speed Drives (VSDs) [86]. These drives controlled the output to their associated positive displacement pumps within the EPP. These pumps in turn help move the process fluid throughout the plant [82] [7]. Research Control Valve branded bellows sealed globe control valves were operated via an

external input of pressurised air [87]. This was controlled by a regulator that is driven by a separate control signal [88].

In the EPP, this control was achieved by a Bellofram electro-pneumatic pressure transducer that is fed a 4-20 mA signal and through a transducer regulates the air supply to a pressure range of 3-15 pounds per square inch (PSI) output [89]. VSDs output an approximated sine wave at the desired frequency. This makes them the ideal component to alter the speed of rotating equipment like motors [90]. Within the EPP, these motors are directly coupled to the pumps they drive. At this initial implementation stage, the plant was an accurate representation of current technology in process control.

UPGRADE 1 – CONTROL (VSDS, CONTROL SYSTEM AND OPERATOR WORK STATIONS)

As part of a continuous improvement effort with the EPP, upgrades were implemented not long after the initial implementation of the plant. The previous VLT5000 model VSD's did not support networking capability or direct connection to a computer. This was one area identified for improvement in the first major upgrade scope of works.

During the delivery of this scope, the ten VLT5000 model VSD's were replaced by Danfoss FC102 VSD's. These later model VSD's supported Modbus communications across a Modbus network that was also established during the implementation of this upgrade [7] [91]. Modbus is a serial communications protocol that enables communication among many devices connected on the same network or bus. It operates as a master-slave type protocol capable of connecting with up to 247 slaves [92].

This was not the only change implemented in the EPP at this time. Another change, if not more important, was the replacement of the previous control system and implementation of new operator workstations for student use. The old system had operated on two distinct network topologies; Distributed Control

Systems (DCS) and SCADA systems. Automation would afterwards be achieved though the Honeywell Experion C300 controller utilising its Process Knowledge System (PKS) DCS [3] [2]. As part of the purchase agreement with Murdoch University, Honeywell undertook the migration of the existing PLC-5 control program to the new C300 controllers [7].

The sheer size of the work scope required to fully implement the control system upgrade meant that this was completed as part of a second thesis the following year. The scope of this was to complete all outstanding actions in the implementation of the new control system and most importantly provide documented guides for how to operate the EPP via Station or Excel. Operation procedures were also devised and submitted with this scope to aid in student understanding of the operation and configuration of the Experion PKS DCS. The plant was also relocated to the newly constructed Engineering and Energy Building that same year [93].

This upgrade brought about many advantages for the end user. For one, the old PLC had a scan time of two seconds and the old SCADA system, SCAN3000 had a refresh time of five seconds. This meant that plant data viewed in Station and utilised by students in automatic plant control in Microsoft excel was up to seven seconds old. By implementing the upgrade to Honeywell C300 controllers with an associated scan time of 50ms, end users would have access to plant information with much less delay. Microsoft Excel Data Exchange (MSEDE) server communication was established during this scope also. This allowed communication with Microsoft Excel with a one second refresh rate. Station R310 HMI displays were also provided as a direct result of this upgrade scope [93].

The Honeywell C300 control hardware and associated I/O modules contain:

- 32 channel digital input module (2 of)
- 32 channel digital output module (2 of)
- 16 channel analogue input module (2 of)
- 16 channel analogue output module (1 of)

This allowed for a much larger selection of plant instrumentation than what was initially conceived during the EPP's initial implementation and also allowed for future upgrades. It also opened up the possibility for installation of wireless and Foundation Fieldbus type instrumentation [93]. Foundation Fieldbus (FF) allows for bi-directional digital communication to multiple field instrument devices and operator stations with human machine interfaces (HMI) on a single pair cable network or bus [48] [94]. This is in contrast with the need for a dedicated cable for each field instrument as with the old control configuration in the EPP. Foundation Fieldbus, however, was not implemented in the pilot plant at this time.

UPGRADE 2 – PILOT PLANT MAINTENANCE AND DEMONSTRATION PROGRAMS

In 2012, the next major scope undertaken in regards to the existing EPP, was maintenance and demonstration programs. This included revising existing control system code to ensure that plant instrumentation was controlled and activated in a new way. This meant that when the mode was set to program, all device control function blocks were to be activated. Sequential control modules (SCM) were utilised to design and implement a maintenance and demonstration program. The maintenance program's intent was to increase the longevity of the EPP by exercising sections of the plant that were susceptible to seizing. This program was set to operate at 0800 hours every weekday morning for one minute. This cycled valves and actuators within the plant approximately 20 times. [8].

A demonstration program was also developed that was similar in nature to the maintenance program. It intended to allow for demonstration of the operation of the EPP when tours are being undertaken. Pumps

were only turned on when predefined conditions were met, negating the need for any input from an operator. This allowed the tour guide to simply press a button to initiate the demonstration program while focusing on explaining to the tour group of how the EPP operates. A final addition of this scope included minor upgrades to the control system code to allow for simpler operation of the EPP in future via the HMI's. All of these changes, however, were only implemented in the first half of the EPP as the second half was being used concurrently by ICE students for their studies. Code for the second half of the plant was written, but not implemented [9].

UPGRADE 3 – PILOT PLANT AUTOMATION

In the same year, another thesis project brought about the completion of the initial scope of automation of the EPP during periods of low utilisation. This was the culmination of separate efforts over several years. Secondary objectives were to improve and document system code, add hardware as required and servicing and replacement of plant components. Testing of this code before final implementation was achieved on a simulated controller implemented as part of an earlier thesis in 2011 [9] [95].

During this scope, issues with the operation of some of the instruments within the EPP was discovered and remedied. An interlock on the product pump that extracts process from the final Continuously Stirred Tank Reactor (CSTR) was resolved. Previously, an interlock compared the values of the product pump recycle flow rate and the other drain stream flow rate. If both values were below 1 the pump would be turned off. If, however, a flow meter was reading a high value when there was no actual flow of fluid, the pump would continue to turn over, potentially causing damage to it. It was eventually found that the recycle flow meter was producing incorrect readings due to air bubbles in the water. This was being caused by leaking seals on the product pump. The pump was repaired by tightening and applying grease to the seals [9].

A momentary push button was also installed on the right-hand side of the EPP main switchboard. This button could be used to initiate the automation program from the plant area allowing demonstrators to demonstrate plant operation with ease. A new light and siren were also installed to visually and audibly warn visitors to the EPP that it was about to start. The code was also amended so that the buzzer and light stay on for 8 seconds when an operator is in charge of the plant and after this time the siren ceases, however, the light stays on. This was done to increase safety in the EPP [9].

UPGRADE 4 – EXPERION SIMULATION AND PILOT PLANT MAINTENANCE

In 2015, a simulated Experion PKS control system was implemented using Laboratory Virtual Instrument Engineering Workbench (LabVIEW) and Open Platform Communications (OPC). OPC is an open standard that facilitates communication between different processes [96]. LabVIEW is a graphic based programming language developed by National Instruments [97]. This was achieved using a C300 controller and a HMI page specifically for this purpose. This work scope was not fully implemented. This was all formally documented for future reference. Existing guides and documentation relevant to the Experion PKS system were refined and restructured to aid future student understanding. At this stage, many interlocks were introduced into the control code to prevent previously existing issues from reoccurring. The code was also restructured and a lot of redundant code was removed to ease understanding [10].

New actuators and sensors were also installed within the EPP within this scope. Three-way valves installed throughout the plant on the Needle Tank underflow, cyclone underflow, lamella underflow and feed stream were a combination of Alternating Current (AC) and Direct Current (DC) pneumatic relays which had rusted. Replacement AC pneumatic relays were ordered but not installed. Solenoid valves were installed on the raw water and air supply points directly after the manual supply valves. This allowed for

the manual valves to be left open and for the maintenance or demonstration program to run at any time [10].

UPGRADE 5 – IMPLEMENTATION OF CONDUCTIVITY SENSORS

In 2016, Modbus conductivity sensors were installed within each of the CSTRs to allow for the implementation of conductivity testing for students. This included the use of a Liquiline CM444 transmitter and three Indumax CLS50D conductivity sensors. An existing dye tank was also utilised. From here an electrolytic solution of predetermined concentration is then pumped to each CSTR. This electrolytic solution comprises of a mixture of raw water and common table salt (NaCl). The clarification stage of the EPP also made use of an existing recycle stream that allows for this concentrate to be recycled back to any of the CSTR's for experimental purposes [11].

Upgrades were performed to the Experion system also to implement these changes into the control system code. The entire purpose of this scope was to increase the complexity associated with the precipitation stage of the EPP. Feedback control was successfully implemented on one and two tank conductivity systems. However, due to the large time constant of the conductivity system, multi-tank conductivity experiments were not completed. It was also identified at completion that the small size of the existing die tank places large restrictions on testing as it required refilling often [11].

APPENDIX B FIM4 EXPERION GUIDES

B.1 FIM4 IMPLEMENTATION INTO EXPERION VIA CONTROL BUILDER GUIDE

In order to implement a new FIM4 device successfully into a project in Experion via Control Builder, first several requirements must be met [53]:

- The user must have logged into “PPserver1” remotely with sufficient privileges;
- Configuration Studio must have been started and the Control Builder application launched;
- The applicable IP addresses for the FTE network and NTP servers must be configured;
- The user must have sufficient privileges to create control strategies within Control Builder;
- An appropriate device index is set on the IOTA via the selection switches for the FIM4 device.

Step 1: Add the FIM4 device to the Project tab of the Assignment Window

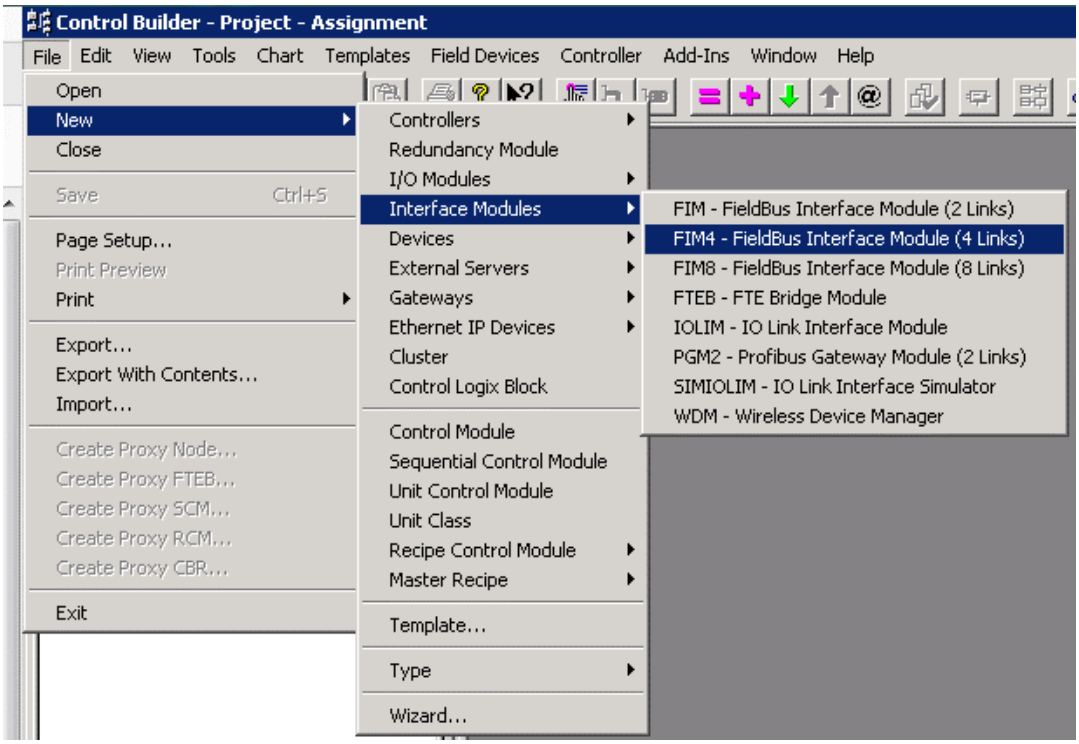

FIGURE 56 ADDING FIM4 DEVICE TO PROJECT TAB WITHIN ASSIGNMENT WINDOW

Path: *File-> New -> Interface Modules -> FIM4 – Fieldbus Interface Module (4 Links)*

If this step has been successful, the module should now appear in the project tab within the assignment window of Control Builder as shown in Figure 57.

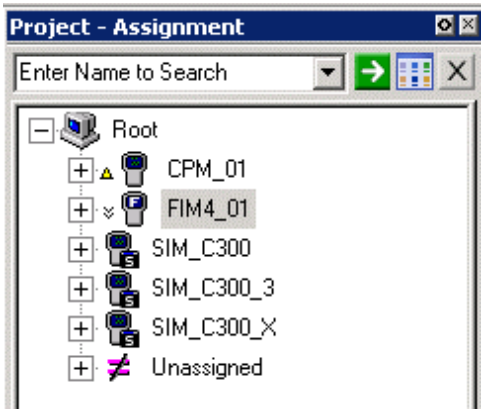

FIGURE 57 FIM4 DEVICE ADDED TO PROJECT TAB

Clicking on the cross located to the left of the FIM4 device in the tree within "Root" should show all the applicable FF links. For a FIM4 device, you should expect to see four of these as shown in Figure 58.

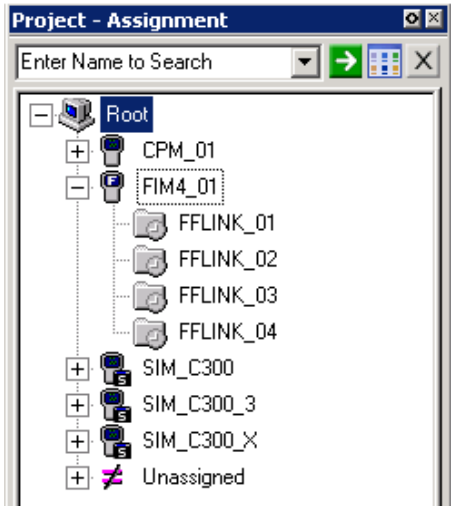

FIGURE 58 FOUNDATION FIELDBUS LINKS WITHIN FIM4 DEVICE IN PROJECT TAB

Step 2: Configure the Module Properties

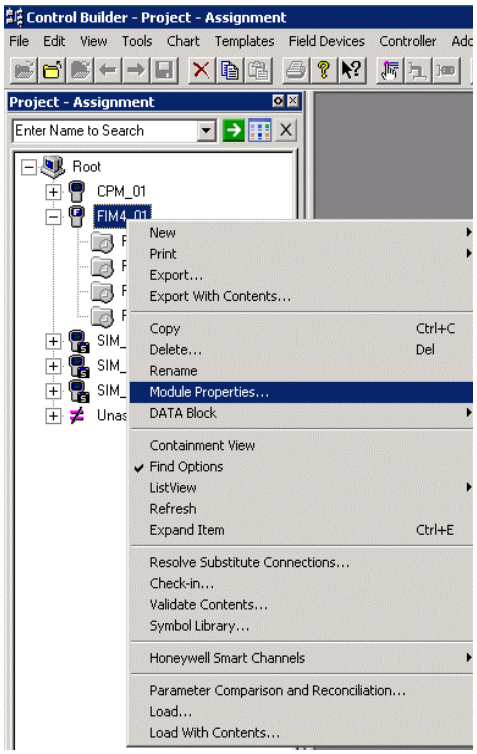

FIGURE 59 FIM4 DEVICE OPTIONS

Access the FIM4 device options menu by right-clicking on it within the project tab. A menu will appear as shown in Figure 59. Select “Module Properties”. The Parameters window shown in Figure 60 will appear. You can either choose to leave the auto-assigned Tag Name or replace it with one more appropriate for the application. Next, the device index must match that set via the physical switches on the IOTA that the FIM4 device is mounted on. The Ethernet IP address should automatically update once the Device Index number is entered. Suppression of the H1 power alarm is application specific. If a power conditioning solution is being utilised that does not integrate with the Series FIM4 device and does not connect to the power conditioner connecter on the IOTA, this should be checked. If you would like to like the device to an asset this detail is entered via the Associated Asset # field.

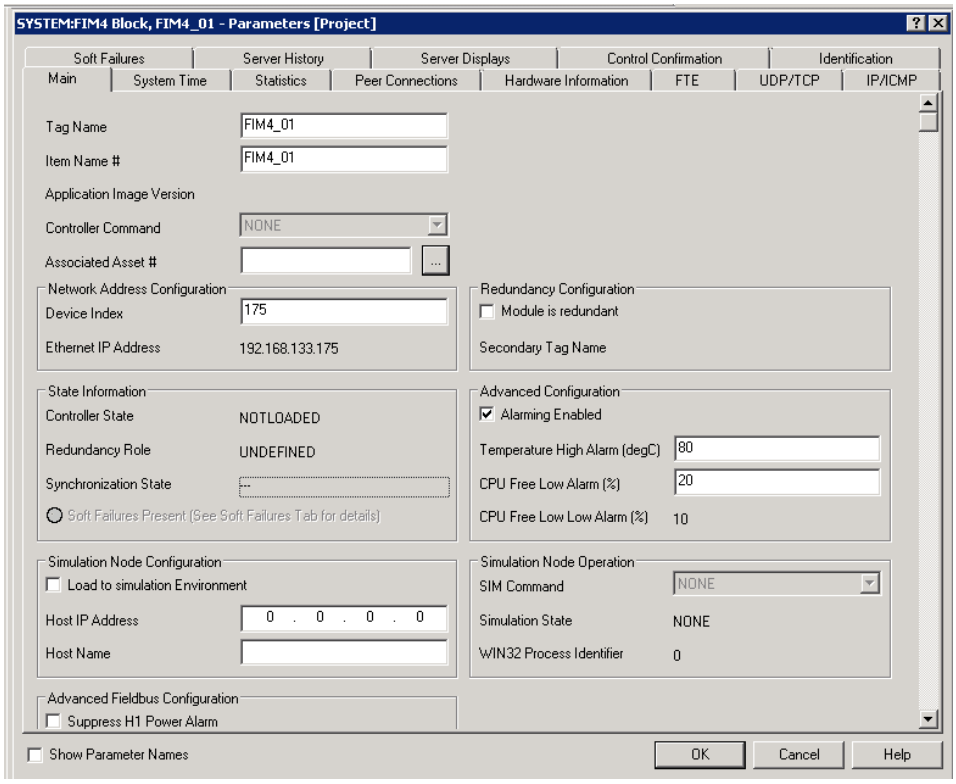

FIGURE 60 FIM4 DEVICE PARAMETERS

Step 3: Load the FIM4 device to the monitoring tab

Right click on the FIM4 device within the project tab as shown earlier in Figure 59. On this occasion select the “Load with Contents” option. A warning screen will appear.

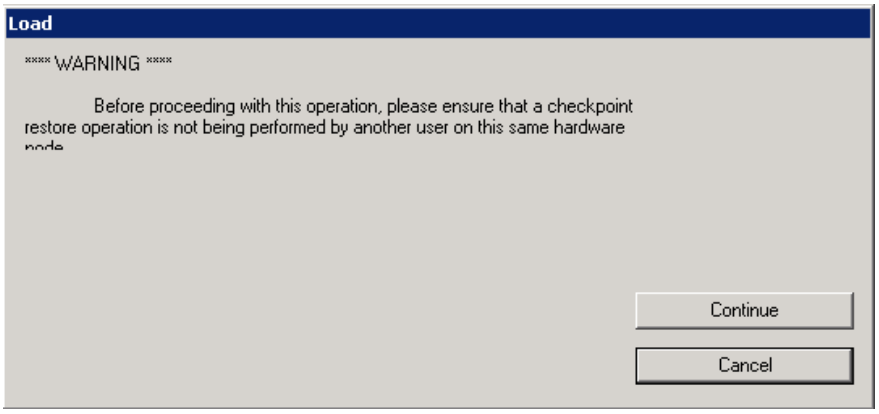

FIGURE 61 LOAD WITH CONTENTS WARNING SCREEN

Select “Continue”. A load dialogue will appear.

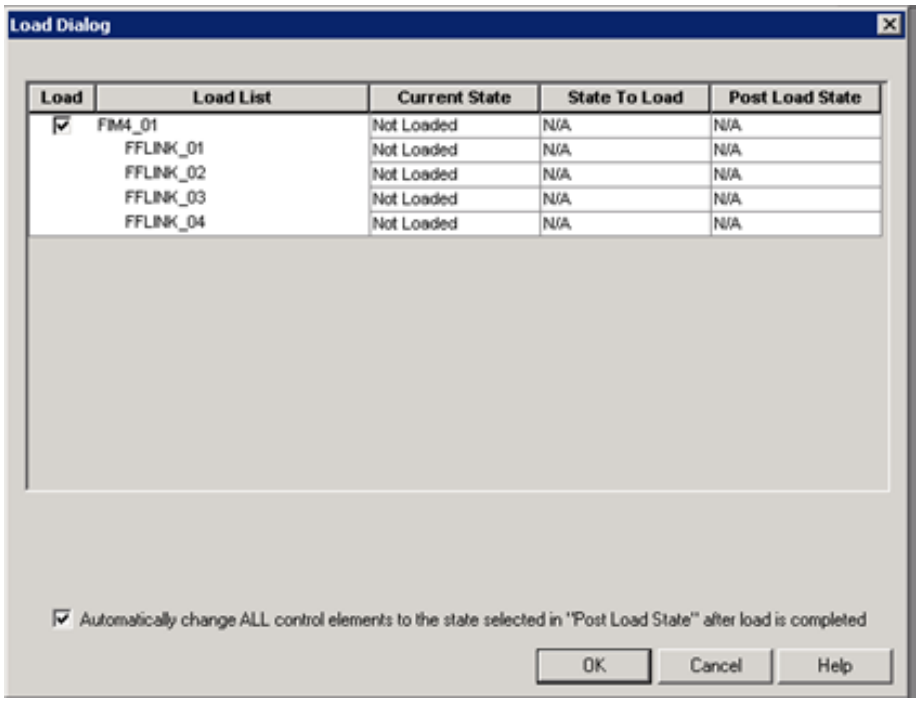

FIGURE 62 LOAD DIALOG WINDOW

Check the box as shown and click “OK”. The device should now appear in the monitoring tab of the assignment window. The device is now ready for use and can be programmed via Control Builder. Green modules are active, while blue modules are those in an idle state.

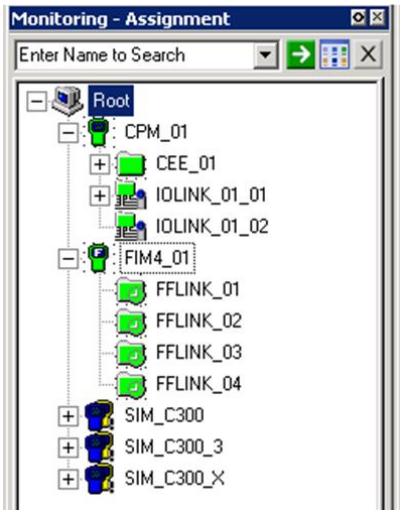

FIGURE 63 FIM4 DEVICE IN MONITORING TAB

Possible errors that may be encountered

Should the user be met with the following error messages when loading the device to the monitoring tab, this means that the firmware on the FIM4 device is not up to date and requires rectification.

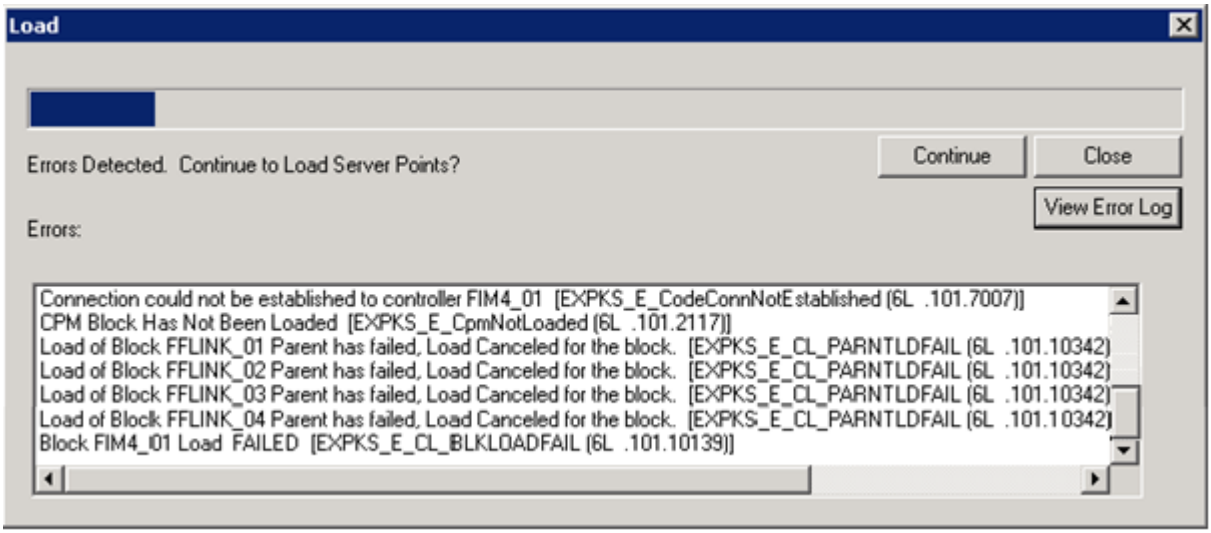

FIGURE 64 SERVER POINT LOAD ERROR MESSAGE

In this instance, please refer to the following guide to upgrade the firmware on the FIM4 device.

For more information on the error codes shown in Figure 64 or any others that may be encountered during this procedure, please refer to the Honeywell Experion PKS Control Builder Error Code Reference document. This can be located in \\mylab\EngShared\Experion Dev\Experion Project\HES-8000 Honeywell Manuals\HES-8000 Imp. Honeywell Manuals RS430 on the Murdoch University server.

It was also found in this instance, that there was several inconsistencies between the project and monitoring tabs of the assignment window. These are denoted by a triangle on that particular icon within Control Builder. This was both within the C300 controller and I/O modules. An example of this is shown in Figure 65.

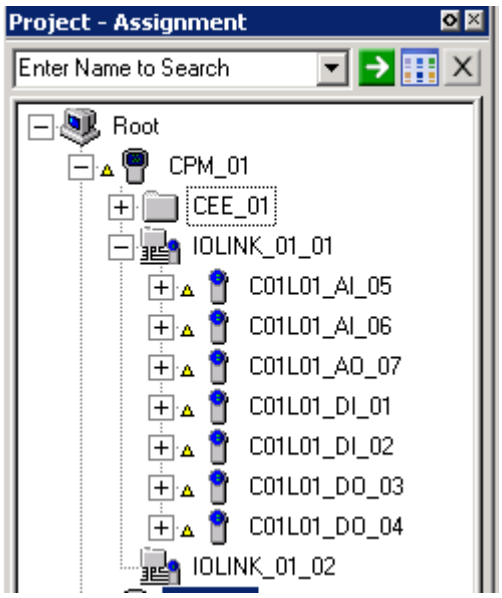

FIGURE 65 ASSIGNMENT WINDOW INCONSISTENCIES

This was also thought to have been another contributor to the errors displayed in Figure 64. This was rectified by loading the latest revision contained in the project tab to the monitoring tab. For direction on how to do this, simply follow the same procedure as shown above in step 3.

B.2 FIRMWARE UPGRADE GUIDE FOR FIM4 DEVICE

In order to upgrade the firmware installed on the Fieldbus Interface Module, the following conditions must be met prior [98]:

- The user must have logged into “PPserver1” remotely with sufficient privileges;
- The user must have sufficient privileges to access the CTools.exe application;
- The corresponding FIM4 device is in an idle state via Control Builder.

Step 1: Access and open the CTools.exe application from Windows Explorer

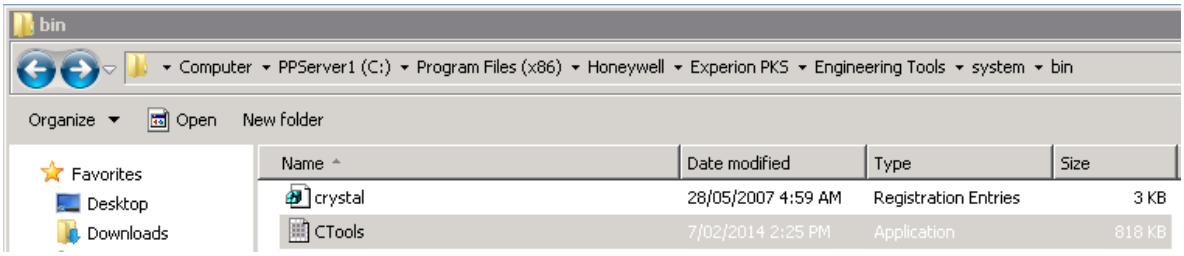

FIGURE 66 CTOOLS.EXE LOCATION

Path: C:\Program Files (x86)\Honeywell\Experion PKS\Engineering Tools\system\bin

If the application has launched correctly, you will be met with the window shown in Figure 67.

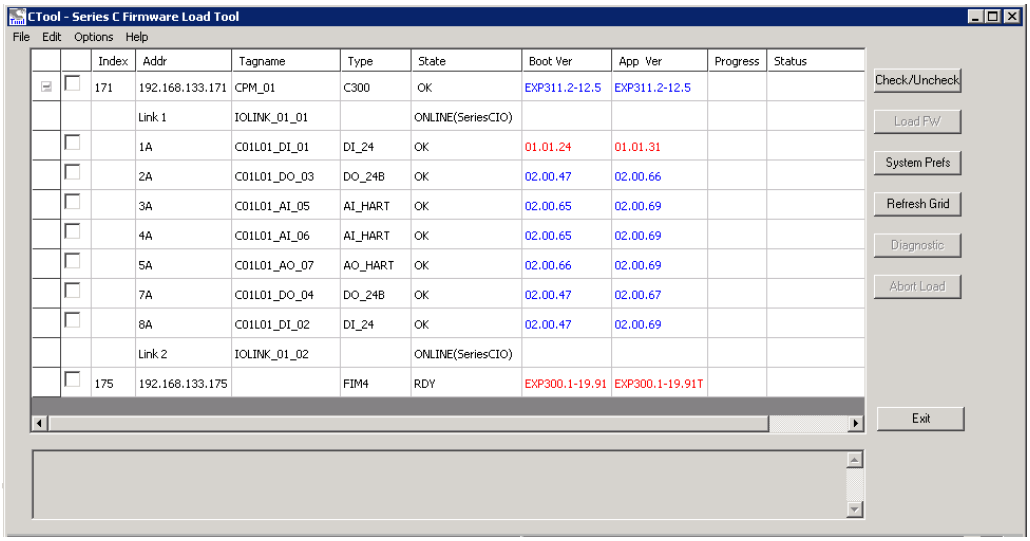

FIGURE 67 SERIES C FIRMWARE LOAD TOOL

In scenarios where the boot version and application version of the firmware are consistent, they will appear blue. In scenarios where this is not the case, they will appear red. This is a clear visual queue that the firmware on the FIM4 device needs to be upgraded, if it appears in red.

Step 2: Confirm the required revision of firmware required

To confirm which version of the firmware is required, refer to the firmware details attributed to the C300 controller in the CTools window. As shown in Figure 68, this was EXP311.2-12.5.

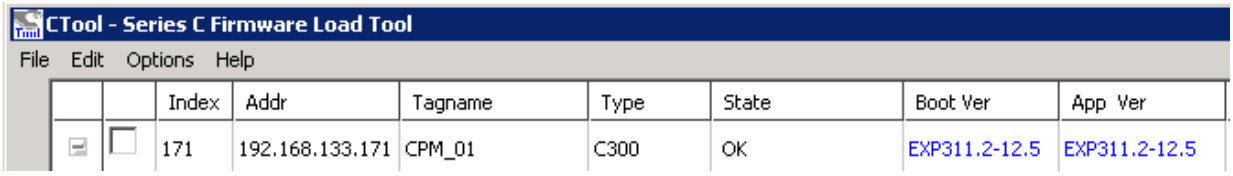

FIGURE 68 C300 EXPERION VERSION VIA CTOOLS.EXE APPLICATION

Step 3: Load the correct version of the firmware to the FIM4 device

To do this, check the box on the left side of the row of the device you wish to upgrade firmware for. Then right click anywhere along the row and a menu will appear as shown in Figure 69.

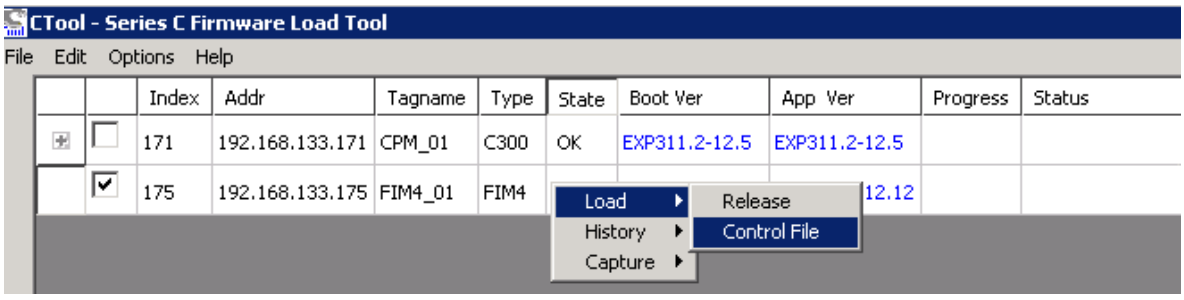

FIGURE 69 FIRMWARE UPGRADE MENU

This will then open another window. You will need to navigate to the appropriate folder containing the .lcf file that is required. An example of the one selected for the previous firmware upgrade is shown in Figure 70. Select the file as shown and press the open button.

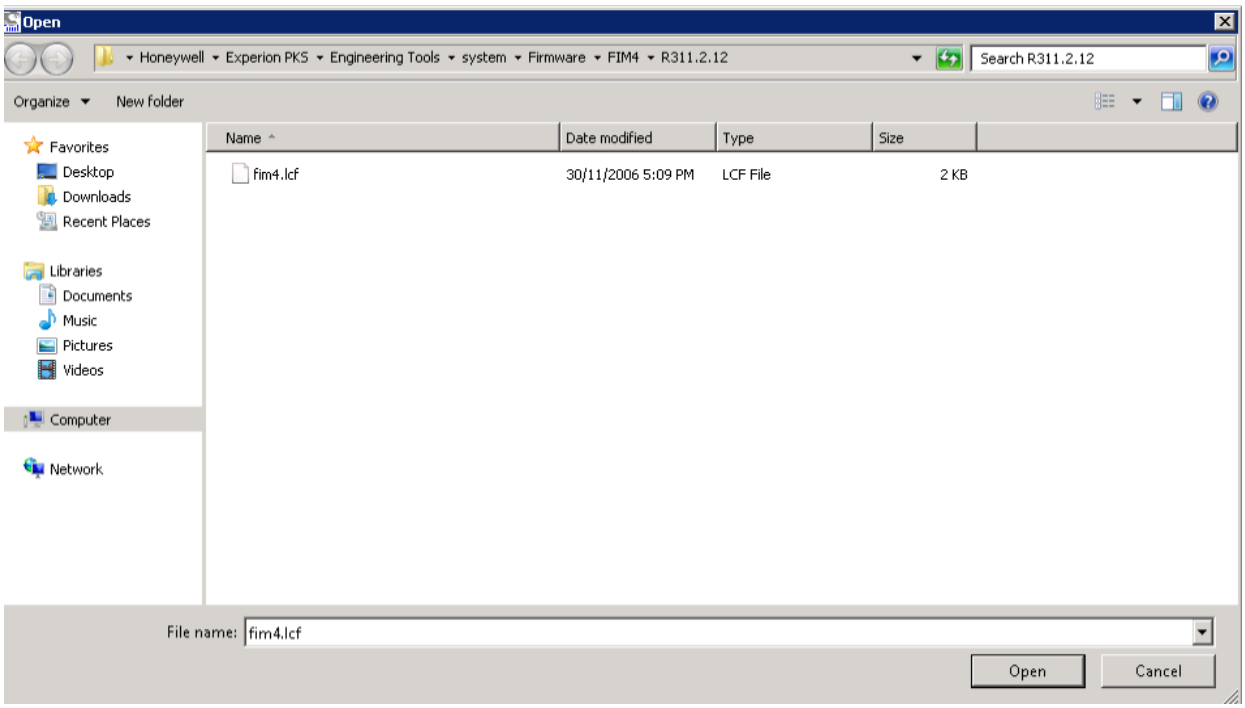

FIGURE 70 FIM4 .LCF FILE FOR FIRMWARE UPGRADE

Path:

C:\Program Files (x86)\Honeywell\Experion PKS\Engineering Tools\system\Firmware\FIM4\R311.2.12

The firmware load operation should commence immediately. The user should expect to see load messages appear in the lower text field of the CTools application and progress of the load showing in the progress column within the window. The status of the firmware load is also shown in the status column. This will appear as displayed in Figure 71.

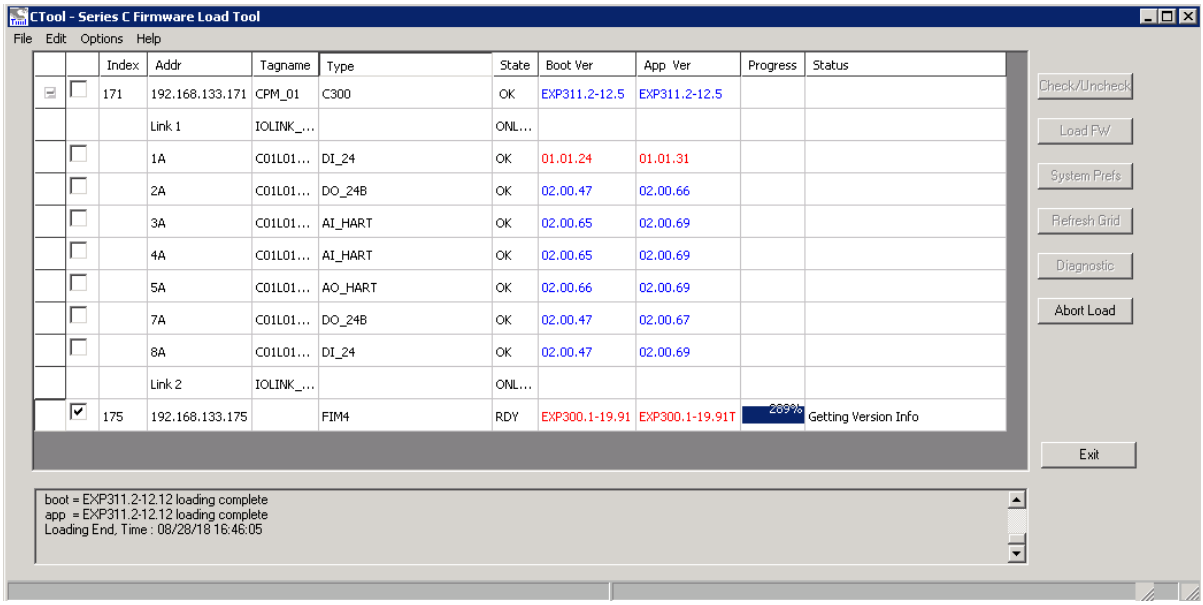

FIGURE 71 CTOOL LOAD PROGRESS SCREEN

Once the firmware has been successfully loaded to the FIM4 device, this should be reflected within the CTool window. The boot version and application version of the firmware for the FIM4 device should match and appear blue. This will appear as shown in Figure 72.

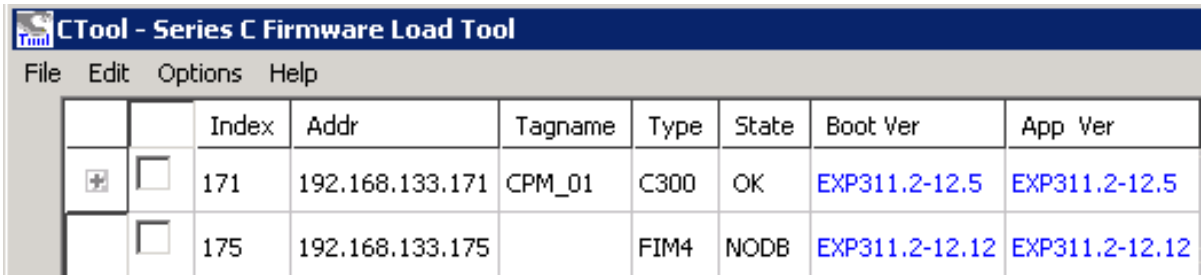

FIGURE 72 FIM4 FIRMWARE UP TO DATE WITHIN CTOOL WINDOW

If this was previously not allowed prior, the FIM4 device can now be loaded to the monitoring tab of the assignment view within the Control Builder application as shown in the previous guide.

APPENDIX C DENSITY OF AN AQUEOUS SOLUTION WITH NACL

TABLE 13 DENSITY (KG/M^3) OF NACL AQUEOUS SOLUTIONS IN DIFFERING CONCENTRATIONS (0 – 45 °C) [67]

	Temperature (°C)									
C (%)	**0**	**5**	**10**	**15**	**20**	**25**	**30**	**35**	**40**	**45**
2	1016	1015	1014	1013	1012	1011	1010	1008	1006	1004
4	1031	1030	1029	1028	1027	1025	1024	1022	1020	1018
6	1045	1044	1043	1042	1041	1040	1038	1037	1035	1032
8	1060	1059	1058	1057	1056	1055	1053	1051	1049	1047
10	1075	1074	1073	1072	1071	1070	1068	1066	1064	1062
12	1091	1090	1089	1088	1086	1085	1083	1081	1079	1076
14	1106	1105	1104	1103	1102	1100	1098	1096	1094	1092
16	1122	1121	1120	1119	1117	1116	1114	1112	1109	1107
18	1138	1137	1136	1135	1133	1132	1130	1127	1125	1122
20	1154	1153	1152	1151	1149	1148	1146	1143	1141	1138
22	1170	1169	1168	1167	1166	1164	1162	1159	1157	1154
24	1187	1186	1185	1184	1182	1180	1178	1176	1173	1170
26	-	-	-	1201	1199	1197	1195	1192	1189	1187

TABLE 14 DENSITY (KG/M^3) OF NACL AQUEOUS SOLUTIONS IN DIFFERING CONCENTRATIONS (50 – 100 °C) [67]

Temperature (50 – 100 °C)											
C (%)	**50**	**55**	**60**	**65**	**70**	**75**	**80**	**85**	**90**	**95**	**100**
2	1002	999	997	994	991	988	985	982	979	975	971
4	1016	1013	1011	1008	1005	1002	999	995	992	988	985
6	1030	1028	1025	1022	1019	1016	1013	1009	1006	1002	998
8	1044	1042	1039	1036	1033	1030	1026	1023	1019	1016	1012
10	1059	1056	1053	1050	1047	1044	1041	1038	1033	1029	1025
12	1074	1071	1068	1065	1062	1058	1055	1051	1047	1043	1039
14	1089	1086	1083	1080	1076	1073	1069	1066	1062	1058	1054
16	1104	1101	1098	1095	1091	1088	1084	1080	1076	1072	1068
18	1119	1116	1113	1110	1106	1103	1099	1095	1091	1087	1083
20	1135	1132	1129	1125	1122	1118	1114	1110	1106	1102	1097
22	1151	1148	1144	1141	1137	1133	1129	1125	1121	1117	1112
24	1167	1164	1160	1157	1153	1149	1145	1141	1136	1132	1127
26	1185	1180	1177	1173	1169	1165	1161	1156	1152	1147	1143

APPENDIX D CONDUCTIVITY OF AN AQUEOUS SOLUTION WITH NACL

TABLE 15 CONDUCTIVITY (S/CM) OF NACL AQUEOUS SOLUTIONS IN DIFFERING CONCENTRATIONS (15 – 50 °C) [67]

	Temperature (°C)								
C (%)	**15**	**18**	**20**	**25**	**30**	**35**	**40**	**45**	**50**
4	4.6604	5.7477	6.0187	6.6943	7.367	8.0364	8.5994	9.1588	9.7143
6	6.5771	8.2279	8.6393	9.6651	10.6865	11.7031	12.4463	13.1844	13.9173
8	8.2289	10.4334	10.9827	12.3526	13.7168	15.0745	15.9489	16.8172	17.679
10	9.6843	12.3839	13.0566	14.7342	16.4049	18.0678	19.0645	20.0542	21.0363
12	11.0685	14.1318	14.8952	16.7987	18.6944	20.5811	21.7497	22.91	24.0615
14	12.4212	15.7195	16.5414	18.5908	20.614	22.6624	24.0403	25.4087	26.7669
16	13.773	17.1954	18.0481	20.1741	22.291	24.3975	25.9847	27.5613	29.1264
18	15.0992	18.5468	19.4057	21.547	23.6787	25.7997	27.5541	29.2969	31.0272
20	16.3654	19.7355	20.5749	22.6674	24.7503	26.8224	28.68	30.5254	32.3576
22	17.5388	20.7237	21.5168	23.4936	25.4609	27.4176	29.3037	31.1774	33.0377
24	18.5547	21.4516	22.1728	23.97	25.758	27.5358	29.3641	31.1802	32.9829

TABLE 16 CONDUCTIVITY (S/CM) OF NACL AQUEOUS SOLUTIONS IN DIFFERING CONCENTRATIONS (55 – 95 °C) [67]

	Temperature (°C)								
C (%)	**55**	**60**	**65**	**70**	**75**	**80**	**85**	**90**	**95**
4	10.2656	10.8266	11.3827	11.9337	12.4791	13.0186	13.7276	14.4288	15.1219
6	14.6444	15.4716	16.2917	17.1042	17.9086	18.7046	19.6305	20.546	21.4505
8	18.5338	19.5973	20.6518	21.6965	22.7309	23.7544	24.8414	25.9157	26.9768
10	22.0101	23.2555	24.4902	25.7134	26.9244	28.1226	29.3728	30.6082	31.8282
12	25.2035	26.5518	27.8882	29.2119	30.5221	31.8182	33.3055	34.7756	36.2277
14	28.1142	29.531	30.9349	32.3251	33.7009	35.0614	36.7879	38.4948	40.1811
16	30.6792	32.1933	33.6934	35.1788	36.6486	38.102	39.9681	41.813	43.6355
18	32.744	34.394	36.029	37.6479	39.25	40.8343	42.7304	44.6045	46.4555
20	34.1757	35.975	37.7581	39.5241	41.2719	43.0006	44.866	46.7091	48.5288
22	34.8835	36.8214	38.7422	40.6449	42.5284	44.3915	46.2064	47.9991	49.7684
24	34.7715	36.8075	38.8258	40.8254	42.8051	44.7639	46.5486	48.3113	50.0508

APPENDIX E SIMULINK SYSTEM MODEL

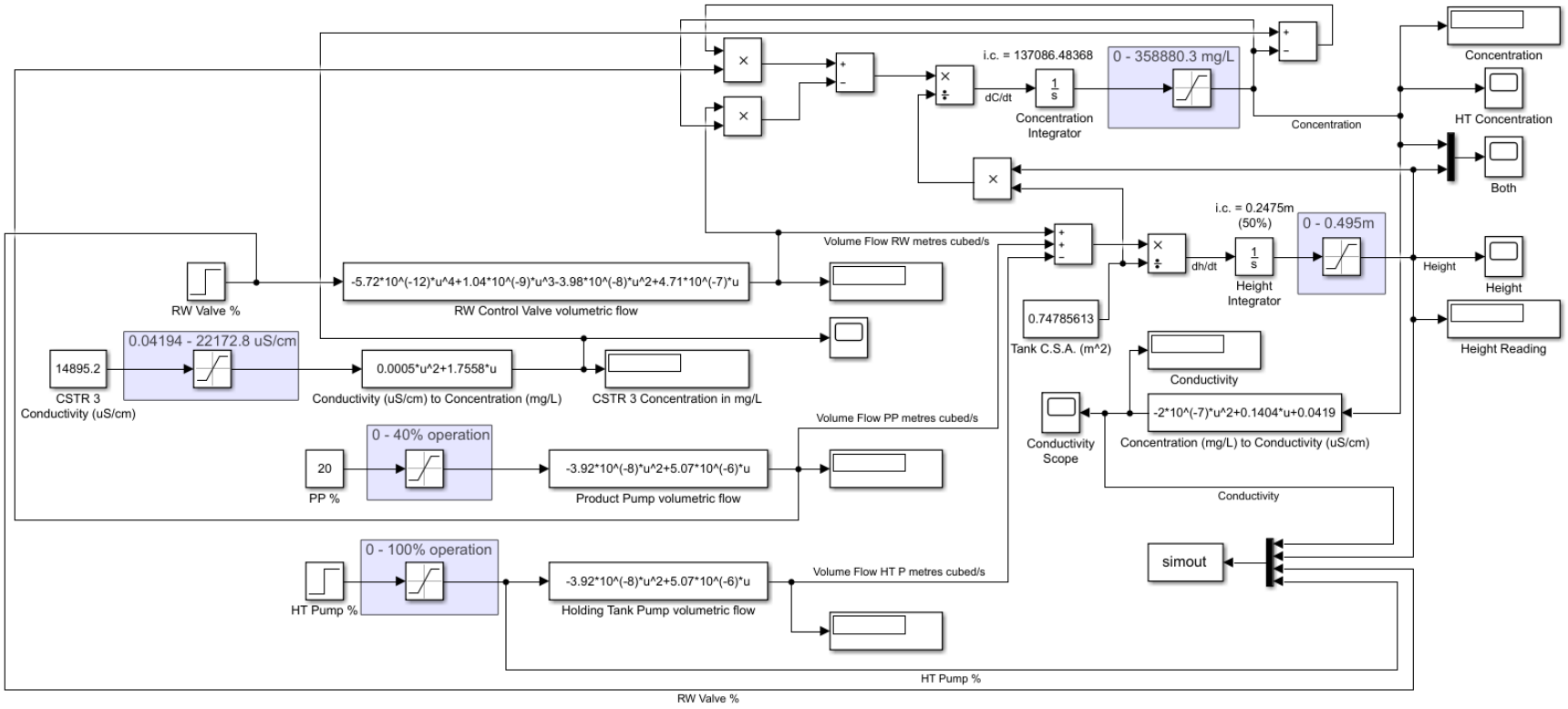

FIGURE 73 SIMULINK DIFFERENTIAL EQUATION SYSTEM MODEL

APPENDIX F SIMULINK SYSTEM MODEL WITH CONTROL

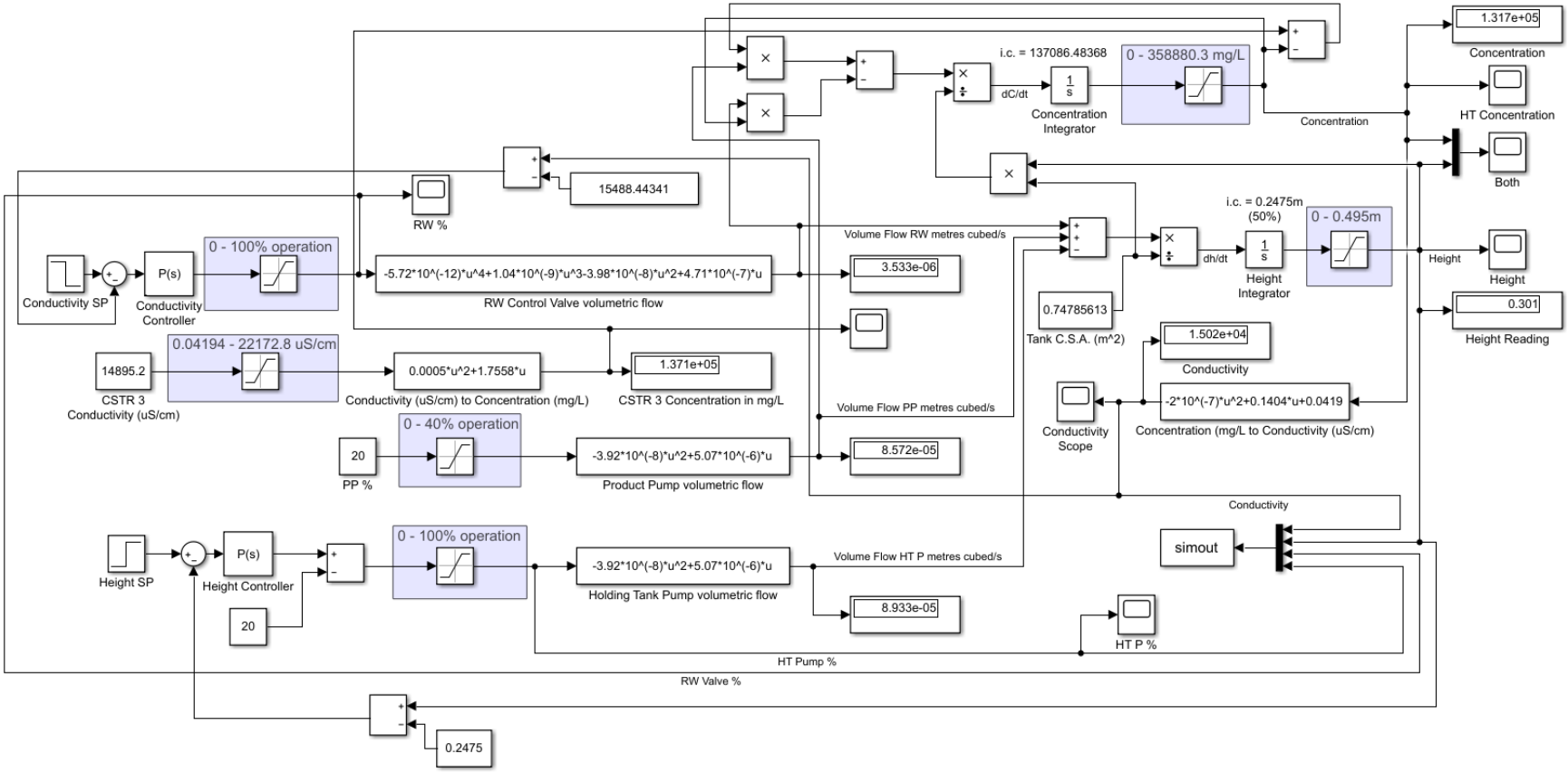

FIGURE 74 SIMULINK DIFFERENTIAL EQUATION SYSTEM MODEL WITH P CONTROLLERS

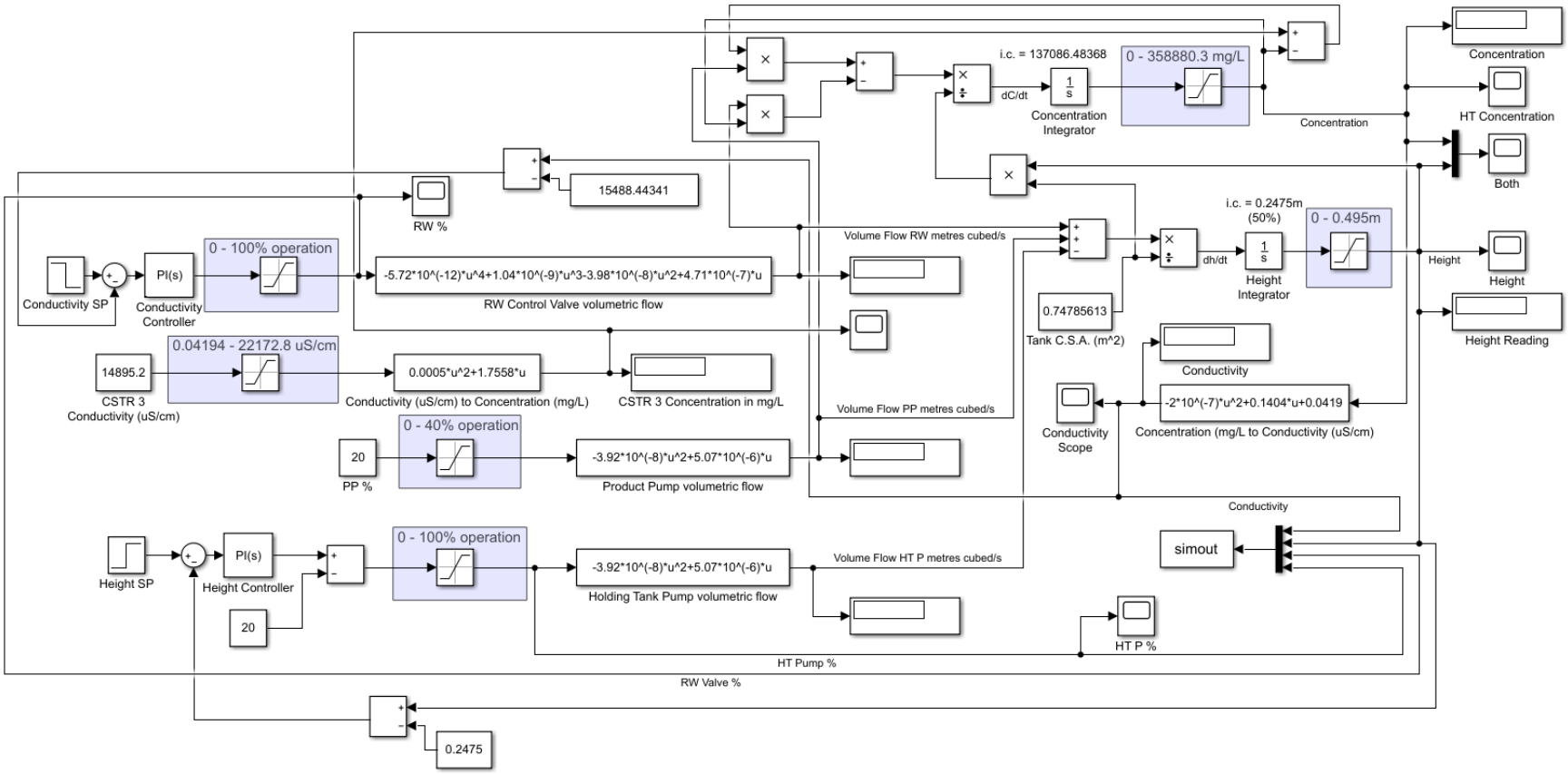

FIGURE 75 SIMULINK DIFFERENTIAL EQUATION SYSTEM MODEL WITH PI CONTROLLERS

APPENDIX G FOUNDATION FIELDBUS DEVICE ADDITION GUIDE FOR EXPERION

In order to successfully implement a new foundation Fieldbus device into Experion via Control Builder, first several requirements must be met:

- An appropriate Fieldbus interfacing device, i.e. FIM4 device and appropriate power conditioning solution must have been implemented both physically and via Control Builder;
- The H1 segment field wiring to the instrument/s must meet Fieldbus wiring standards and utilise terminators and segment couplers as required;
- The user must have logged into "PPserver1" remotely with sufficient privileges;
- Configuration Studio must have been started and the Control Builder application launched;
- The user must have sufficient privileges to create control strategies within Control Builder.

Step 1: Look for the new un-commissioned device in the Monitoring tab of the Assignment Window

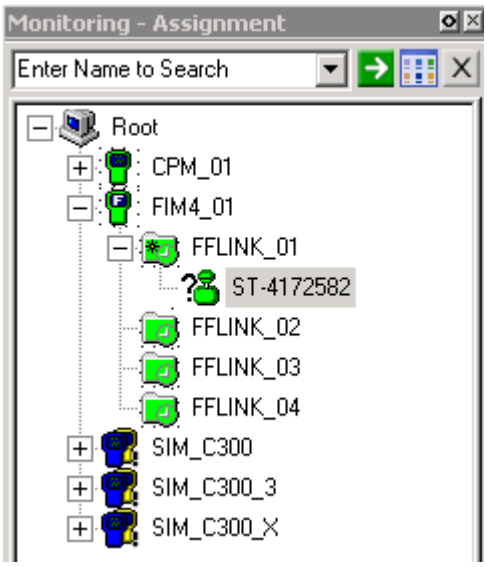

FIGURE 76 UN-COMMISSIONED DEVICE IN MONITORING TAB

New un-commissioned devices will appear underneath the segment (FFLINK_01) that they have been successfully physically implemented on.

Step 2: Ensure the device description (DD) file is available

First check that the DD file is not already on the server in the appropriate folder. The easiest way to access this folder is to double click on the un-commissioned device as shown in Figure 76. This will bring up a parameters window.

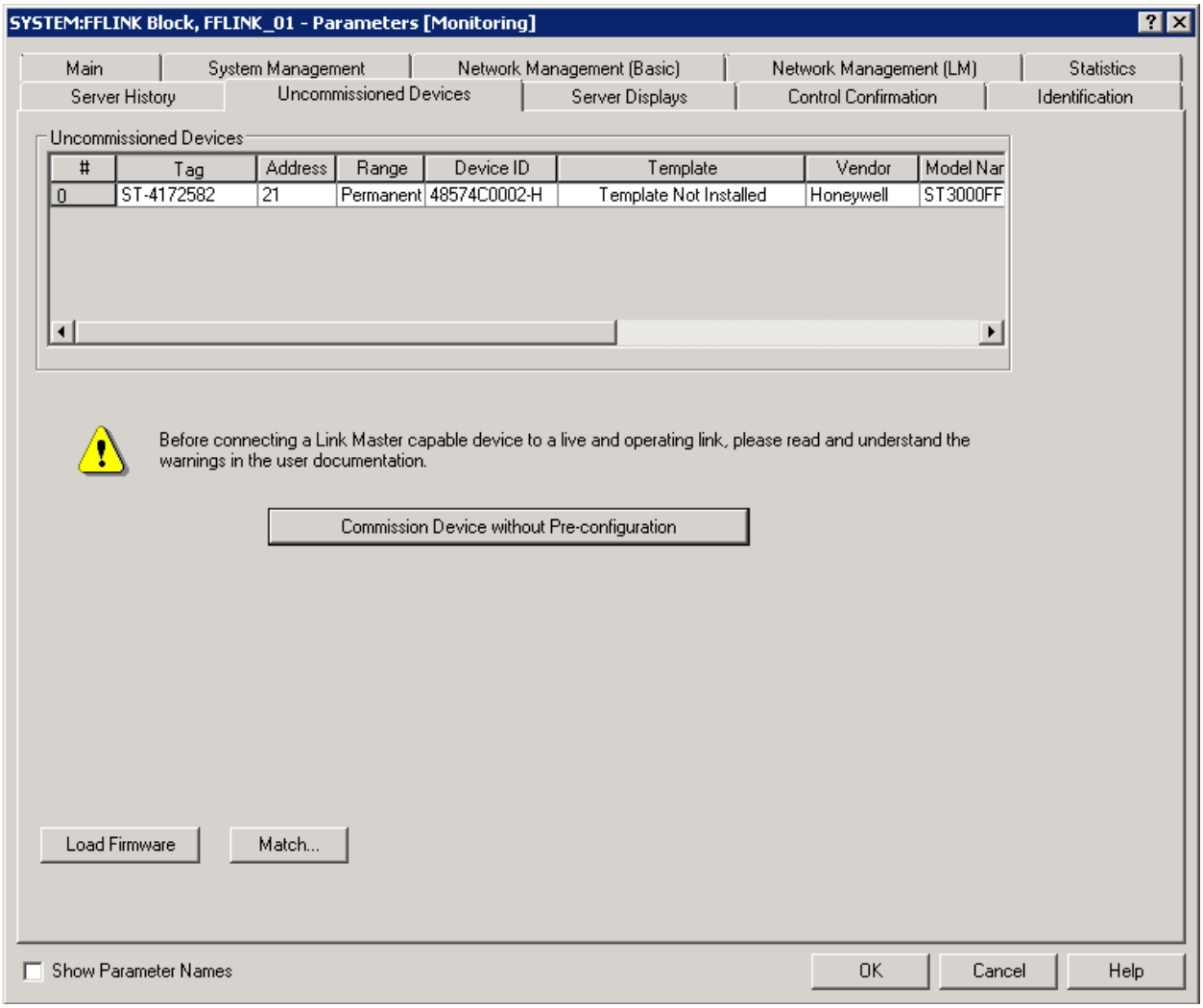

FIGURE 77 FOUNDATION FIELDBUS DEVICE PARAMETER WINDOW

From here, select the “Commission Device without Pre-configuration” button in the centre of the Un-commissioned Devices tab of the window. This will bring up a Device Template window.

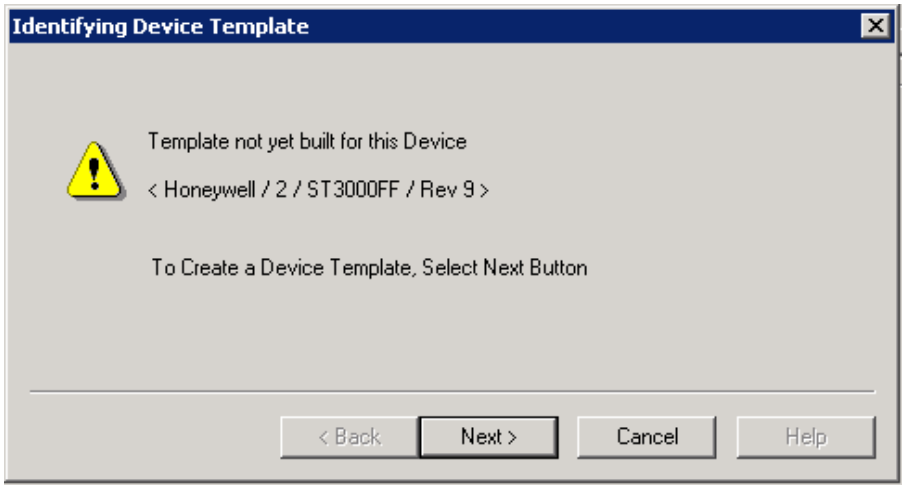

FIGURE 78 IDENTIFYING DEVICE TEMPLATE WINDOW

Clicking next will open a select device type window.

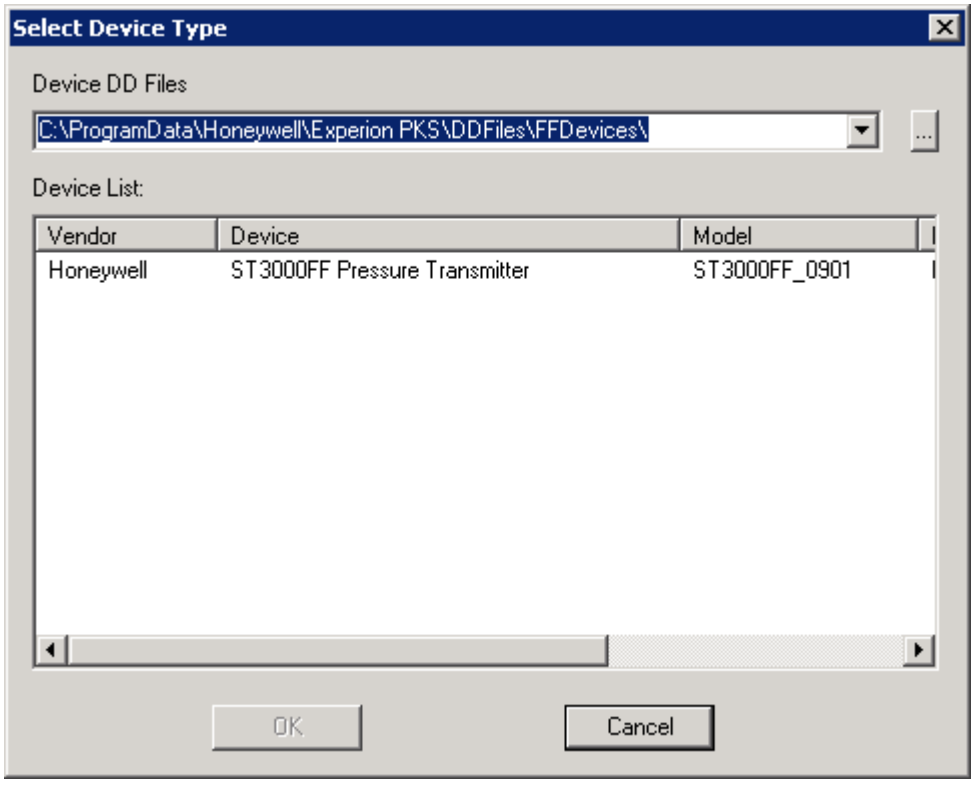

FIGURE 79 SELECT DEVICE TYPE WINDOW

This will take the user to the file path pre-established for any relevant pre-loaded device description files within Experion. The device list will state in instruments that have had data pre-loaded prior.

Path: *C:\ProgramData\Honeywell\Experion PKS\DDFiles\FFDevices*

If the device data file is not present this will need to be obtained from the vendor's relevant software support website online. Once downloaded, the user will need to open the relevant data folder (usually zipped) and copy three files to the relevant directory. Those required are a combination of device description files (.ffo and .sym) and capabilities files (.cff) highlighted in Figure 80.

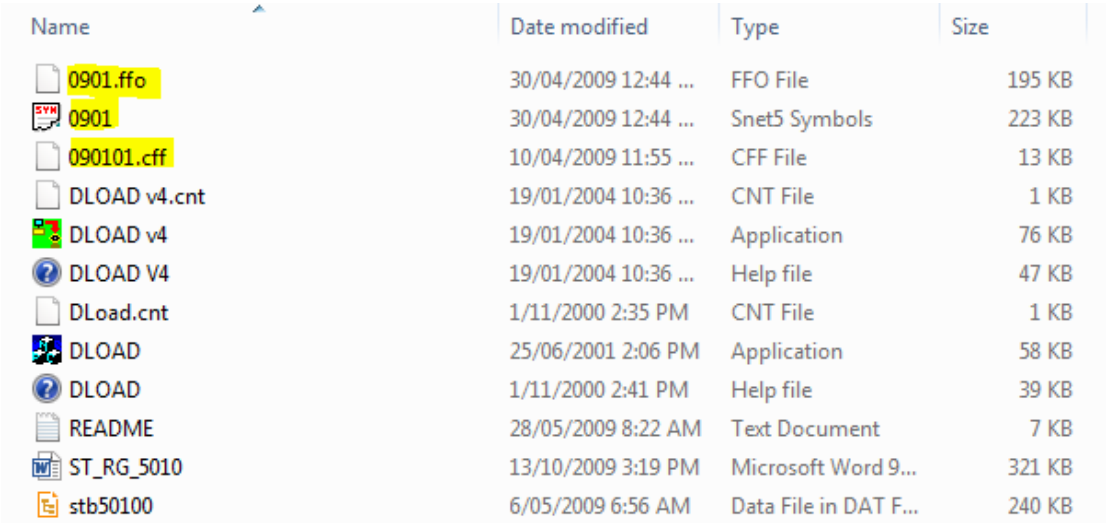

FIGURE 80 DEVICE DATA FOLDER AND CONTENTS REQUIRING EXTRACTION TO THE RELEVANT DIRECTORY

Step 3: Commission the un-commissioned device

Return to the select device type menu as shown in Figure 79. Select the desired instrument. Click the OK button. This will be available for interaction once a relevant device is selected from within the window. This will implement a device data upload to the Experion system. Should this be successful, the user will be presented with several system messages.

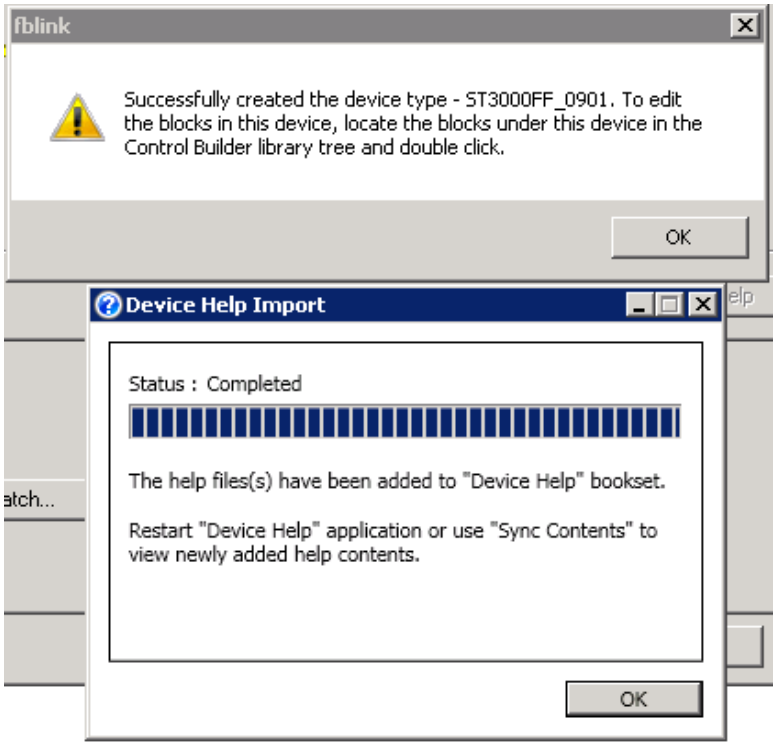

FIGURE 81 DEVICE TYPE CREATION SUCCESSFUL MESSAGE

The fblink message is advising the user that the relevant device type is now imported into Experion Control Builder. After clicking OK, the user will be presented with a user authorisation window.

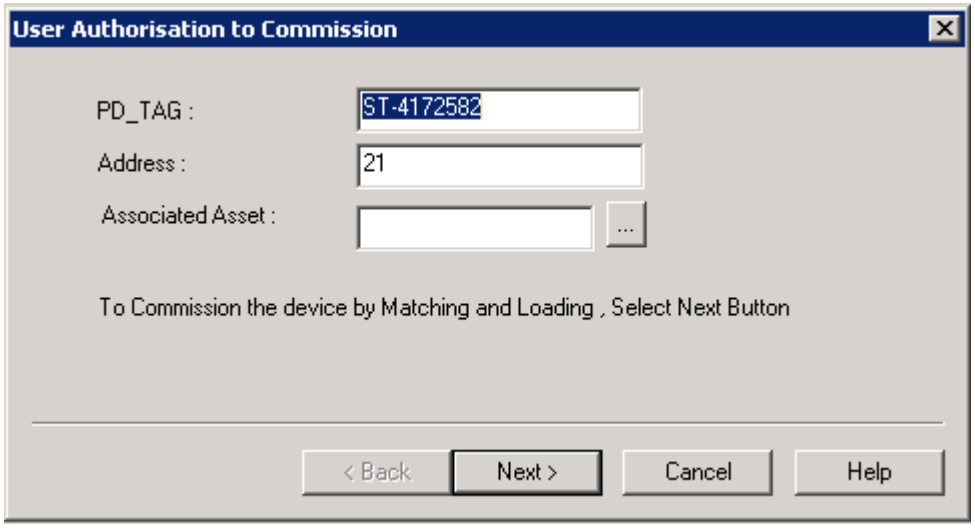

FIGURE 82 USER AUTHORISATION TO COMMISSION WINDOW

This window allows the user to either accept the auto-populated information for the device or enter their own as desired. There is also the option to enter an associated asset as desired. To proceed with asset allocation, select the button with 3 dots next to the empty window in Figure 82. This will bring up a point selection window.

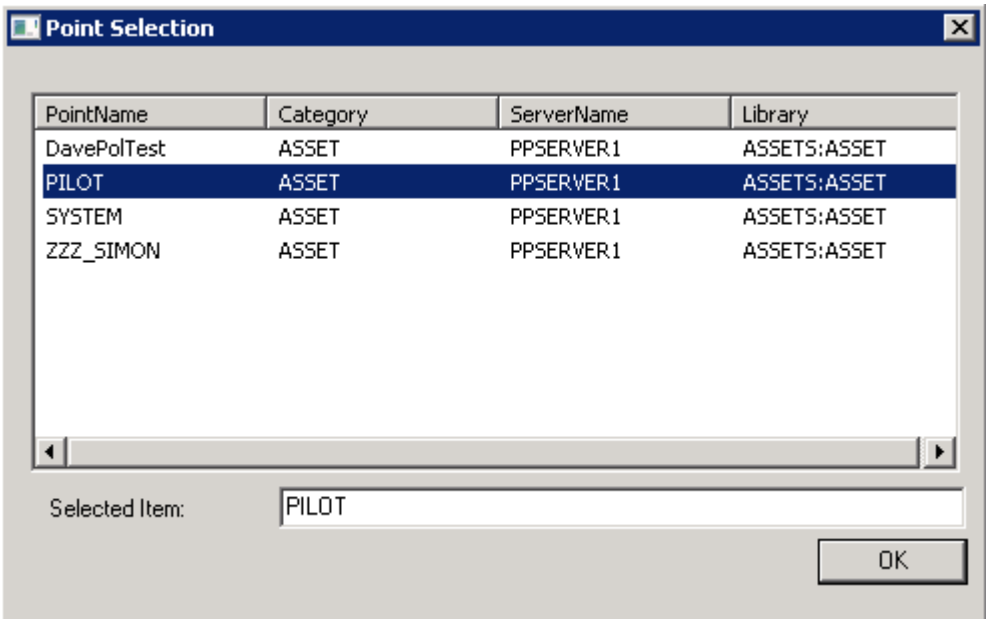

FIGURE 83 POINT SELECTION WINDOW

For consistency, it is advisable to select PILOT as the asset for implementation of new devices onto PPServer1. Selecting OK will take the user back to the user authorisation window in Figure 82. From here select next to commission the device by Matching and Loading.

Step 3: Add the created device via the Project tab of the Assignment Window

To do this access the project tab of the assignment window. Left click on the desired segment (FFLINK_01) and choose the selection path: *New* → *Devices* → **Device**

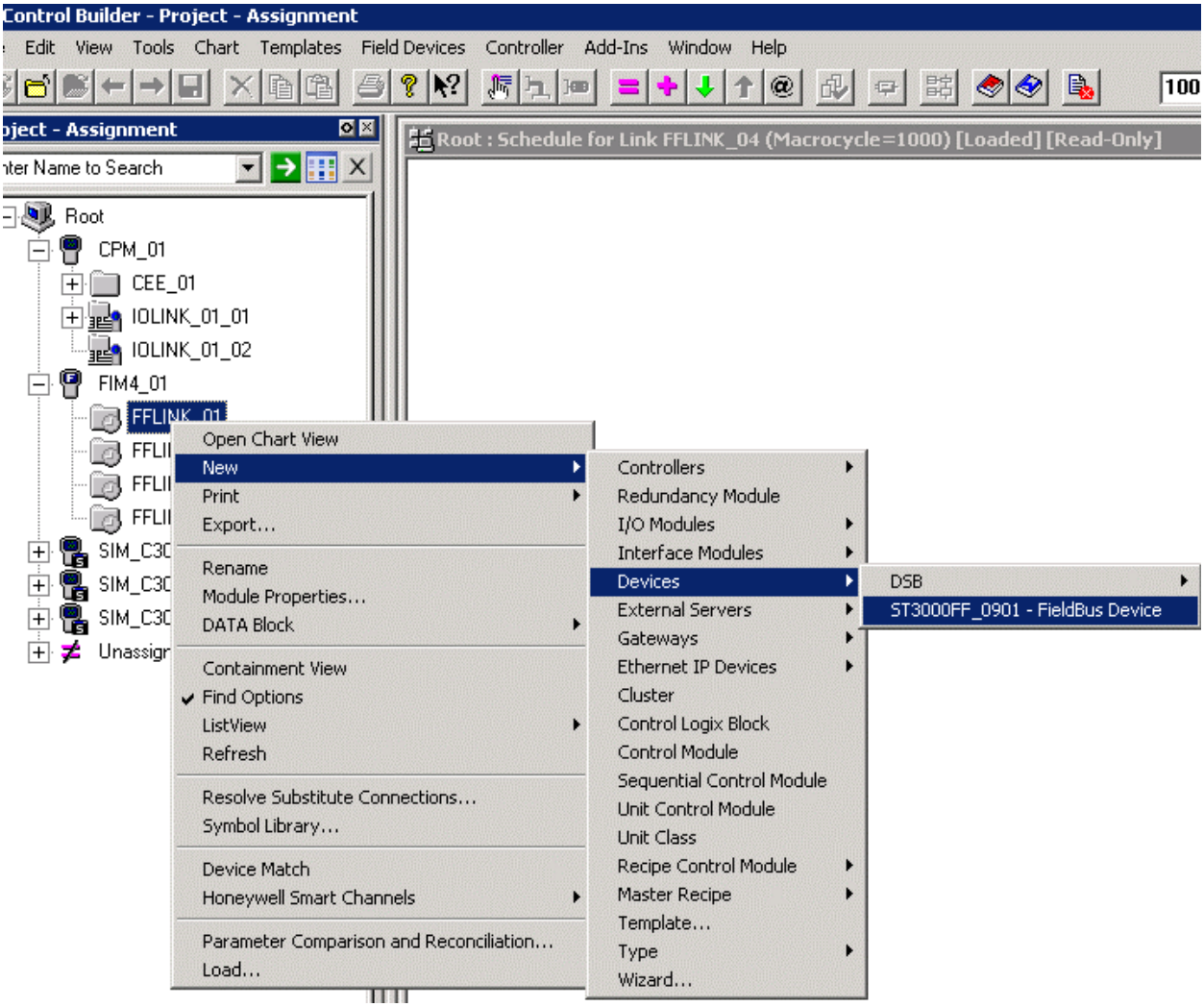

FIGURE 84 NEW DEVICE SELECTION IN PROJECT TAB

Selecting the desired device, in this instance being ST3000FF_0901 – Fieldbus Device will automatically open the associated device's parameters window. As before, the associated asset can be chosen.

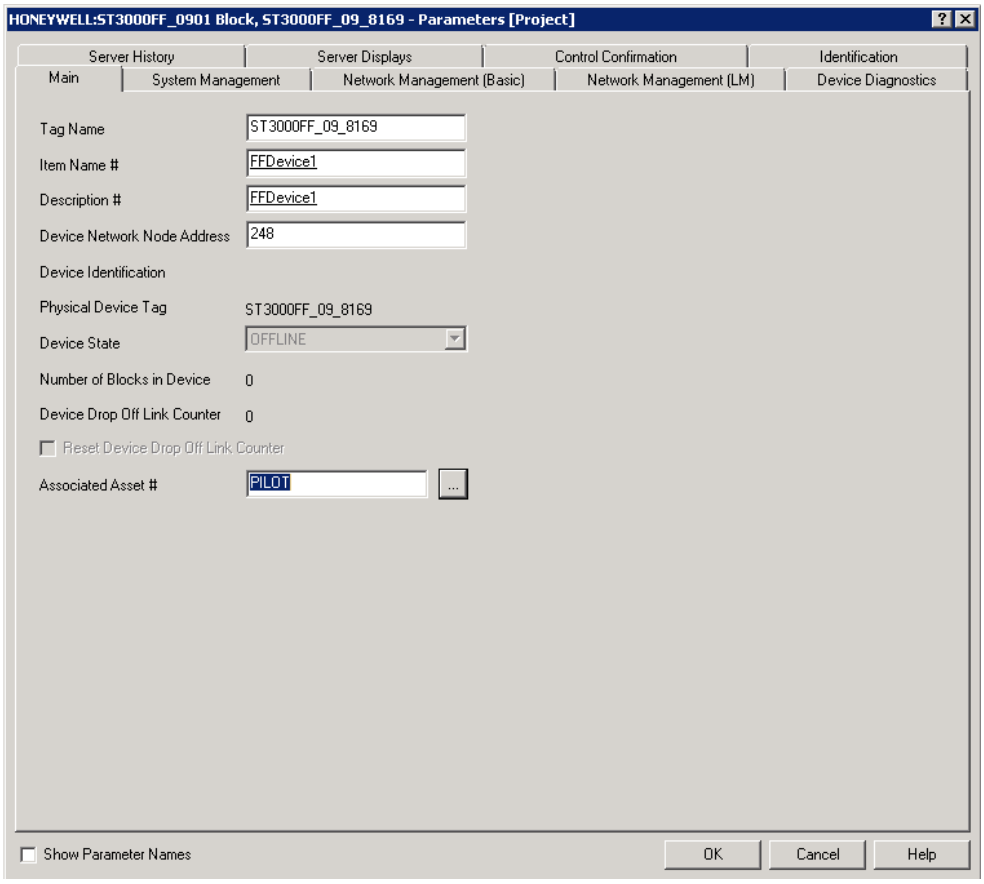

FIGURE 85 FIELDBUS DEVICE PARAMETERS WINDOW MAIN TAB

This new device will then appear under the Unassigned subset within the project tab as shown in Figure 86

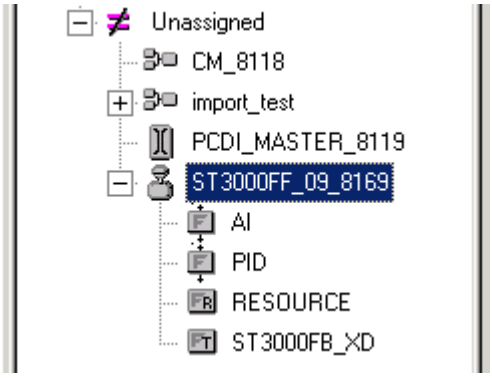

FIGURE 86 NEW FF DEVICE UNDER UNASSIGNED FOLDER

The device can now be assigned to the appropriate segment (FFLINK_01) by selecting the device and clicking the assign button found towards the top of the user window. This will bring up an Execution Environment Assignment Window. Select the desired device and its intended destination and then press assign as shown in Figure 87.

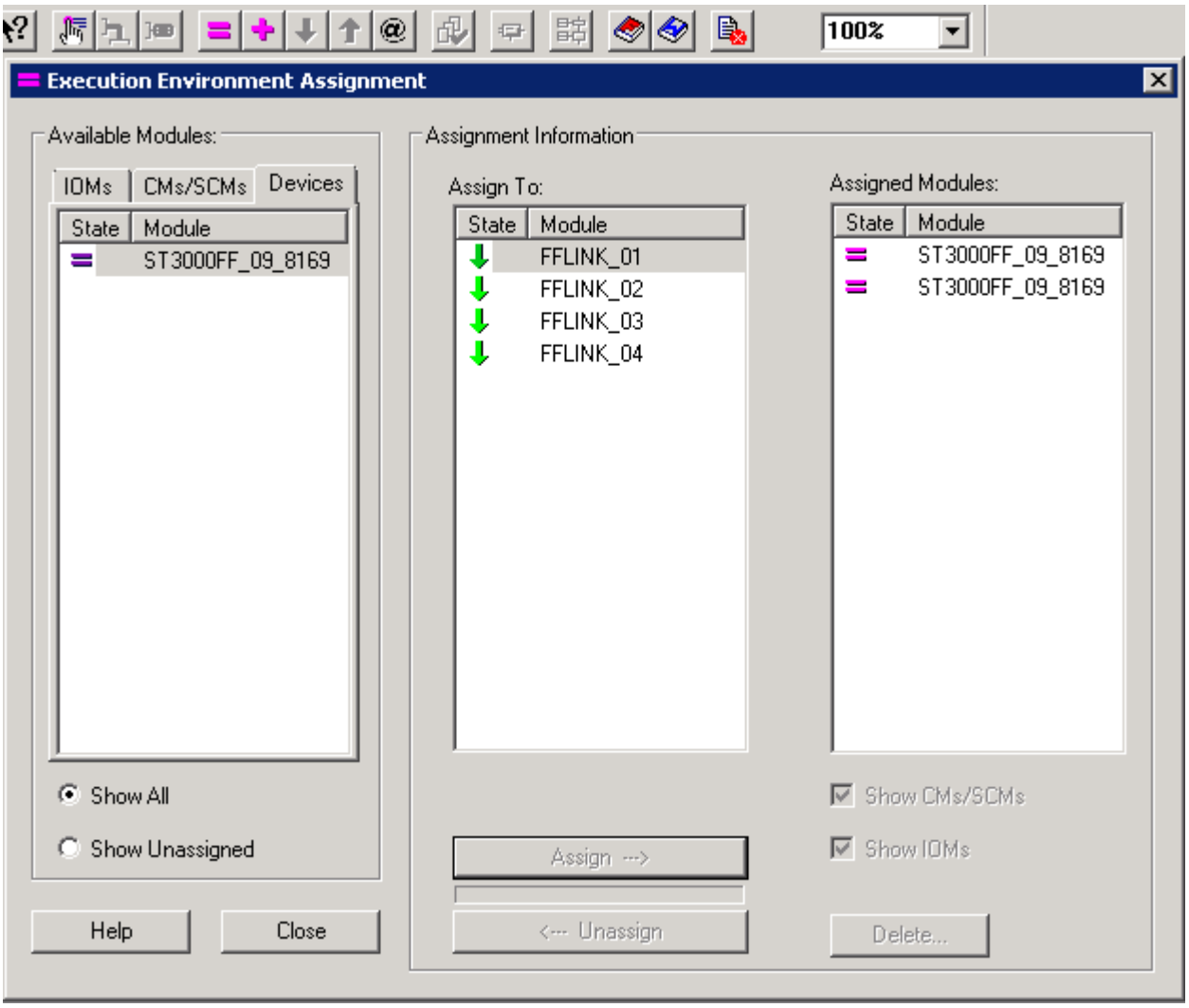

FIGURE 87 EXECUTION ENVIRONMENT ASSIGNMENT WINDOW

After this, return to the device parameter window as shown in Figure 77 and press match. The window that appears should look as that shown in Figure 88.

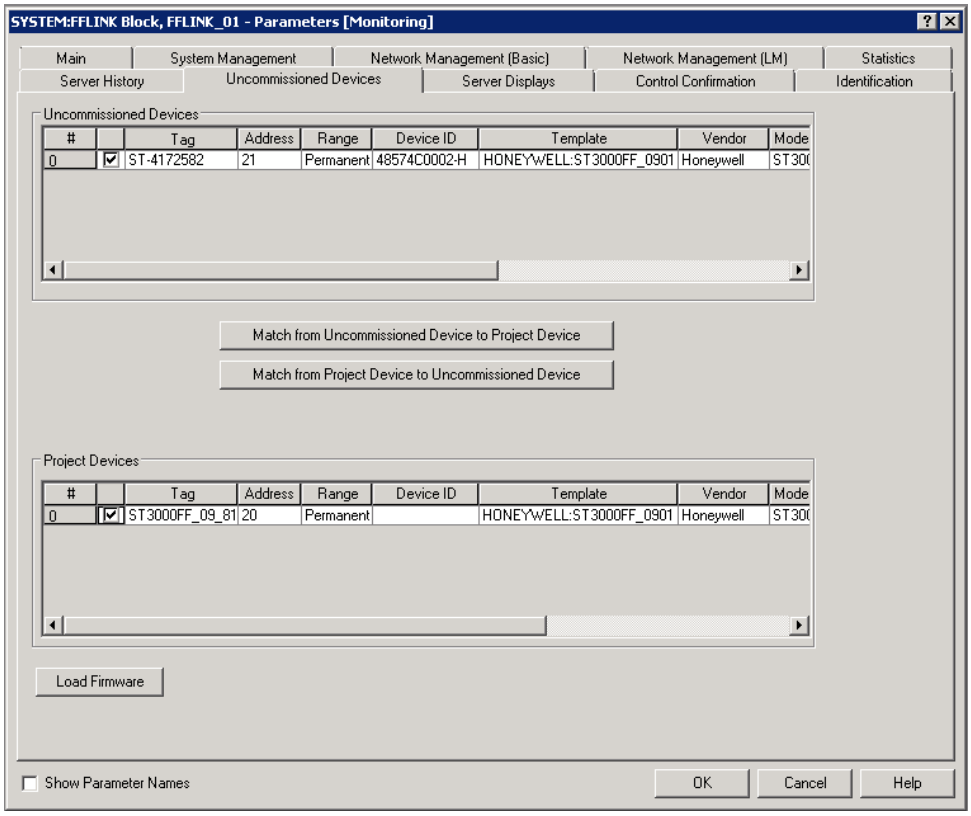

FIGURE 88 MATCHING FROM UN-COMMISSIONED TO COMMISSIONED AND VICE VERSA

Select the match from Project Device to Un-commissioned device button at this stage. A device matching progress window will then appear.

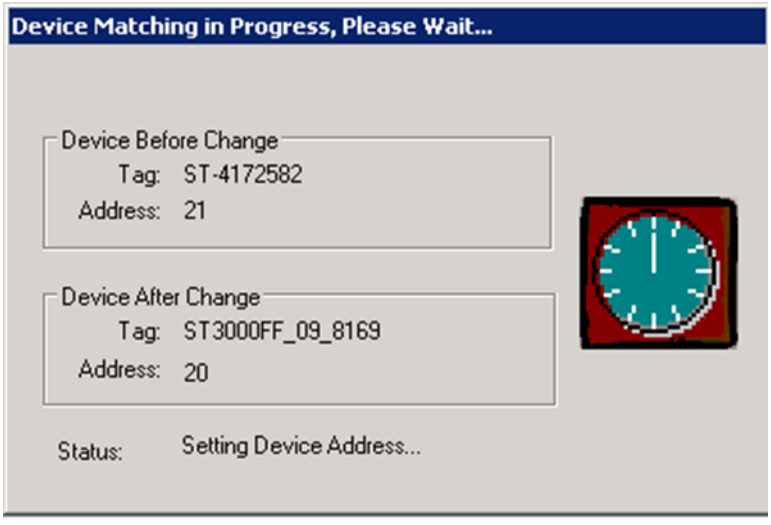

FIGURE 89 DEVICE MATCHING PROGRESS WINDOW

Once this has completed, return to the project view and select the desired segment (FFLINK_01) and select load with contents. A load dialog box will then appear as shown in Figure 90. Press ok to enable the download.

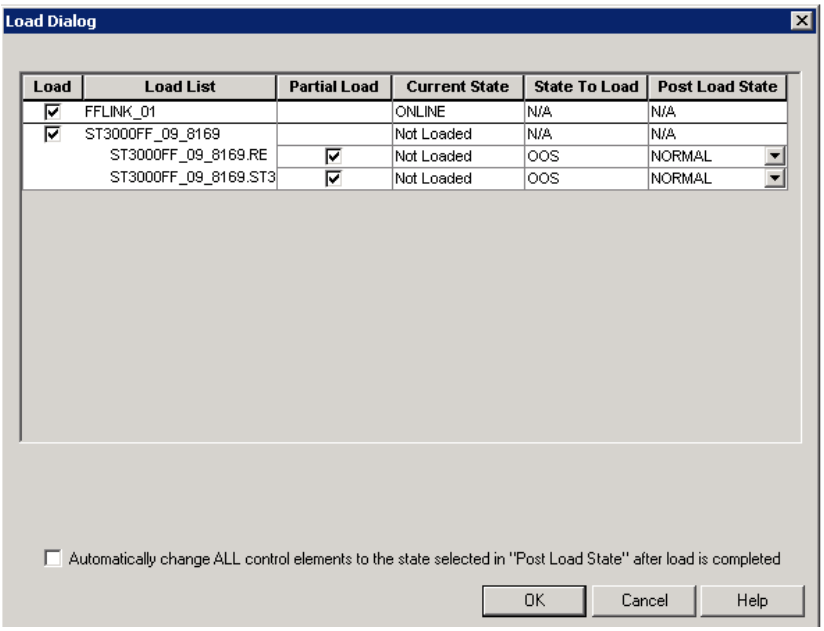

FIGURE 90 DOWNLOAD FROM PROJECT TO MONITORING TAB

A warning screen will then appear.

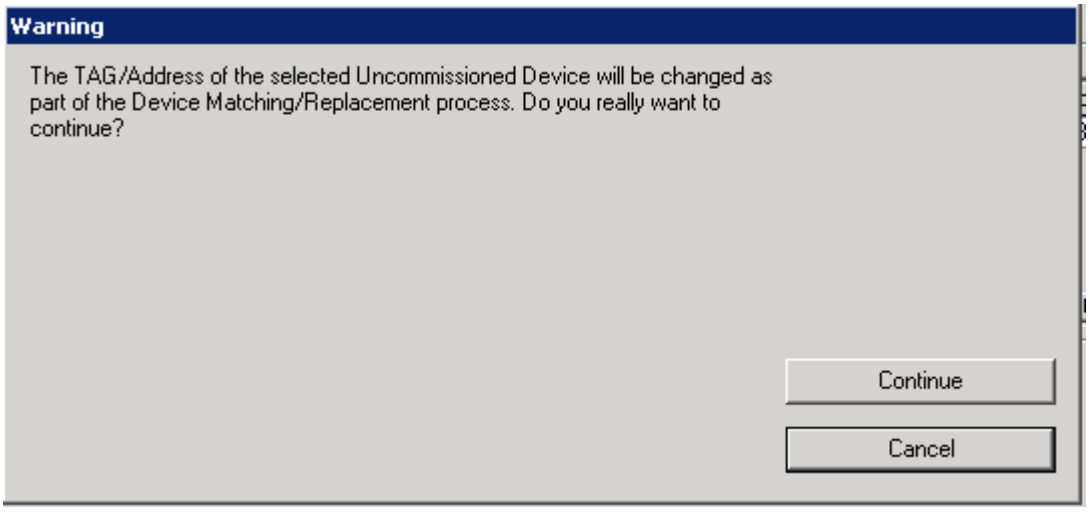

FIGURE 91 WARNING SCREEN CONCERNING TAG/ADDRESS UPDATE

Press continue and a load progress window will appear.

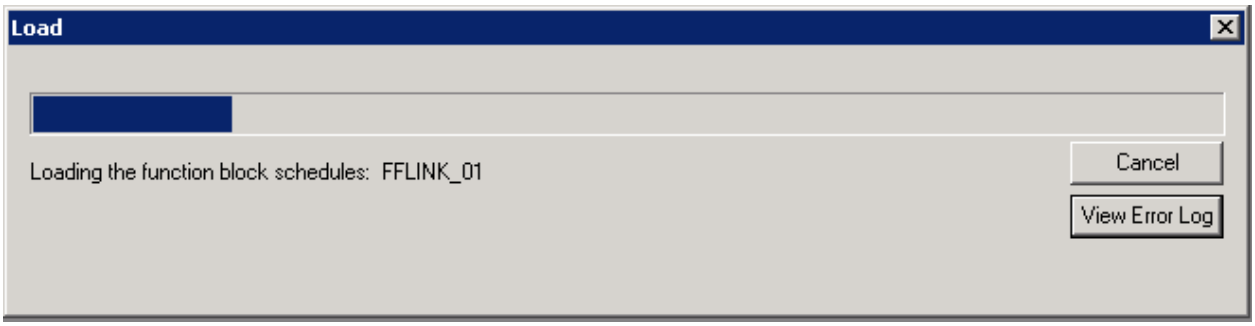

FIGURE 92 LOAD PROGRESS WINDOW

If this is successful, the previously un-commissioned device will now appear as a commissioned device in the monitoring tab of the assignment window.

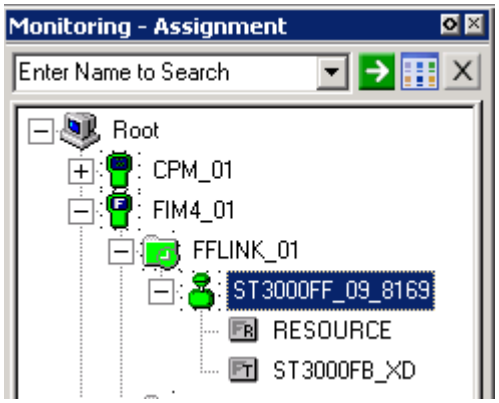

FIGURE 93 COMMISSIONED FF DEVICE IN MONITORING TAB

APPENDIX H EPP FOUNDATION FIELDBUS H1 NETWORK WIRING DIAGRAM

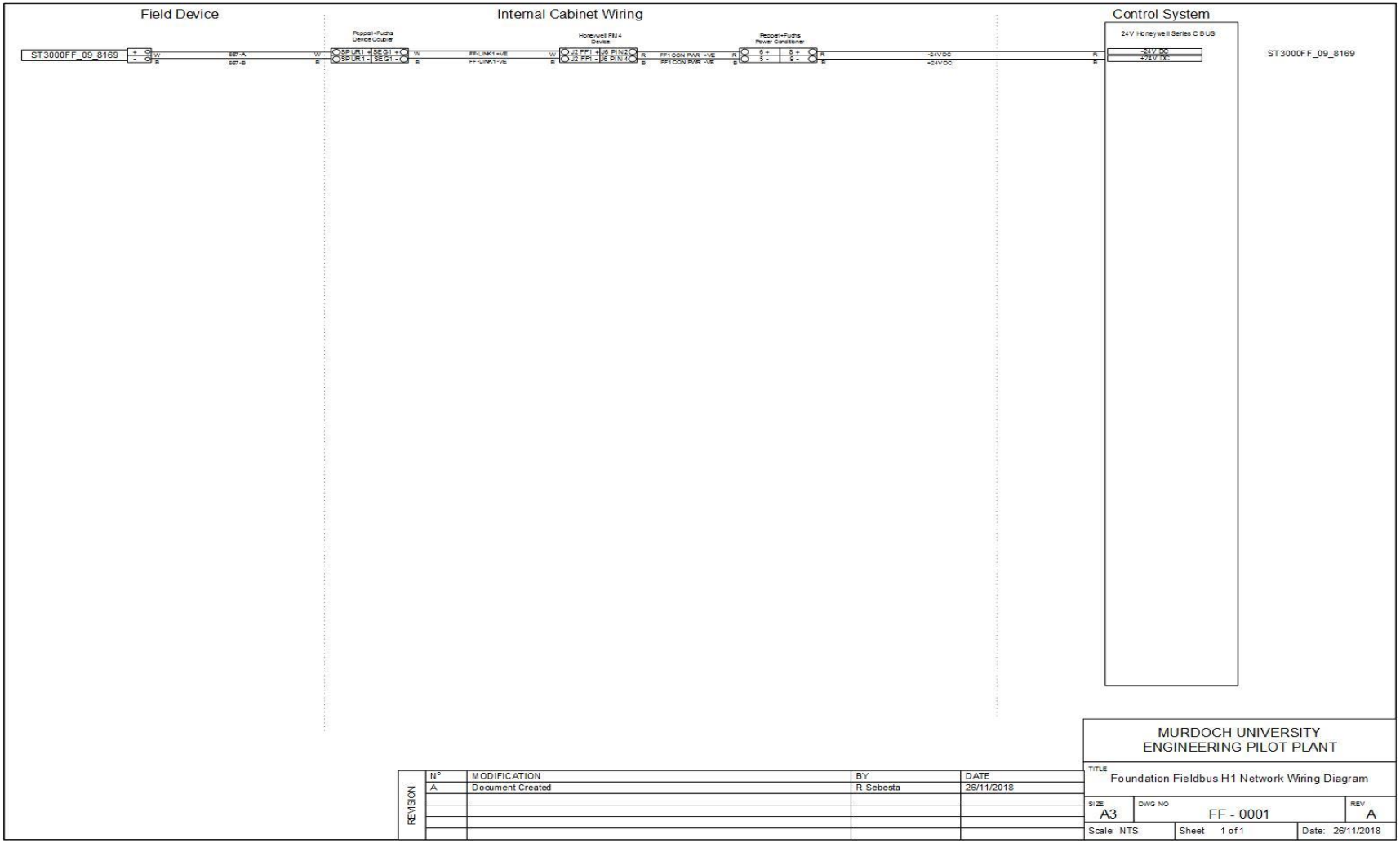

FIGURE 94 EPP FOUNDATION FIELDBUS H1 NETWORK WIRING DIAGRAM